Advanced Numerical and Experimental Transient Modelling of Water and Gas Pipeline Flows Incorporating Distributed and Local Effects

YOUNG IL KIM

Thesis for Doctor of Philosophy (PhD)
School of Civil, Environmental and Mining Engineering
July 2008

CHAPTER 6

THE EFFECT OF LEAKAGES ON TRANSIENT PIPE FLOWS

Leakages are unintentional releases of quantities of product from pipelines into the environment. In addition to its direct product losses, possible environmental pollution, land subsidence due to soil loss, and additional energy expenses due to pressure drop may all be significant. Leaks generally originate from damage to a pipeline, corrosion of pipe material, equipment failure and/or errors in pipeline design and operation. One of the best opportunities to mitigate pipeline accidents and subsequent leaks comes from implementing better pipeline monitoring and leak detection system. An effective and appropriately implemented leak detection program can reduce spill volumes and increase the public confidence. Significant cost saving due to leak reduction will accrue from the implementation of leak detection techniques. One of the most promising pipeline monitoring and fault detection systems is to use controlled transients. The advantage of the use of transients over steady flow for pipeline assessment or fault detection is the increase of flow information and sensitivity. However, a transient model based system requires a highly accurate transient analysis model. This chapter shows the effect of leakages during transients in water and gas pipelines. Leakage is estimated using an orifice equation for water transients and isentropic flow theory is applied to simulate leak behaviour in transient gas pipeline. Various experimental data and simulation results show the dynamic behaviour of leakages during water and gas transients according to leak locations and sizes.

6.1 LEAKAGES IN PIPELINE SYSTEMS

Continually, new water pipeline systems are being installed and old pipelines are under repair and replacement. The American Water Works Association (AWWA) estimates that 19,000 kilometers of new water distribution pipelines are installed annually around the world [Smith et al., 2000]. However, leaks are common faults in pipeline systems, which may occur through cracks in pipes and at couplings and connections. The daily water loss by leaks from a pipe network may be a major percentage of the total daily water consumption. Water loss from unaccounted water may be from 15% to 30% even in well-maintained networks and as high as 50% or higher in old or poorly maintained networks. The data investigated by the Asian Development Bank reported that the unaccounted for water varies from 8% (Singapore) to 62% (Dhaka, Bangladesh) in water distribution networks and the average unaccounted water is around 36%. These values were arrived at by surveying a total of 38 utilities from 23 developing countries in the Asian and Pacific region [Rao and Sridharan, 1996]. The average water loss of pipeline in some North America cities comes up to around 25% [Makar and Chagnon, 1999].

Natural gas is currently one of the most widely used sources of energy and its consumption is rapidly increasing worldwide because natural gas is the cleanest fossil fuel in terms of its combustion characteristics and economical due to its low production costs and superior thermal efficiency. Moreover, it is found all over the world and convenient to control because most natural gas is distributed through pipeline systems. During the last 30 years, large gas pipeline networks have been constructed in order to transport natural and industrial gases from source of production to consumption sites across long distances. However, all gas pipelines are in danger of accidents by outside forces, corrosion, and operating errors. Gas leaking from a natural gas pipeline is an undesirable event because it is a potential safety hazard and the loss of product. If leaking gas comes in contact with a lit match or a spark from a vehicle, an explosion or fire could result. Taking into account that a considerable proportion of gas networks are installed in highly populated zones, the consequences of such an explosion could be severe.

It is necessary to provide a quick response to pipeline failure to reduce the loss of valuable materials and to minimize the environmental damage. Leak detection systems for

distribution and transmission pipeline would make it possible to secure production without additional development of substitute resources.

6.2 LEAK DETECTION TECHNIQUES

Large leaks cause significant changes in pressure gradients and differences in mass flow rates at measurement points, and therefore are relatively easy to detect by simple equipment or even the naked eye. On the other hand, small leaks are more difficult to detect because changes in the usual process measurements are small. However, leaks as small as 1% of the nominal flow rate can cause the discharge of a large amount of water or dangerous fluid before they are detected. Leak detection has been the focus of research and the concern of water authorities for many years. The early detection of leaks is the main goal of a leak detection system.

Current leak and blockage detection methods along a pipeline can be divided into two categories, hydraulic and non-hydraulic based methods (see Chapter 2 for the detailed literature review). Non-hydraulic based methods detect the property of a pipe material, fluid, or noise emission using traditional procedures such as online or offline observation and surveillance as well as technologies using electric and sampling devices. Table 6.1 shows the summary of non-hydraulic based leak detection techniques mentioned in Section 2.1.1.

Table 6.1 Non-hydraulic Based Leak Detection Techniques

Simple Techniques	Sophisticated Technologies	Sensing Devices
· Biological Method · Bubble Test · Listening Device	· Robotic Pig Based Technique · Radioactive Technique · Ground Penetrating Radar · Magnetic Flux Technique · Electromagnetic Technique · Ultrasonic Technique · Micro-Cantilever Technique · Acoustic Technique	· Temperature Sensing · Vapour and Gas Sensing · Liquid Sensing

Hydraulic based methods, also known as computational pipeline monitoring or computational based methods, use instruments to monitor internal pipeline parameters such as pressure, flow, and temperature. These parameters are input data for inferring faults of

pipeline by processors. The use of computer systems in pipeline monitoring allows the greatest amount of data to be collected, analyzed, and acted upon in the shortest amount of time. For these reasons, most pipeline systems employ some form of computer based monitoring. Leak detection is one of many functions performing computer-based systems [Furness and van Reet, 1998]. These systems are generally composed of a supervisory computer with associated software, instruments, and communication links. Table 6.2 shows the summary of hydraulic based leak detection techniques mentioned in Section 2.1.1.

Table 6.2 Hydraulic Based Leak Detection Techniques

Flow and Pressure Change Methods	Transient Model Based Method
· Single Point Pressure Analysis · Real Time Statistical Method · Mass or Volume Balance Method · Pressure Analysis Method	· Inverse Transient Method · Transient Damping Method · Inverse Resonance Method · Resonance Peak-Sequencing Method · Wave Reflection Method

Unfortunately none of the existing methodologies can offer good performance for all the conditions. Each leak detection technique may be suitable for the specific operational condition of a pipeline while not applicable to others. The fault detection system based on a simulation model is usually accomplished through the successive and simultaneous application of various techniques. The characteristics of some techniques favor their use in certain pipeline and surrounding situations. The best combination of fault detection techniques must be used to produce the optimum results.

The performance of transient model based fault detection techniques is, so far, unsatisfactory because these methods require an extremely accurate transient model and largely depend on the sensitivity and calibration of instruments. However these techniques may present the future direction of fault detection as well as real-time pipeline monitoring by improving pipeline analysis and system measurement. The advantage of the use of transients over steady flow for detection problems is to increase the amount of information about the pipeline through measurement of the flow time history. In addition, transients are more sensitive to pipeline flow components. The flow information analysis of transients can be usefully applied to pipeline fault detection, calibration of roughness factors and minor losses, and pipeline assessment. The study introduced in this research is

focussed on the understanding and interpretation of the effects of leaks on transients and better uses of transients for pipeline fault detection. The development of an appropriate and accurate numerical dynamic model of transients in pipelines is an essential prerequisite for detecting leaks as well as pipeline monitoring systems.

6.3 NUMERICAL MODELS FOR LEAK ESTIMATION

Leakage in a pipe may be simulated at nodal points in a computational grid by a discontinuity in discharge. The sum of the flows entering (positive) Q_{in} and the flows exiting (negative) Q_{out} at a node with the leakage flow Q_L is equal to zero.

$$Q_{in} - Q_{out} - Q_L = 0 \tag{6.1}$$

In the case of water in a pipe flow, the leakage flow at a node can be described by the orifice equation.

$$Q_L = C_d A_L \sqrt{2g(H_L - z_L)} \tag{6.2}$$

where C_d = discharge coefficient, A_L = area of the leak hole, H_L = hydraulic head at the leak, and z_L = elevation of the pipeline at the leak. Eq. 6.2 is valid when the pressure at the node is above zero (atmospheric). Occasionally, water can find its way back into the pipeline when the pressure inside the pipe becomes lower than that outside of the pipe. A leak hole at a negative pressure can be the injection pathway of non-potable water during transient events. Injection of non-potable water into water distribution systems has the possibility of pathogen intrusion that may result in the outbreak of water borne diseases [Funk et al., 1999]. The expression below allows leakage described at negative pressures. The sign operator ϕ_L is dependent on the hydraulic head at the leak (+1 if H_L-$z_L \geq 0$ and -1 if H_L-$z_L < 0$).

$$Q_L = C_d A_L \phi_L \sqrt{2g|H_L - z_L|} \tag{6.3}$$

The lumped leak coefficient C_dA_L is usually assumed to be independent of the Reynolds number of the flow through the leak during transient events because of computational

simplicity, therefore the lumped leak coefficient empirically calibrated in the initial flow condition is generally used for leak estimation during unsteady pipe flow. However, in a real pipe system, the discharge coefficient is dependent on the leaking flow that changes during transients. Rouse [1978] indicated that discharge coefficient is almost constant for a Reynolds number of greater than 10,000. The dependence of discharge coefficient on the leaking flow is not expected to be a major problem because most leaks may have a high Reynolds number due to high pressure condition [Víkovský, 2001]. Chapter 8 introduces the fully frequency dependent unsteady minor loss models for orifices and axial-extended orifices. This model can be used for simulating the dynamic behaviour of leaking flow during transient events. However, leak estimation is not a simple problem because pipeline systems have various shapes of leak hole, and the leak opening itself can easily deform and change the effective leak area and shape when the pipe is stressed.

For leak estimation of gas transients, reversible adiabatic flow condition (frictionless adiabatic or isentropic flow) is used for simulating gas inflow and outflow through the leak hole in the pipeline system [Shapiro, 1953; Liepmann and Roshko, 1957; Saad, 1985]. All possible states have constant entropy. The flows of real gases are affected by temperature, pressure, and properties of the substance, thus ideal flows such as isentropic flow cannot be reached in the flow of real gases. However, the friction effect and heat exchange are minor in the flow through a leak opening because the effective friction length of the leak hole is very short and the mass flow rate by a leak is relatively small compared with the volume of a pipeline, so the pipeline provides enough heat capacity to hold the temperature close to the fluid temperature. Thus the gas inflow and outflow through a leak hole can be regarded by isentropic flow conditions.

The mass flow rate (accidental release) of gas through a leak hole depends on the values of pressure p_o, absolute temperature T_o, density ρ_o, velocity V_o, enthalpy h_o, and Mach number M_o through the leak hole, as well as the pressure p, absolute temperature T, density ρ, velocity V, enthalpy h, and Mach number M within the pipe under the assumption of frictionless and steady state flow condition (shown in Fig. 6.1). The pipe is considered to be like a tank.

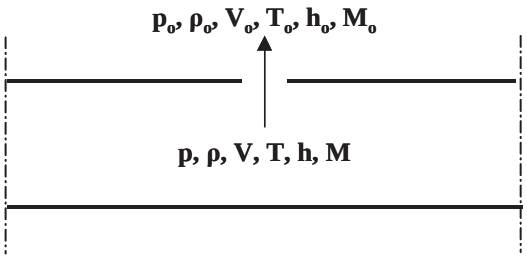

Figure 6.1 Accidental Gas Release through a Leak Hole

The velocity at the leak hole is derived by using perfect gas law relations (Eq. 3.29 and 3.31) and first law of thermodynamics ($h = h_o + V_o^2/2$).

$$V_o = \sqrt{2C_p(T - T_o)} = \sqrt{\frac{2\gamma}{\gamma - 1} R(T - T_o)} \tag{6.4}$$

After rearranging by using $C_p = \gamma R/(\gamma\text{-}1)$ and $a^2 = \gamma RT$.

$$\frac{T}{T_o} = 1 + \frac{\gamma - 1}{2} \frac{V_o^{\,2}}{a_o^{\,2}} = 1 + \frac{\gamma - 1}{2} M_o^{\,2} \tag{6.5}$$

where M is Mach number, flow velocity / wavespeed = $V/a = V/(\gamma RT)^{0.5}$. Eq. 6.5 shows that temperature ratio only depends on the specific heat ratio of the gas and the Mach number. This relationship is valid for both adiabatic and isentropic flows. T is the same for all points in the flow, provided that the flow is adiabatic.

The particular properties at the critical flow state (sonic flow) of leak opening are found when the gas is flowing at Mach number 1, where the mass flow per unit area is a maximum. The properties are usually identified by means of an asterisk to distinguish them from properties at other Mach values. The critical properties are used as a reference point in describing properties at different sections of the flow. Thus the particular value of the temperature ratio at the critical state follows that

$$\frac{T}{T^*} = \frac{\gamma + 1}{2} \quad by \quad V^* = a^* \quad or \quad \sqrt{\frac{2\gamma}{\gamma - 1} R(T - T^*)} = \sqrt{\gamma RT^*} \tag{6.6}$$

When a perfect gas flows isentropically, the relations between pressure, temperature, and density for an isentropic process can be presented as

$$\frac{T_o}{T} = \left(\frac{p_o}{p}\right)^{(\gamma-1)/\gamma} = \left(\frac{\rho_o}{\rho}\right)^{\gamma-1} \tag{6.7}$$

Substitution of Eq. 6.7 into Eq. 6.5 yields the pressure and density ratios as function of Mach number in isentropic process.

$$\frac{p}{p_o} = \left(1 + \frac{\gamma-1}{2} M_o^{\,2}\right)^{\gamma/(\gamma-1)} \tag{6.8}$$

$$\frac{\rho}{\rho_o} = \left(1 + \frac{\gamma-1}{2} M_o^{\,2}\right)^{1/(\gamma-1)} \tag{6.9}$$

Also, the particular values of the pressure and density ratios at the critical state (sonic flow) are found by setting $M = 1$ in the above equations.

$$\frac{p^*}{p} = \left(\frac{2}{\gamma+1}\right)^{\gamma/(\gamma-1)} \tag{6.10}$$

$$\frac{\rho^*}{\rho} = \left(\frac{2}{\gamma+1}\right)^{1/(\gamma-1)} \tag{6.11}$$

Mass flow rate through a leak hole can be expressed by using leak opening area A_L and perfect gas law relations.

$$\dot{m} = C_d A_L \rho_o V_o = C_d A_L \frac{p_o}{RT_o} V_o = C_d A_L \frac{p_o V_o}{\sqrt{\gamma RT_o}} \sqrt{\frac{\gamma}{R}} \sqrt{\frac{T}{T_o}} \frac{1}{\sqrt{T}} \tag{6.12}$$

The mass flow rate through a leak hole may be derived in terms of Mach number by eliminating p_o in Eq. 6.12 and by using the isentropic relations in Eq. 6.5 and 6.8.

$$\dot{m} = C_d A_L \sqrt{\frac{\gamma}{R}} \frac{p}{\sqrt{T}} \frac{M_o}{\left(1 + \frac{\gamma - 1}{2} M_o{}^2\right)^{(\gamma+1)/2(\gamma-1)}} \tag{6.13}$$

Eq. 6.13 shows that, for a given Mach number, the flow is proportional to the pipe pressure and inversely proportional to the square root of the pipe temperature. Eq. 6.13 may be rearranged by using the isentropic relations and perfect gas law after eliminating the Mach number by using Eq. 6.8. If the pipe flow is subsonic, the mass flow at the leak hole is either sonic or subsonic flow. In addition, this mass flow rate is dependent on whether the flow is sonic or subsonic. Supersonic flow ($M > 1$) seldom occurs in the general gas transmission or distribution pipe system. Eq. 6.14a and 6.14b represent the mass inflow and outflow rate through leak hole during subsonic flow condition ($M < 1$), and the mass flow rate is expressed in terms of pressure ratio between inside the pipe and outside the pipe [Shapiro, 1953; Liepmann and Roshko, 1957; Streeter and Wylie, 1985; Wylie et al., 1993; Swaffield and Boldy, 1993]. Critical pressure ratio of Eq. 6.11 establishes the flow conditions that differentiate between subsonic and sonic flow and between inflow and outflow.

Subsonic Mass Inflow Rate

$$\dot{m} = +C_d A_L \sqrt{2 p_o \rho_o \frac{\gamma}{\gamma - 1} \left\{ \left(\frac{p}{p_o}\right)^{2/\gamma} - \left(\frac{p}{p_o}\right)^{(\gamma+1)/\gamma} \right\}} \qquad \textit{when} \quad p_o > p > p_o \cdot \left(\frac{2}{\gamma+1}\right)^{\gamma/(\gamma-1)} \tag{6.14a}$$

Subsonic Mass Outflow Rate

$$\dot{m} = -C_d A_L \cdot p \sqrt{\frac{2}{RT} \frac{\gamma}{\gamma - 1} \left\{ \left(\frac{p_o}{p}\right)^{2/\gamma} - \left(\frac{p_o}{p}\right)^{(\gamma+1)/\gamma} \right\}} \qquad \textit{when} \quad p_o / \left(\frac{2}{\gamma+1}\right)^{\gamma/(\gamma-1)} > p > p_o \tag{6.14b}$$

These equations are applicable when the flow at the leak hole is subsonic. The maximum mass flow rate $\dot{m}_{maz}$ can be obtained by using Eq. 6.6, Eq. 6.11, and perfect gas law or by directly setting the Mach number is unity to the Eq. 6.13.

Sonic (Critical) Mass Inflow Rate

$$\dot{m}_{\max} = +C_d A_L \sqrt{\frac{\gamma}{R}} \frac{p_o}{\sqrt{T_o}} \left(\frac{2}{\gamma+1} \right)^{(\gamma+1)/2(\gamma-1)} \qquad (6.15a)$$

$$when \quad p \le p_o \cdot \left(\frac{2}{\gamma+1} \right)^{\gamma/(\gamma-1)}$$

Sonic (Critical) Mass Outflow Rate

$$\dot{m}_{\max} = -C_d A_L \sqrt{\frac{\gamma}{R}} \frac{p}{\sqrt{T}} \left(\frac{2}{\gamma+1} \right)^{(\gamma+1)/2(\gamma-1)} \qquad (6.15b)$$

$$when \quad p \ge p_o / \left(\frac{2}{\gamma+1} \right)^{\gamma/(\gamma-1)}$$

Eq. 6.14a to 6.15b can be applied to the loss of gas through a leak hole from a pipeline. The specific heat ratio γ is 1.401 when the flow medium is air. These equations may also be used for modelling an air valve to protect a pipeline from vacuum conditions and to release air from a pipeline [Wylie et al., 1993; Chaudhry, 1987; and Swaffield and Boldy, 1993].

6.4 NUMERICAL INVESTIGATION OF LEAKAGE

When the flow in a pipe changes suddenly, a pressure transient starts propagating along the pipeline. Pipeline features, such as leaks, blockages, entrapped air, minor losses, and appurtenances alter the inherent propagation of the pressure transients. The change of time-domain wave signal affected only by wall friction is a low frequency signal with square pressure wave. If the pressure propagation is affected by a leak, the transient flow may be composed of two parts, both low frequency flow signal for transient basic flow affected by wall friction and high frequency flow signal (rapid change of pressure wave) damped by a leak.

Fig. 6.2 shows a single pipeline of 37.53 m in length composed of 4 pipe segments and 5 nodes, which is used to demonstrate the effect on a pressure wave by the changes of leak magnitude and location. This pipeline is identical to the laboratory pipeline described in Chapter 4. The pipeline is connected to a reservoir to a flow control valve. Transients are

generated by the fast closure of the flow control valve and pressure wave is measured at the end of pipeline.

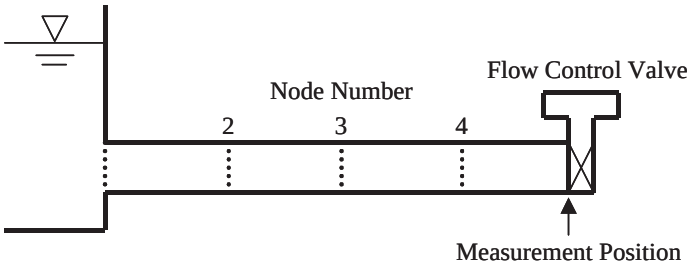

Figure 6.2 Single Pipeline for Numerical Experiments

Numerical simulations demonstrate that the attenuation of pressure wave occurs in a pipeline due to leaks. Fig. 6.3 shows pressure wave variations when the lumped leak coefficient C_dA_L changes at node 3. The leak areas used for this simulation are $1.0*10^{-7}$, $2.0*10^{-7}$, and $4.0*10^{-7}$ m^2. The pressure wave variations with time affected by leaks are compared with the pressure wave of intact pipe. Pressure profiles are clearly classified according to leak area changes. Leaks in the pipeline contribute to the shape and damping of transient traces. Fig. 6.4 shows pressure variations when the leak location changes (leak from node 2, 3, and 4 in Fig. 6.2). A lumped leak coefficient of $7.0*10^{-7}$ m^2 is used for all simulation cases. The shapes of pressure traces are different according to leak location changes and the positions of sudden pressure drop in the first pressure rise indicate the exact leak location. Obvious pressure damping, change of pressure shape, and position of sudden pressure drop due to a leak leads to a method and possibility of detecting the location and magnitude of the leak.

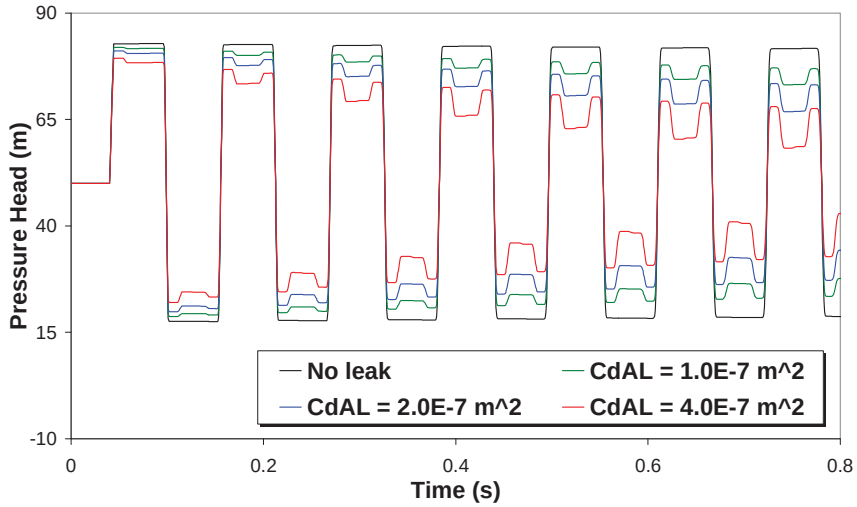

Figure 6.3 Pressure Variations according to a Change of Leak Area in Water Pipe

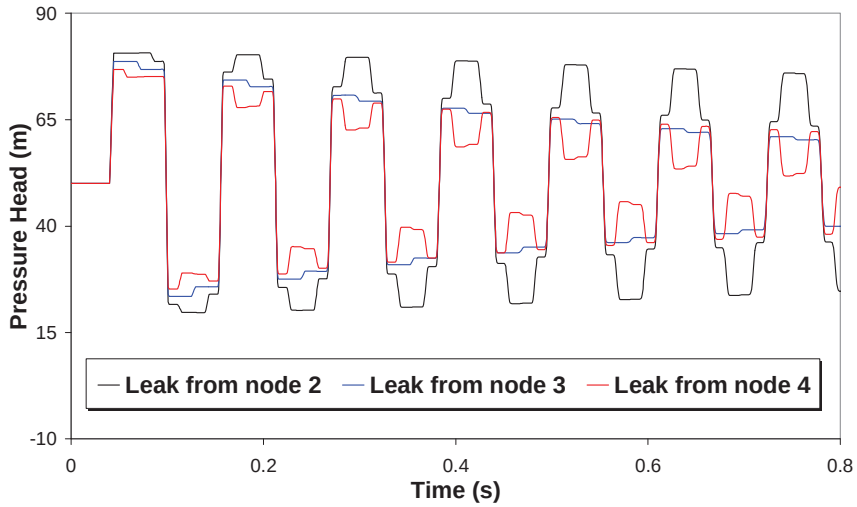

Figure 6.4 Pressure Variations according to a Change of Leak Location in Water Pipe

Leak detection methods using transient flow simulation are based on the analysis of pipeline pressure variations with time along the pipeline. Attributes of pressure waves affected by a leak provide potential methods for leak detection. The behaviour of pressure waves is gradually altered by the specific properties of the pipelines such as leaks, blockages, wall shear stress, and minor loss components. The wave disturbed by a leak retains a substantial amount of information concerning the leak. The magnitude and location of leaks can be detected by analyzing the behaviour of pressure waves during transients.

Figs. 6.5 and 6.6 show the comparison of simulation results according to the change of leak size and location in the gas transients. The test situation and pipeline system with air is the same as the above system used for numerical experiments of water transients. The lumped leak coefficients used for numerical tests according to the change of leak areas are $3.0*10^{-6}$ and $5.0*10^{-6}$ m^2 in Fig. 6.5 and the lumped leak coefficient used for a numerical test according to the change of leak locations is $5.0*10^{-6}$ (leak from node 2, 3, and 4 in Fig. 6.2). Although the simulation results are similar with the results of water transients, the impact due to leaks on pressure waves appear to be smaller than that for water transients. Gas compressibility blunts the impact of leaks during transient events and is still dominant physical phenomena for analysis.

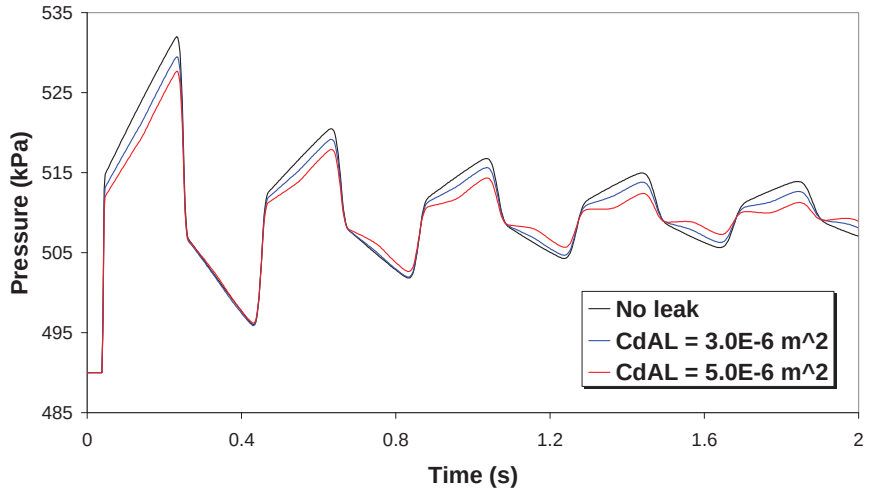

Figure 6.5 Pressure Variations according to a Change of Leak Area in Gas Pipe

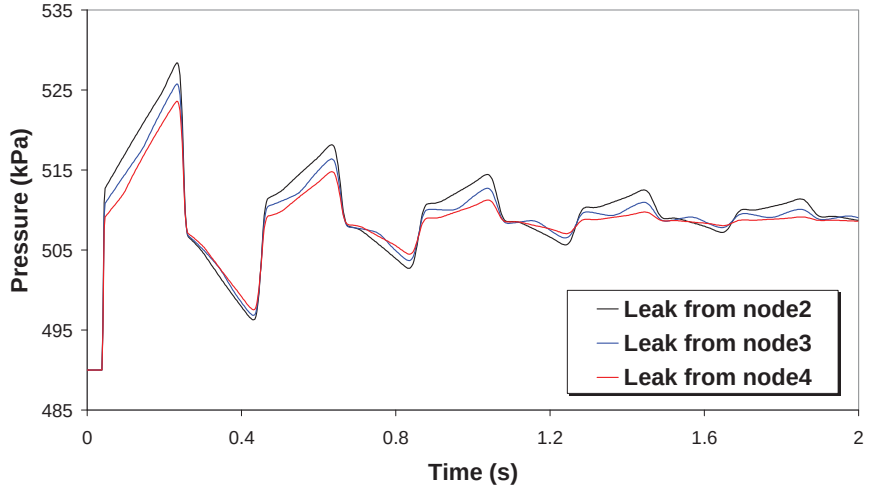

Figure 6.6 Pressure Variations according to a Change of Leak Location in Gas Pipe

6.5 EXPERIMENTAL VERIFICATION FOR LEAKAGES

Laboratory experiments have been undertaken for the verification of unsteady friction models for water and gas transients of a tank-pipe-valve system. The experimental apparatus is described in Chapter 4. The layout of the pipeline system is repeated in Fig. 6.7.

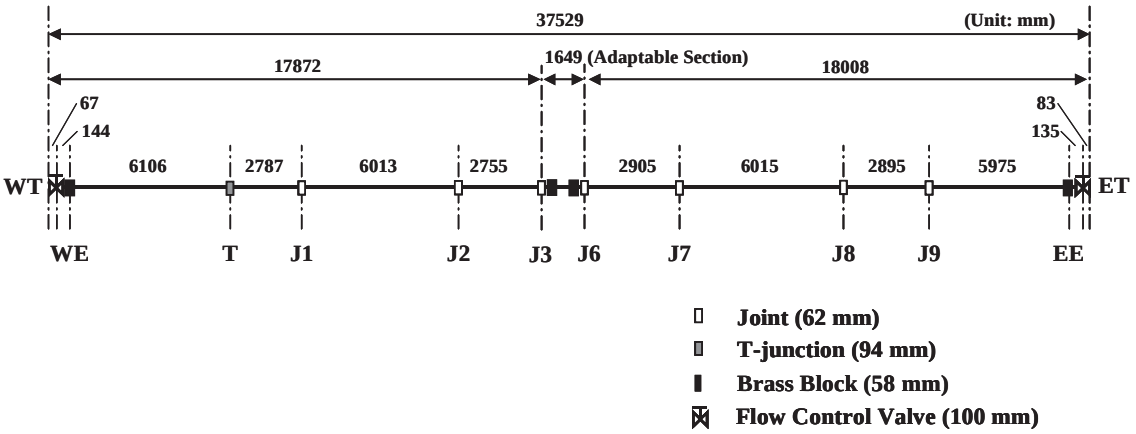

Figure 6.7 Laboratory Pipeline System Layout

6.5.1 Leak Location Tests from Leaking Joints

This section shows the test data for locating leaks. Leaks were originated from pipeline joints by slightly loosening the fittings. The laboratory pipeline system has 7 or 9 high precision Swagelok 1 inch straight fittings depending on the test conditions and one T-junction. Transient events are generated by fast closing solenoid valve at the WE (west end). The pipeline system is a tank-pipe-valve system. The sampling frequency of measurement data at a west end brass block is 2 kHz. Fig. 6.8 shows measured pressure profiles for changes of leak location. Each measured pressure trace has different shape according to the location of leaking joint. The sudden pressure drops in the first pressure rise indicate the exact leak locations. Fig. 6.9 shows the details of sudden pressure drops in the first pressure rises. The thick gray arrows point out the location of leaking joint and the position of sudden pressure drop. The positions of sudden pressure drops indicate the exact leak locations.

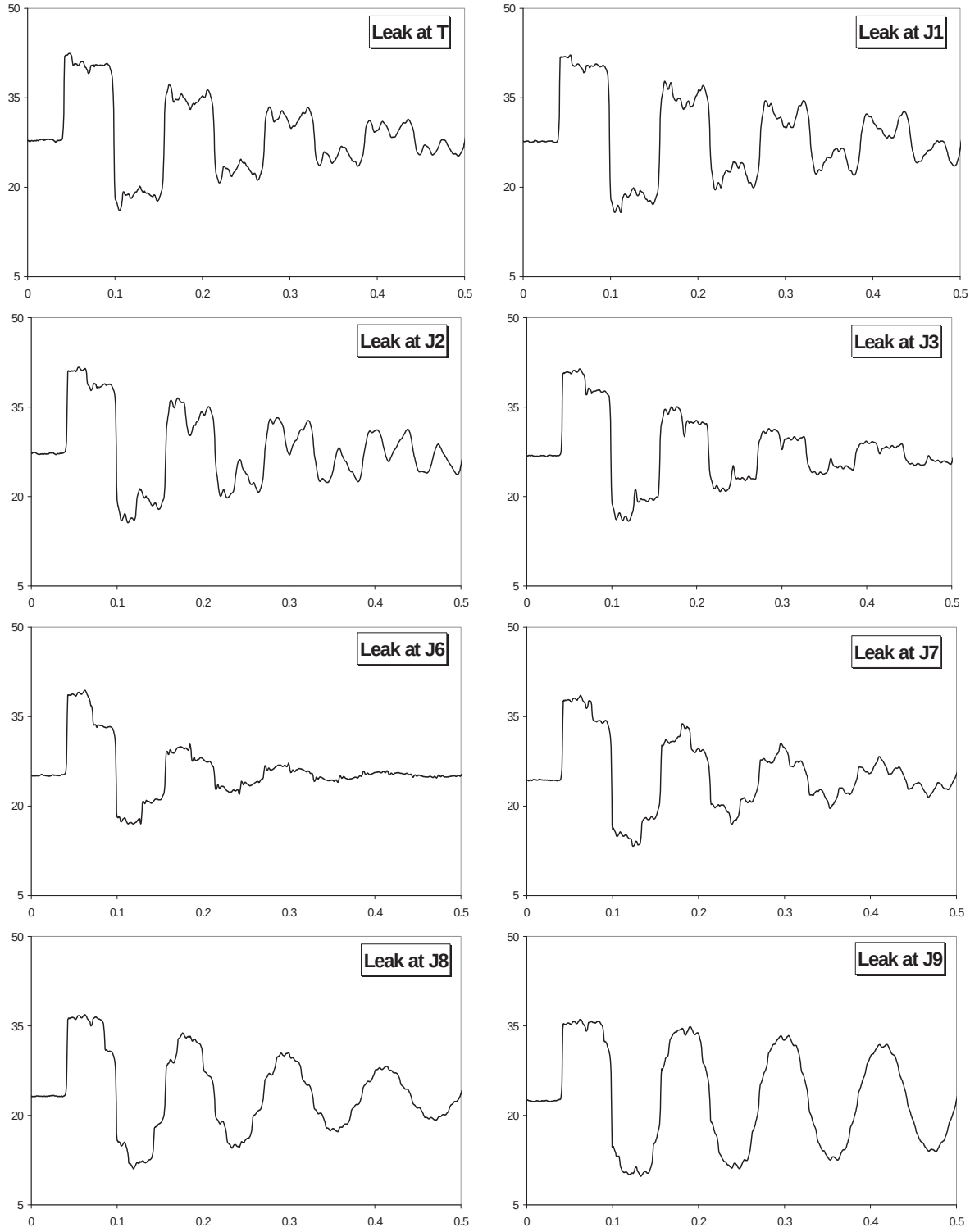

Figure 6.8 Pressure Profiles for Leaking Joints

(x-axis: measured time (s) and y-axis: pressure head (m))

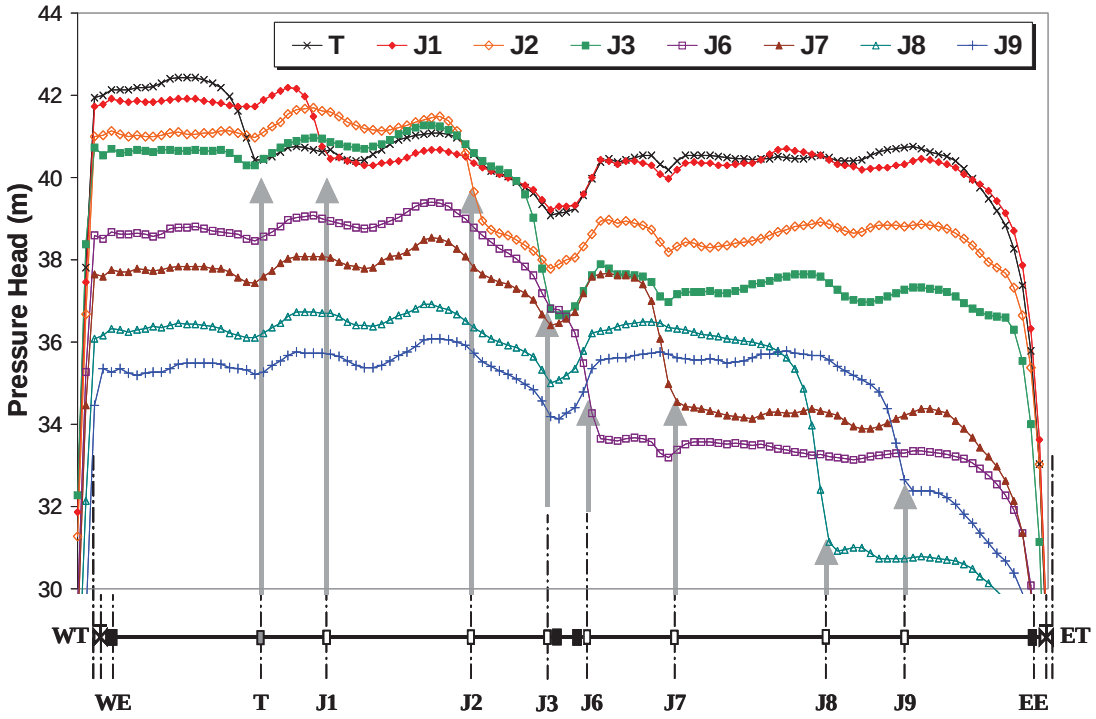

Figure 6.9 Details of Sudden Pressure Drops in the First Pressure Rise

6.5.2 Resonance (Auto-Oscillation) by a Leak

An auto-oscillation (resonance) condition caused by a leak accidentally appeared during the above tests for leaking joints. Excessive pressure fluctuations and noise were produced when the pipeline has a leak at the joint J2. Figs. 6.10 and 6.11 show the measured pressure waves during the resonance condition. Although flow disturbances generated by accidental or normal operation generally attenuate and disappear in the hydraulic system with time, occasionally a flow disturbance is amplified that results in severe pressure and flow oscillations. This condition depends on the characteristics of the fluid system and of the excitation. Such an oscillation that leads to pressure amplification in the fluid system is defined as resonance, also known as self-excited oscillation or auto-oscillation [Wylie et al., 1993].

Pressure amplifications occur when the frequency of a certain system element is matched to one of the critical and natural frequency of the pipeline system. The system element can be regarded as an exciter to develop the pressure amplifications. A typical example of an exciter is a leaking valve or a leaking seal [Jaeger, 1977]. Resonance is serious physical phenomena because unexpected resonance can be destructive in practical hydraulic

systems. It is accompanied by instability, noise, system vibration, and possible destruction of the system due to severe pressure fluctuation and overstress. Pejovic and Boldy [1992] showed some examples of the fluid systems ruined by hydraulic resonance.

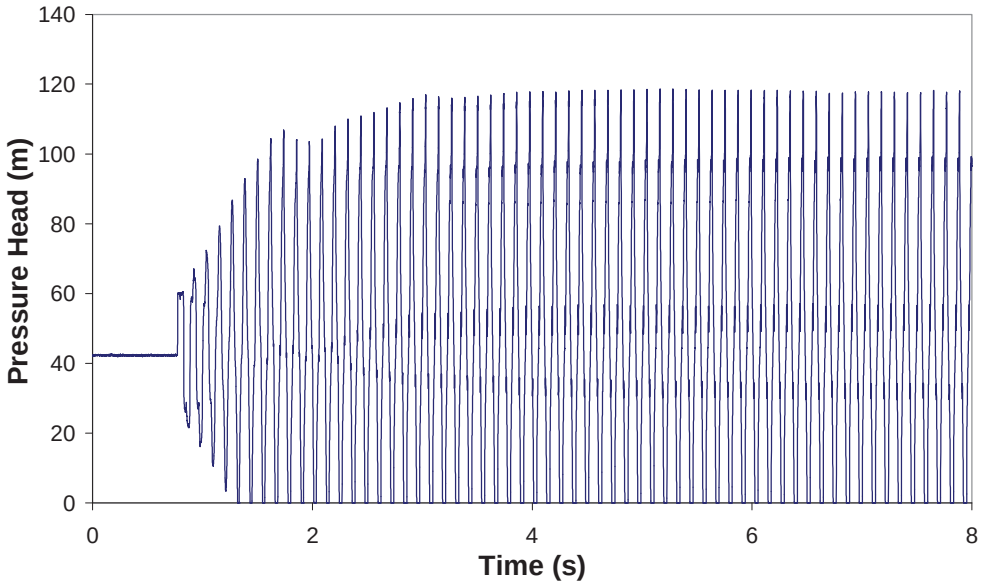

Figure 6.10 Measured Resonance Caused by Leaking Joint (at the end of pipe)

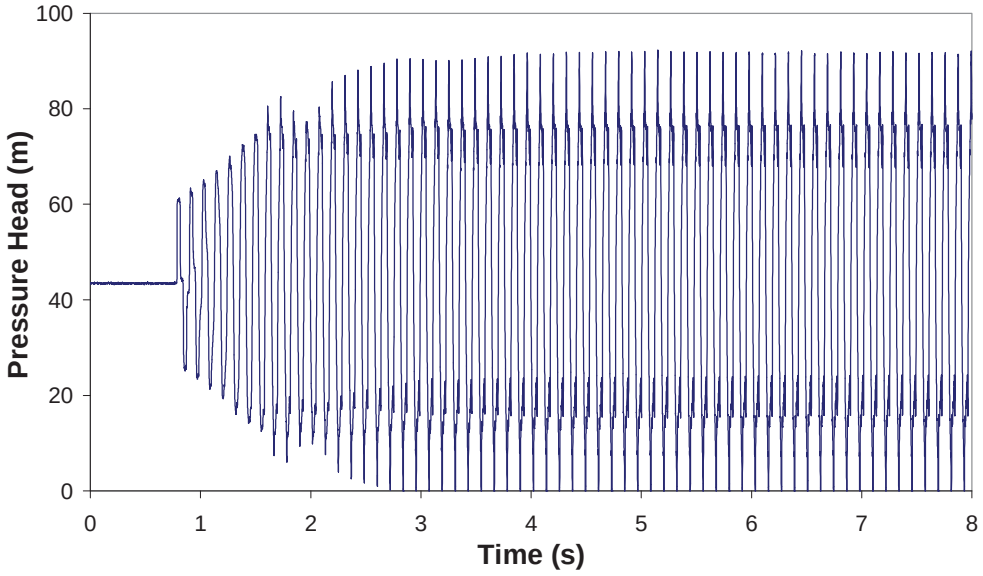

Figure 6.11 Measured Resonance Caused by Leaking Joint (at the middle of pipe)

In this test condition, the leaking joint (J2) is an exciter that develops the resonating condition. The measured pressure waves show excessive pressure oscillations and the oscillations maintain an almost constant magnitude of pressure wave with time. The upper

bound of the pressure magnitude is almost double at the end of pipe when compared to the first pressure rise generated by transients. The lower bound drops below the set point (zero pressure head in this case of tests) of data acquisition system. The oscillations were finally stopped by opening the flow control valve at the end of pipe to protect laboratory pipeline system from the excessive and continual pressure fluctuations. This test result indicates another undesirable situation of a leakage in the pipeline system in terms of dangerous pressure oscillations.

When the frequency ω_L of leaking joint is the matched to natural frequency ω_n of pipeline system, the measured pressure wave shows the initial development of a beat from 0.8 to 3 seconds in Figs. 6.10 and 6.11. Transient oscillation increases in this section. Then the oscillations become almost constant after 3 seconds. These oscillations with constant amplitude are called steady oscillatory flow. The amplitude of the pressure oscillations depends on the frequency ratio ω_L/ω_n and system conditions. If the frequency of a leaking joint is equal to the natural frequency of pipeline system and the system is frictionless, the amplitude of steady oscillations becomes infinite and the oscillations are amplified without any bound. The reason for this is that the total energy of the system keeps on increasing with each cycle because no energy is dissipated in the system. However, the pipeline system has wall shear stress, so the amplitude of the oscillations grows until the energy input and energy dissipation by friction are equal and the system oscillates with finite amplitude. The steady-oscillatory flows in a hydraulic system are generally analysed in the frequency domain by using impedance or transfer matrix method [Chaudhry, 1987].

6.5.3 Comparison between Measured Data and Simulation Results

Leakages generate additional damping of a transient pressure wave. Fig. 6.13 shows the comparison between measured data and simulation results by using a conservative scheme including a leak estimation model to show the damping effects of pressure waves by leaks. Tests were executed by using a leak component shown in the upper part of Fig. 6.12. This leak component is composed of leak valve and screw type orifice with various bore sizes (0.5, 1, 2, 3, 4, and 5 mm). Transient events were generated by closure of a fast operating solenoid valve at the WE and the leak component is assembled into EM brass block shown in Fig. 4.4 (near the middle of pipeline). Leak tests were conducted with various leak bore sizes under various flow conditions shown in Table 5.4. They have similar test results

according to flow condition and leak size, therefore this section shows the results of tests conducted under condition 5.

Figure 6.12 Leak Component

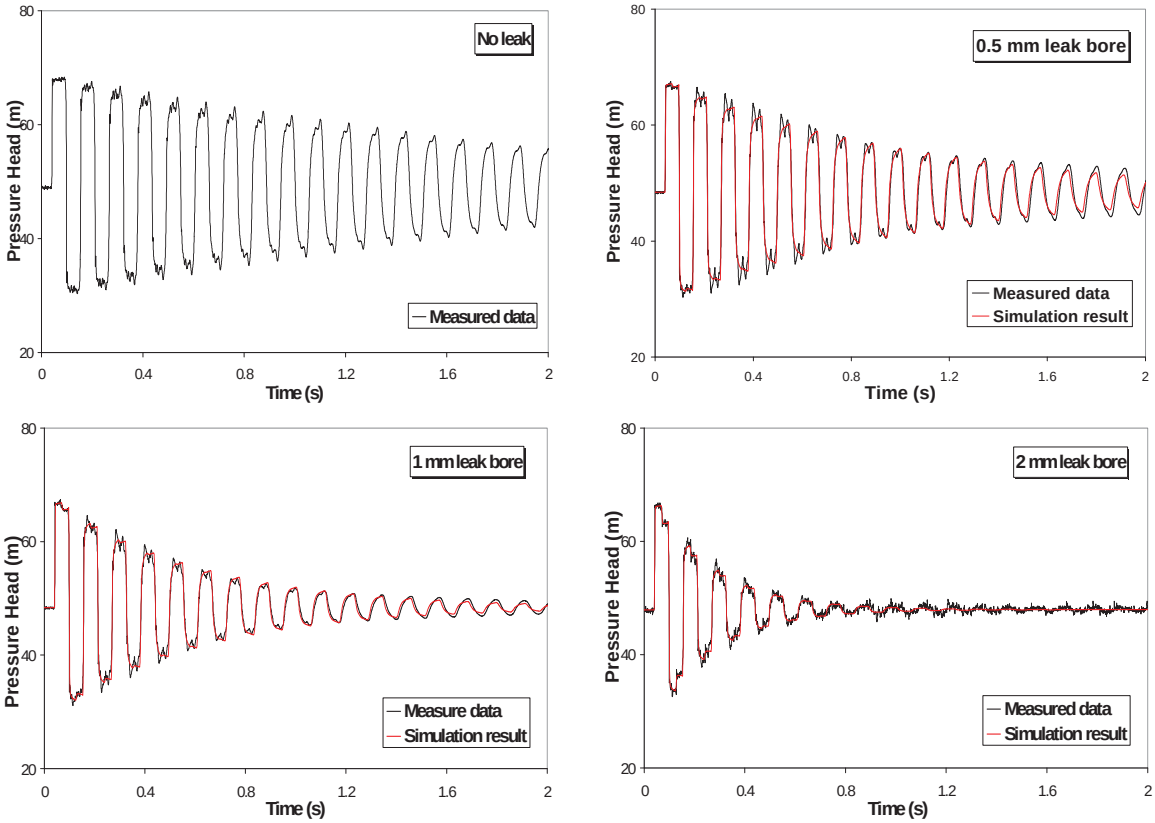

Figure 6.13 Transient Damping Effects of Leaks

During these laboratory tests, inflow to the system Q_{in}, outflow from the system Q_{out}, and flow rate by leaks Q_L were measured by volumetric method to find the exact lumped leak coefficient C_dA_L with measured pressure data. Table 6.3 shows the details of flow information and lumped leak coefficients according to leak bore sizes.

Table 6.3 Flow Information and Lumped Leak Coefficients

Leak Size	Q_{in} $*10^{-5}$ (m^3/s)	Q_L $*10^{-5}$ (m^3/s)	Q_{out} $*10^{-5}$ (m^3/s)	Q_L / Q_{in} (%)	C_dA_L $*10^{-6}$ (m^2)
No Leak	5.248	-	5.248	-	-
0.5 mm Leak	6.210	0.974	5.236	15.7	0.319
1.0 mm Leak	7.301	2.122	5.179	29.1	0.696
2.0 mm Leak	10.805	5.646	5.159	52.3	1.862

Fig. 6.13 clearly indicates that the damping of pressure wave during transients increases as the leak size increases. There is good agreement between measured pressure data and simulation results. Figs. 6.14 to 6.16 show the comparison between measured data with leaks and their simulation results by proposed conservative scheme model at the end and middle of pipeline. Generally, the model performs well, accurately modelling the phase, magnitude and shape of the experimental data.

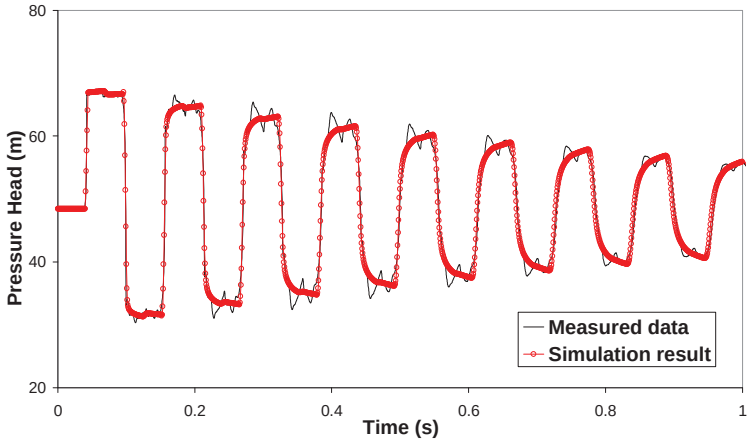

(a) At the End of Pipeline

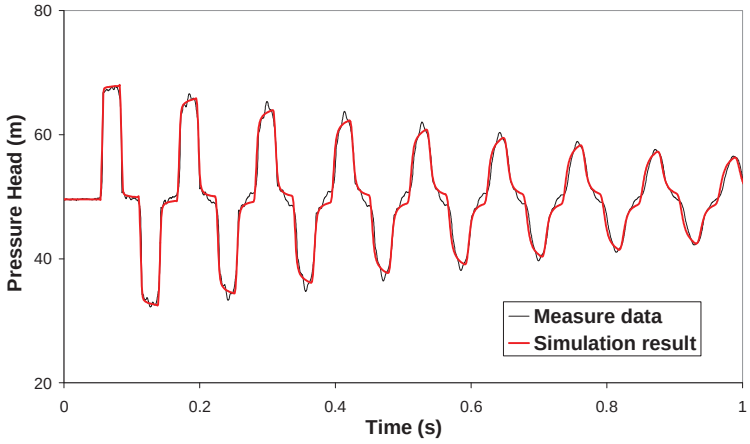

(b) At the Middle of Pipeline

Figure 6.14 Simulation Result for a 0.5 mm Leak Bore

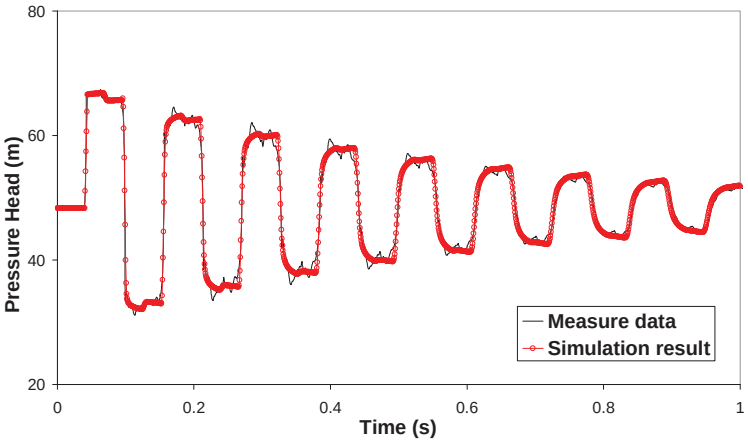

(a) At the End of Pipeline

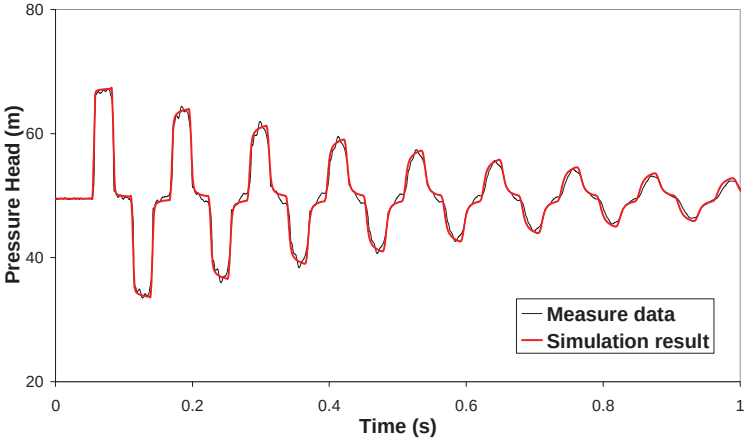

(b) At the Middle of Pipeline

Figure 6.15 Simulation Result for a 1.0 mm Leak Bore

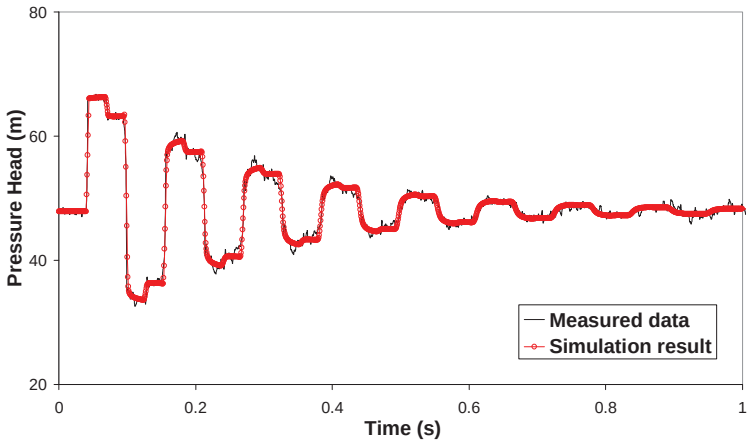

(a) At the End of Pipeline

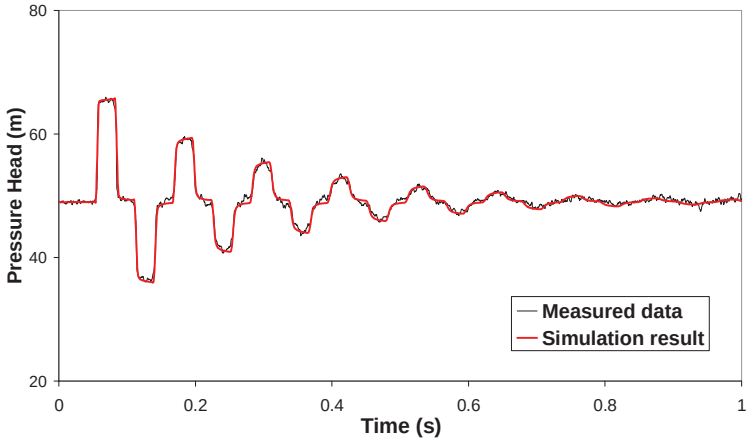

(b) At the Middle of Pipeline

Figure 6.16 Simulation Result for a 2.0 mm Leak Bore

6.5.4 Leakages in Transient Gas Pipe Flows

Similar to the experiments for verification of unsteady friction model in the water pipeline, experiments of transient gas flow with a leakage were conducted after draining and drying the pipeline and tanks. Dry air supplied by an air compressor through air filters was used as the fluid medium. Transient events were generated by fast closing solenoid for low Mach number gas flows ($M < 0.03$) and flow control valve for relatively high Mach number gas flows ($M > 0.1$). Both valves were located at the downstream end. Both pressure and temperature were measured at the tank, middle of pipe, and end of pipe during transients.

1) Low Mach Number Flows

Figs. 6.17 and 6.18 show the measured pressure wave at the end and middle of pipeline for different leak bore sizes for low Mach number gas flows. The initial velocity and maximum pressure change are both small. The pressure data are plotted at the same scale on the graphs (the range of the x-axis and the y-axis are 8 seconds and 16 kPa respectively) to compare each pressure variation and pressure wave shape. Table 6.4 shows the flow information during these tests. The mass inflow to the pipe $\dot{m}_{in}$, mass outflow from the pipe $\dot{m}_{out}$, mass flow rate by leaks $\dot{m}_L$, and their ratios are obtained by the relationship between the pressure of the constant tank volume and mass flow rate in Eq. 4.5. During these experiments, the maximum temperature change of whole process is smaller than 0.5^{o}C, therefore temperature change is negligible for the variable of transient analysis.

Table 6.4 Flow Information for Low Mach Number Flow

Leak Size	Mass Inflow $\dot{m}_{in}$ (kg/s)	Mass Flow by a Leak $\dot{m}_L$ (kg/s)	Mass Outflow $\dot{m}_{out}$ (kg/s)	Leak Rate $\dot{m}_L / \dot{m}_{in}$ (%)	Initial Pressure (kPa)	Mach Number
No Leak	$9.796*10^{-3}$	-	$9.796*10^{-3}$	-	486.7	0.013
0.5 mm Leak	$9.898*10^{-3}$	$4.666*10^{-4}$	$9.431*10^{-3}$	4.7	472.5	0.012
1.0 mm Leak	$1.072*10^{-2}$	$1.364*10^{-3}$	$9.353*10^{-3}$	12.7	477.3	0.012
2.0 mm Leak	$1.379*10^{-2}$	$4.916*10^{-3}$	$8.869*10^{-3}$	35.6	467.7	0.011
3.0 mm Leak	$1.949*10^{-2}$	$1.110*10^{-2}$	$8.392*10^{-3}$	56.9	464.8	0.011

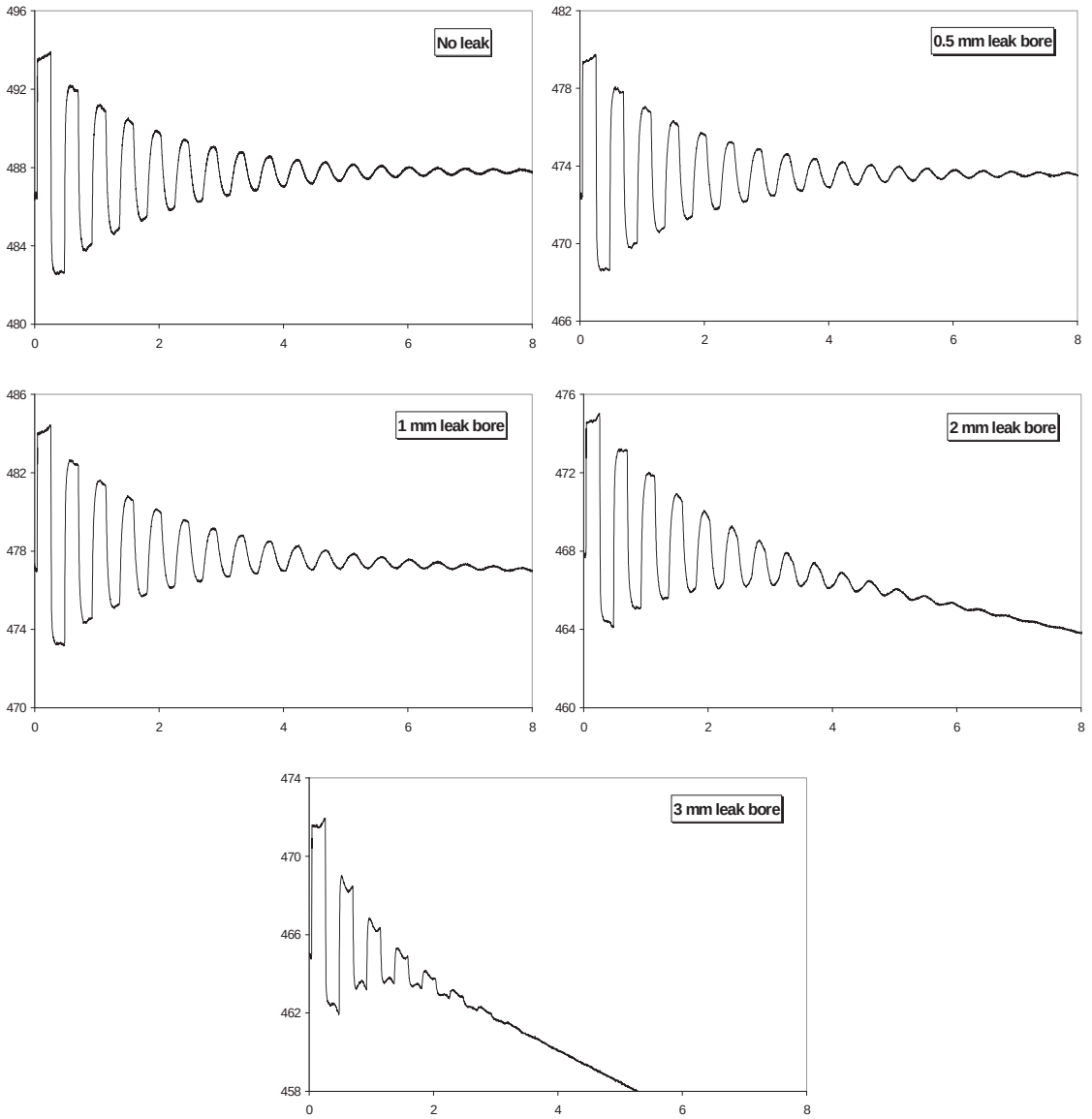

Figure 6.17 Measured Data at the End of Pipe for Low Mach Number Flows

(x-axis: measured time (s) and y-axis: pressure (kPa))

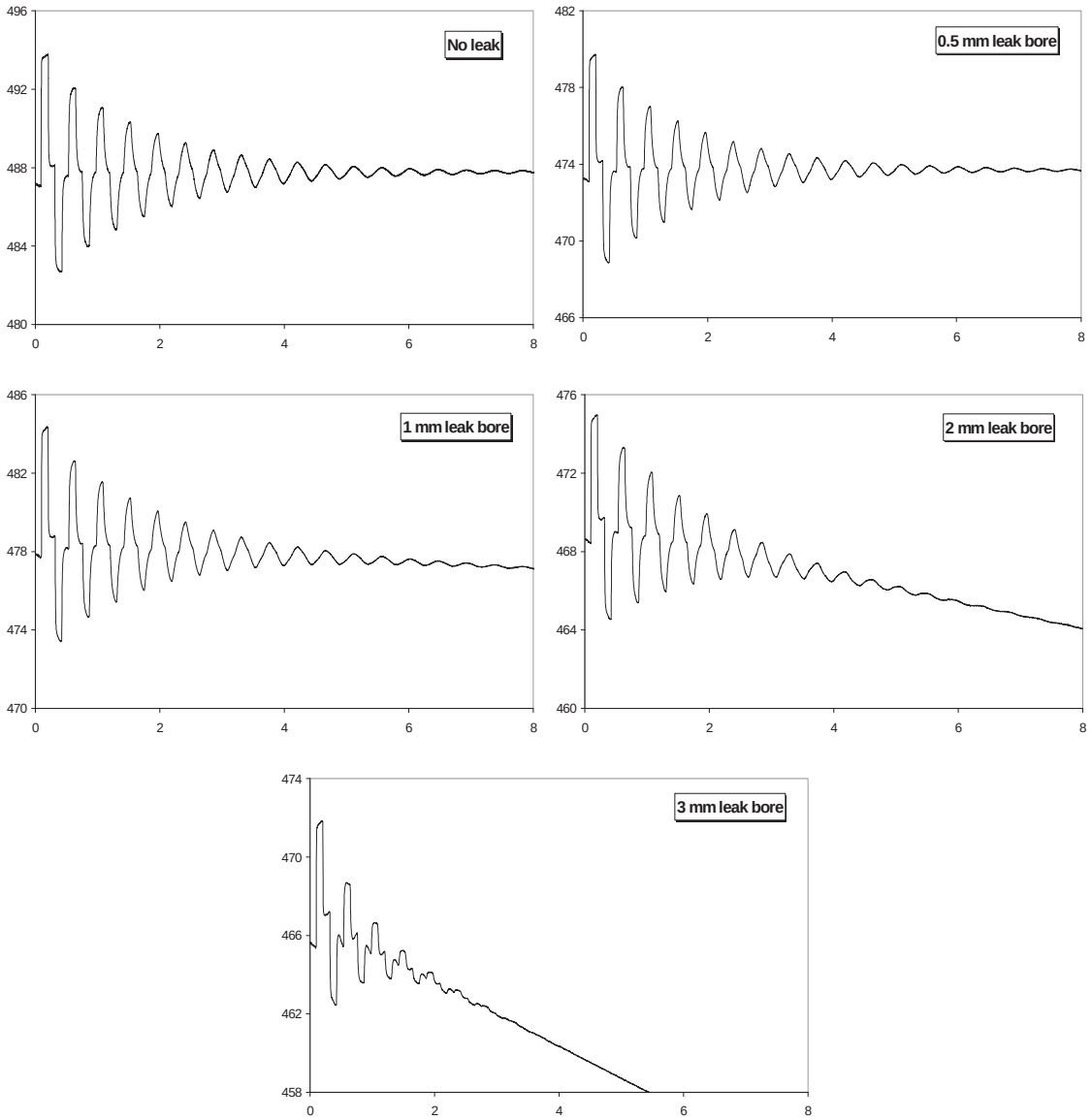

Figure 6.18 Measured Data at the Middle of Pipe for Low Mach Number Flows

(x-axis: measured time (s) and y-axis: pressure (kPa))

Similar to the test results of condition 1 in Figs. 5.21 and 5.22, the measured data for low Mach number gas flows almost have no line-packing effect due to the low Mach number flow by small transient events (maximum pressure change by transients is almost 11 kPa). The fluid can be regarded as slightly compressible flow and the fluid compressibility is not a dominant physical process for low Mach number gas transient analysis. The downward trends in the pressure profiles represent the leak discharge of the system and the inclination of downward trend increases as the leak size grows. Unlike the results of water transients with leaks, the damping effect of pressure waves by a leak for gas flows is not clear. When the pipeline has over 35.6% leak rate, the pressure wave starts damping. In addition,

although the results of water transients with leaks clearly show the change of pressure shape and sudden pressure drop by a leak, there is no change of pressure shape in the measured data of low Mach number gas transients except for the large leak with the 56.9% leak ratio. These insensitive responses of gas transients by leaks may be caused by the less inertial effect of gas flows.

2) Higher Mach Number Flows

Figs. 6.19 and 6.20 show the measured pressure wave at the end and middle of pipeline according to the leak bore sizes in the relatively high Mach number gas transients (*M > 0.1*). The pressure data are plotted at the same scale (the ranges of x-axis and y-axis are 4 seconds and 70 kPa respectively) to compare each pressure variation and pressure wave shape. Table 6.5 shows the flow information for these tests. The temperature is negligible for the variable of transient analysis because the maximum temperature change of whole process is smaller than 1.0^{o}C during transient tests.

Table 6.5 Flow Information for Relatively High Mach Number Flow

Leak Size	Mass Inflow $\dot{m}_{in}$ (kg/s)	Mass Flow By a Leak $\dot{m}_L$ (kg/s)	Mass Outflow $\dot{m}$ (kg/s)	$\dot{m}_L / \dot{m}_{in}$ (%)	Initial Pressure (kPa)	Mach Number
No Leak	$5.179*10^{-2}$	-	$5.179*10^{-2}$	-	211.6	0.149
0.5 mm Leak	$5.085*10^{-2}$	$3.126*10^{-4}$	$5.054*10^{-2}$	0.6	248.6	0.129
1.0 mm Leak	$4.039*10^{-2}$	$1.229*10^{-3}$	$3.916*10^{-2}$	3.1	251.2	0.107
2.0 mm Leak	$4.889*10^{-2}$	$4.332*10^{-3}$	$4.457*10^{-2}$	8.9	200.6	0.136
3.0 mm Leak	$5.243*10^{-2}$	$9.173*10^{-3}$	$4.326*10^{-2}$	17.5	172.1	0.133
4.0 mm Leak	$4.998*10^{-2}$	$1.746*10^{-2}$	$3.252*10^{-2}$	34.9	178.0	0.110
5.0 mm Leak	$5.066*10^{-2}$	$2.616*10^{-2}$	$2.450*10^{-2}$	51.6	140.8	0.104

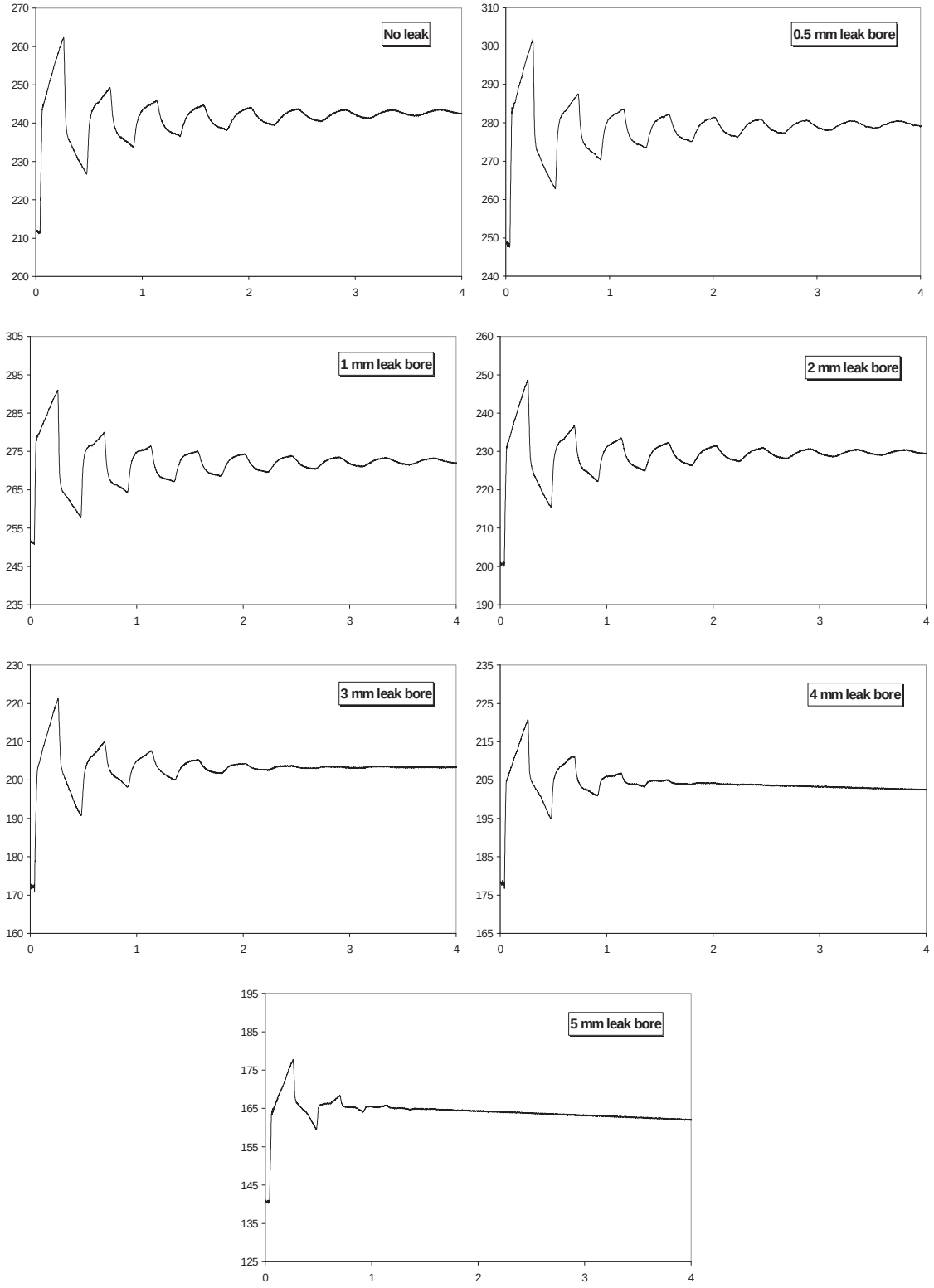

Figure 6.19 Measured Data at the End of Pipe for Relatively High Mach Number Flows (x-axis: measured time (s) and y-axis: pressure (kPa))

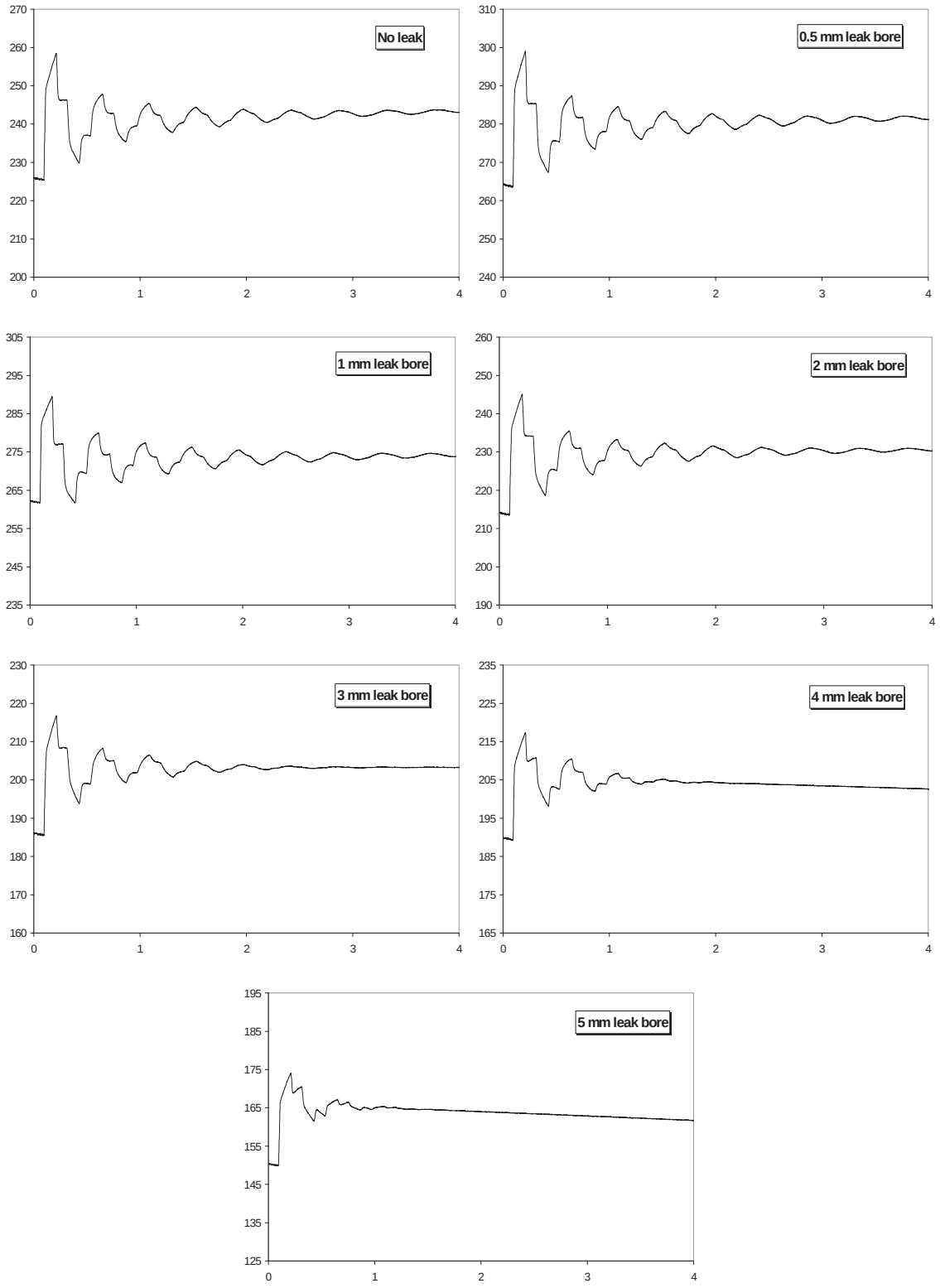

Figure 6.20 Measured Data at the Middle of Pipe for Relatively High Mach Number Flows (x-axis: measured time (s) and y-axis: pressure (kPa))

In the case of the relatively high Mach number gas transients, the situation is much the same with the measured data for low Mach number gas flows, although the line-packing increases as transient event increases. The slightly upward trends of pressure profiles with below 8.9% leak ratio represent the pressure recovery from the large pressure drop as shown in Fig. 5.20 and the downward trends of pressure profiles with above 17.5% leak ratio represent the leak discharge. Similar to the measured data for low Mach number gas flows, the damping effect of pressure wave by a leak is not clear when the pipeline has less than 8.9% leak ratio. The rapid pressure damping starts when the pipeline has over a 17.5% leak ratio. Also, there is no change of pressure shape by a leak.

Fig. 6.21 shows the comparison between measured data with 3 and 4 mm leak bores and simulation results. The polytropic process gas transient analysis model has been used for gas transient analysis with leaks because the temperature change is small during transient events. The polytorpic process exponent, which considers heat exchange of the system, is obtained by comparison between measured data and simulation results. The calibrated polytropic process exponent is 1.18. The lumped leak coefficients C_dA_L for 3 and 4 mm leak bores have been calibrated by using the relationship between the measured pressure of tank with constant volume and leak mass flow rate in the steady-state flow condition. The calibrated lumped leak coefficients for 3 and 4 mm leak bores are $5.014*10^{-6}$ and $9.489*10^{-6}$ respectively. The initial fluid velocities in the pipeline are 47.9 and 37.5 m/s with 3 and 4 mm leak bores respectively. Similar to the results of gas transients for unsteady friction estimation in Chapter 5, the simulation results of models overestimate the line-packing effect, although the model can predict the overall transient traces. These discrepancies may come from the characteristics of gas compressibility. The Mach numbers of flow conditions for gas transient tests with 3 mm and 4 mm leak bores are 0.14 and 0.11 respectively. These values are smaller than that of compressible subsonic flow (Mach number > 0.3) that has complete characteristics (noticeably asymmetrical pressure communication) for compressible flow. The transient gas flows for experiments may still have the property of incompressible flow (nearly symmetrical and instantaneous pressure communication). Therefore, the measured data of tested flows do not show complete storage capacity of a pipeline due to an increase in pressure, especially for the initial pressure rises of transient events. After the third pressure wave cycle, there is good agreement between measured data and simulation results because the effect of line-packing decreases.

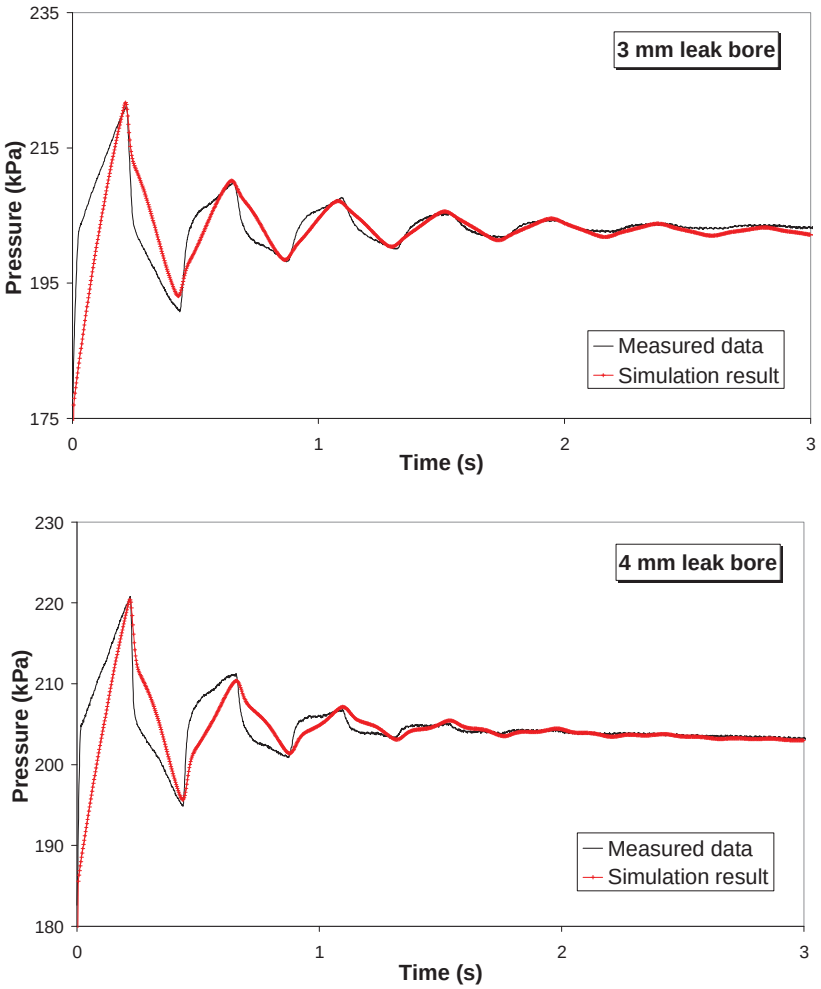

Figure 6.21 Comparison between Measured Data and Simulation Results

6.6 SUMMARY AND CONCLUSIONS

A leak in a pipe has been simulated at nodal points in the grid line of the computational space by a discontinuity in discharge. Leaks have been estimated using an orifice equation for water transients and frictionless adiabatic (reversible adiabatic or isentropic) flow theory has been used to simulate gas inflow and outflow through the leak hole in the transient gas pipeline. Various experimental data and simulation results show the dynamic behaviour of leaks during water and gas transients for various leak locations and sizes. Also, the fully frequency dependent unsteady minor loss models for orifice and axial-extended orifice as introduced in the Chapter 8 can be used for simulating the dynamic behaviour of leaking flow during transient events. The measured data and simulation results show that the shapes of pressure waves are different according to the changes of

leak location and size. Pressure waves affected by leaks, including pressure damping, a change of pressure shape, and the position of sudden pressure drop, provide a potential method for detecting the location and magnitude of the leak.

The leak model for water transients accurately predicts the phase, magnitude and shape of pressure waves of the experimental data. Unlike the measured data of water transients with leaks, the change of pressure wave by a leak has been shown to be small for gas transients. The compressibility of gas diminishes the impact of leaks during transients. Similar to the simulation results of gas transients for the estimation of unsteady friction, the transient model including a leak estimation term overestimates the effect of line-packing because of the characteristic of gas compressibility of low Mach number tested flows, however, the model is able to predict the whole transient trace.

A resonance condition (auto-oscillation or self-excited oscillation) caused by a leak was detected accidentally during one of the leak tests. Excessive pressure fluctuations were measured. Although the pressure wave generated by accidental or normal operation usually attenuates and disappears in the hydraulic system with time, occasionally a pressure wave may be amplified that results in severe pressure and flow oscillations when the frequency of a certain system element matches one of the critical and natural frequencies of the pipeline system. The system element can be regarded as an exciter that develops the pressure amplifications. A typical example of an exciter is a leaking valve or a leaking seal. Resonance is serious physical phenomena because unexpected pressure variation can be destructive in practical hydraulic systems. The measured resonance showed excessive pressure oscillations and the pressure wave oscillations keep on at an almost constant magnitude. This measured data indicates another undesirable situation of a leakage in the pipeline system.

CHAPTER 7

THE EFFECT OF ENTRAPPED AIR POCKETS ON TRANSIENT PIPE FLOWS

This chapter investigates entrapped air pockets that affect the dissipation and dispersion of pressure waves in transient pipe flows. Air pockets can be developed in a liquid pipeline by gas bubble entrainment through the action of pump suction, rapid filling of pipeline, air release during low-pressure transients, cavitation and/or column separation. The presence of the gas cavities has a significant effect on the character of transients in the pipeline. Gas cavities suppress or increase the maximum pressure in the pipe. A gas cavity can be considered as spring or air cushion. A pressure pulse compresses the spring during transients, so even small bubbles greatly decrease the wavespeed and change the amplitude of pressure wave. The existence of entrained air bubbles and the presence of developed air pockets complicate the analysis of the transient flows and make it increasingly difficult to predict the pressure wave phenomena during surge pressures. A mathematical model for simulating the effect of an entrapped air pocket on transient pipe flows can be developed by using an air accumulator (small air chamber) model that yields practical results. Incorporating the mathematical model for an entrapped air pocket into the conservative solution scheme leads to the discrete gas cavity analysis model for single or multiple isolated cavities. Unlike the traditional transient analysis model based on the method of characteristics, this model does not need the wavespeed equation for gas-liquid mixture to initially decide the whole computational domain following the restricted relationship between time and space step because the conservative scheme directly calculates the variation of fluid density and describes the variable wavespeeds and pressure traces of gas-

liquid mixture flows during transient events. The model is effective in treating relatively small gas volumes, for which the gas volume is significantly less than the liquid volume. The discrete gas cavity model is applied to a number of numerical and experimental examples with the pressure dependent wavespeeds and shock waves during transient events. Various experimental data and their simulation results show the dynamic behaviour of entrapped air pocket during transients.

7.1 GAS CAVITY IN LIQUID PIPELINE SYSTEM

Gas accumulations in the liquid pipeline systems are often unintentional and unavoidable situation. Moreover, in most cases gas cavities cannot be quantified and it is difficult to find the exact locations of gas cavities. The control of gas pockets is one of the major problems in pipeline systems used for water supply. Air may be found in water pipelines mainly as stationary pockets or moving bubbles of various sizes. Air pockets can reduce the effective pipe cross section due to the reduction of pipe capacity when air becomes trapped in parts of the pipeline. Sometimes, the water flow is completely blocked by the air. The bulk properties of the fluid with gas cavities are changed, particularly with regard to the density and elasticity of the fluid. The change of fluid properties makes the analysis of systems more complicated. The presence of air changes the structure of flow turbulence and possibly the wall shear and enhances corrosion (especially in sewer systems) by making more oxygen available for the process. In addition, large air pockets can cause vibrations of the structure and surging of the flow because transition from partly full to full flow.

7.1.1 Development of Air Pocket

Air pockets can develop in a pipeline by bubble entrainment at the inflow/outflow location and by gas release as the water pressure reduces. The former can result from poor suction design and operation cycling of pump, which permit excessive drawdown before pump switching or shutdown, vortices at an inlet or intake, and turbulence in shaft. Also, air release valves can contain air if the air discharge is not properly controlled. Lee [1999] presented the air influence on hydraulic transients on fluid system with air valves and Lee and Leow [2001] showed a numerical study on effects of check valve closure flow conditions on pressure surges in pumping station with air entrainment. Air transport with

large pockets of air can occur during filling and emptying of pipelines. Air movement along the pipeline can be slow during filling the pipeline and air column can become trapped adjacent to a closed valve at the end of the pipeline or can separate into two water columns at the high points of an undulating profile in the system. Martin [1976] demonstrated a theoretical model to calculate pressure changes in a single pipe with a trapped air pocket at the end of pipe based on a rigid column of fixed length and polytropic compression and expansion of the entrapped air. Cabrera et al. [1992] indicated the rigid column model could significantly overestimate the pressure rise for certain conditions.

The effects of trapped air on transients in a rapidly filling pipe have been investigated both experimentally and analytically [Zhou et al., 2002 and 2004; Liou and Hunt, 1996]. They showed huge peak pressure surges and severe pressure oscillations by air entrapment, which can damage urban infrastructure. Also, air can be entrained by a leak of pipeline where the pressure is negative [Lauchlan et al., 2005]. In horizontal pipelines or pipes having mild slopes, the liquid flow has a tendency to occupy the lower part of the pipe and the air or vapour move toward the higher elevation in pipelines due to the effects of gravity on fluids with different densities and the buoyancy of gas cavities. The air easily collects at the top of the conduit, pipe cracks, valves, fittings, joints, pipe wall roughness, and forms air pockets.

The evolution of additional gas bubbles from the dissolved gas depends upon the pressure reduction and temperature increase. Most liquids contain dissolved air or gas. Water at atmospheric pressure contains about 2% of saturated air by total volume [Fox, 1977]. A liquid saturated with gas at some relatively high-pressure (above atmospheric pressure) releases dissolved air and gases during a low-pressure process or the passage of negative transient pressure events and the turbulent passage (eddy effect) of water through the coarse wall surface, bends, valves and other pipeline fittings, but the rate at which they can be reabsorbed is so slow that can be ignored in the process. This process is highly time dependent and the volume of the bubbles can be large if the drop in pressure is large. The exact amount of released gas is unknown in most cases. The increase of temperature can also promote air release, as the vapour pressure of water increases with temperature. This can be an important consideration for pipeline design in hot climates or subjected to high thermal variations.

The transient pressure can be reduced to the vapour pressure of a liquid in low-pressure systems and systems having rapid transient events, which produce vapour cavities in the flows. They will continue to grow rapidly and sometimes, cause the liquid column to separate by the vapour cavities occupying the entire cross section of pipe (column separation). If the surrounding pressure of cavities is above vapour pressure, the bubbles become unstable and collapse. The sudden collapse of the cavities may create violent pressure rises, potentially causing severe damage to the pipeline systems with unpleasant secondary effects, such as noise, vibrations, and erosion damage to the system. A number of numerical and experimental studies have been executed for gas release and column separation on transient pipe flows [Simpson and Wylie, 1987 and 1991; Simpson and Bergant, 1994a and 1994b; Bergant and Simpson, 1999; Nakagawa and Takenaka, 1995; Miwa et al., 1989; Mitosek, 2000; Greco, 1990; Bughazem and Anderson, 1996 and 2000] and many hydraulic textbooks about hydraulic pressure surge provide useful numerical and experimental information of cavitation flows [Wylie et al., 1993; Chaudhry, 1987; Almeida and Koelle, 1992; Thorley, 2004; Tullis, 1989; Swaffield and Boldy, 1993; Fox, 1989]. Also, Bergant et al., [2006] presented an extensive literature review about water hammer with column separation. This research focuses on the investigation of the effect of fully developed gas or vapour pocket on transients.

7.1.2 Effect of Entrapped Air on Transients

Transient pipe flow analysis in two-phase (gas-liquid mixture) flows is more complicated than that of single-phase flows (pure liquid transients or water hammer phenomenon) because of the presence of a compressible component such as air or vapour cavities. The effects of entrapped or entrained air on surge pressures in the pipeline systems can be either beneficial or detrimental, with the outcome being entirely dependent on the characteristics of the pipeline, the amount and location of the air, and the nature and cause of the transients. The existence of entrained air bubbles and the presence of developed air pockets complicate the analysis of the transient flows and make it increasingly difficult to predict the pressure wave phenomena on surge pressures.

Air bubbles or pockets in a liquid pipeline system, even in very small volumetric proportions, not only significantly reduce wave propagation velocity (wavespeed), but also cause a major change in the shape and attenuation of the transient pressure waves.

Naturally the influence of air is most significant at low pressurised systems. The sudden and rapid change in fluid velocity when the pipeline has an air pocket creates pressure spikes that are either greater than or less than those that would occur without any air due to the reflection from the boundary surface between the two-phase and single-phase flows. Burrows and Qiu [1995] demonstrated how the presence of air pockets could severely exacerbate surge peaks during pump shut-down in single water pipeline systems. The most severe case occurs during the rapid acceleration of a liquid column toward a volume of air that is completely confined. The peak of surge pressure can be markedly higher than the initial imposed pressure if the transient is generated rapidly, which can cause damage to the pipeline and its fittings, whilst a large air cavity acts as an effective accumulator (air cushion) and suppresses the maximum pressure excursions because of the increase in elasticity of the mixture. Numerical and experimental examples of high pressure surges associated with the presence of entrapped air in pipeline are shown in transient research about single-component and two-component two-phase flows [Wylie et al., 1993; Martin, 1976; Fujii and Akagawa, 1993 and 2000; Akagawa et al., 1982, 1983, and 1986] and Fuertes et al. [1999] and Izquierdo et al. [1999] demonstrated a mathematical model for the assessment of pressure head maximum (peak pressure) in pipelines with entrapped air pockets during transient events.

The presence of very low volumetric proportion of gas or vapour cavity significantly reduces the propagation velocity of a pressure wave (wavespeed) in pipeline systems that is strongly pressure dependent and affects the application of the traditional transient analysis model (the method of characteristics) through the Courant criterion and the slope of the characteristic curves in the x-t plane. A comparison between predicted and measured wavespeeds in a free gas liquid mixture is presented by Swaffield et al. [1978a and 1978b]. The effect of gas cavity is difficult to quantify and the behaviour of gas cavity is very unpredictable, therefore many researchers tend to utilize a combination of wavespeed and sensitivity analysis approach in order to ensure that these effects do not lead to a misleading result. The standard treatment outlined by Wylie [1984] is widely employed to predict the wavespeed of an air-water mixture with isolated small volume of free air. A void fraction, α_v, is used to describe the ratio of volume of gas cavity, $\forall_g$, to the total volume of mixture, $\forall$. For a given mass of gas cavity M_g, α_v is a function of pressure.

$$\alpha_v = \frac{\forall_g}{\forall} \tag{7.1}$$

If the perfect gas law is used and isothermal behaviour for the gas cavity with small void fraction is assumed, the gas cavity obeys the following equation.

$$p_g^* \forall_g = M_g RT \tag{7.2}$$

where p^*_g = absolute partial pressure of gas cavity, R = gas constant, T = absolute temperature, total absolute pressure p^* is absolute partial pressure of gas cavity p^*_g plus absolute vapour pressure p^*_v by Dalton's law. The wavespeed a_m of gas-liquid mixture can be written in the same manner in Eq. 3.36.

$$a_m = \sqrt{\frac{K_m / \rho_m}{1 + (K_m / E)(D/e)}} \quad where\ \rho_m = \rho_g \frac{\forall_g}{\forall} + \rho_l \frac{\forall_l}{\forall} = \rho_g \alpha_v + \rho_l (1 - \alpha_v) \tag{7.3}$$

where ρ_g = density of gas cavity, ρ_l = density of liquid, ρ_m = density of gas-liquid mixture, K_m = the bulk modulus of elasticity of the gas-liquid mixture, and $\forall_l$ = volume of liquid. The mass density of the gas-liquid mixture can be assumed the same as that of the liquid, $\rho_m \approx \rho_l$, because small void fractions are considered.

$$a_m = \sqrt{\frac{K_m / \rho_l}{1 + (K_m / E)(D/e)}} \tag{7.4}$$

The variation of pressure in a pipeline system is defined by the following equation excluding thermodynamic effects.

$$\Delta p = -K_l \frac{\Delta \forall_l}{\forall} = -K_g \frac{\Delta \forall_g}{\forall} = -K_m \frac{\Delta \forall}{\forall} \tag{7.5}$$

Therefore, the bulk modulus of elasticity of gas-liquid mixture is the following equation.

$$K_m = \frac{K_l}{1+\alpha_v\left(\frac{K_l}{K_g}-1\right)} \quad by\ \ \Delta\forall = \Delta\forall_g + \Delta\forall_l \tag{7.6}$$

Eq. 7.6 is rearranged to show the bulk modulus of elasticity of mixture to depend on absolute partial pressure of gas cavity and void fraction without considering the bulk modulus of elasticity of gas cavity by using the definition of the mass of gas cavity per unit volume of mixture $m_g = M_g/\forall$ and isothermal assumption $\Delta p_g^* \forall_g + p_g^* \Delta\forall_g = 0$.

$$K_m = \frac{K_l}{1+\frac{m_g RT}{p_g^*}\left(\frac{K_l}{p_g^*}-1\right)} \quad where \begin{cases} p_g^* \forall_g = M_g RT \Rightarrow \alpha_v = m_g RT / p_g^* \\ p_g^* = -\dfrac{\Delta p_g^*}{\Delta\forall_g/\forall_g} = K_g \end{cases} \tag{7.7}$$

Eq. 7.7 is simplified by $K_l/p_g^* >> 1$ when considering practical transient problems.

$$K_m = \frac{K_l}{1+\frac{m_g RT \cdot K_l}{p_g^{*2}}} \tag{7.8}$$

Therefore, the wavespeed of gas-liquid mixture is

$$a_m = \sqrt{\frac{K_l/\rho_l}{\left\{1+\frac{m_g RT \cdot K_l}{p_g^{*2}}\right\}\cdot\left\{1+\frac{K_l D}{Ee}\cdot\frac{1}{1+\frac{m_g RT \cdot K_l}{p_g^{*2}}}\right\}}} \tag{7.9}$$

Most of standard transient analysis models based on the method of characteristics (MOC) use Eq. 7.9 to obtain the initially constant wavespeed of a system with gas cavities for deciding the whole computational domain. The wavespeed is an important factor with regard to the stability condition of solution (see the Section 3.6 for the detail of MOC). In the MOC, the time step for computational discretisation is limited by stability criteria based on the Courant number that restrict the relationship between time and space step

over the whole computational domain. This limitation causes problems when the MOC is applied to the system with variable wavespeeds.

The volume of a gas cavity must change during transients, thus the wavespeed is variable during transient events. The solution using the initial wavespeed becomes unstable in the method of characteristics because the Courant number changes with location and time. In this case, MOC requires spatial and temporal interpolations or wavespeed adjustment that introduce important attenuation and dispersion errors in the solution. Although there are dynamic equations for the method of characteristics to describe the variable wavespeed of gas-liquid mixture during transients [Wylie, 1984], the characteristic lines are curved, which need other approximations that can also lead to inaccurate results. There are numerous mathematical models to calculate variable wavespeed and dynamic phenomena of the system with gas or vapour cavities. However, each method has limitations and none is universally accepted.

7.2 NUMERICAL MODEL FOR ISOLATED GAS CAVITIES

Numerical modelling of a system containing gas cavities is difficult due to the uncertainty of the size and location of gas cavities. If a cavity is assumed to be collected at computational section, it can be treated as single pocket. Each volume of gas or vapour may be assumed to expand and/or contract according to the polytropic gas process relation under the perfect gas law condition as the pressure changes. Liquid mass conservation is preserved at each cavity by applying a local continuity relationship.

In this research, the effect of single or multiple isolated air pockets on transient pipe flows is calculated by using accumulator (air chamber) boundary condition inside the pipeline as shown in Fig. 7.1. This accumulator model for gas cavities is effective when the gas volume is much less than the liquid volume between sections at standard conditions (see the screw bolt type devices for experiments of air pockets in Fig. 7.11). The air is allowed to expand and contract with varying pressure conditions, but is not allowed to move through the pipeline. Air pocket gets trapped in the wall of an accumulator. The computational process is similar to the general air chamber or accumulator in Wylie et al. [1993]. The pressure at any instant is assumed to be the same throughout the gas volume.

Both frictional effects and the variation of elevation inside the accumulator are neglected in the computational process because of the small air volume.

If the head losses at the junction are neglected, then

$$H_1 = H_2 \tag{7.10}$$

When the flow toward the chamber is considered as positive, the local continuity relationship is

$$Q_1 = Q_2 + Q_3 \tag{7.11}$$

If the air is assumed to enclose at the top of the chamber, the entrapped gas in accumulator is assumed to follow the polytropic process relationship in accordance with the perfect gas law [Wylie et al., 1993].

$$H_A V_a^n = C_A \tag{7.12}$$

where V_a is air volume at the end of the time step, n is the polytropic exponent, H_A is the absolute head equal to the gage plus barometric pressure heads, $H_A = H' - z + H_b$, and C_A is a constant whose value is determined from the initial conditions.

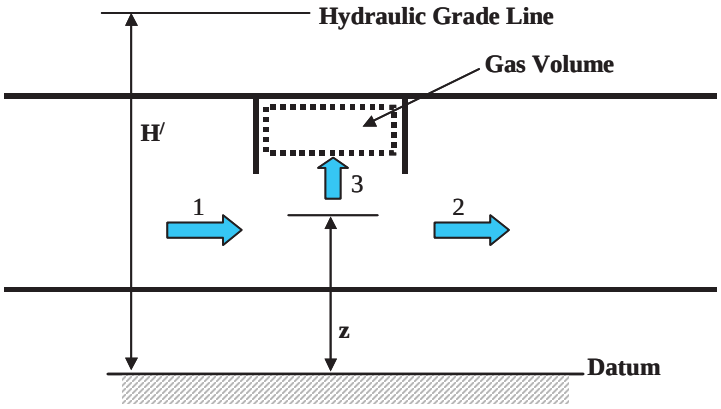

Figure 7.1 Air Chamber for a Gas Pocket

The exponent n depends on the heat exchange process followed by the air volume in the air chamber. Values in the range 1.0 (isothermal) to 1.4 (isentropic or reversible adiabatic) are

normally used for air that follows the perfect gas law. If significant heat exchange occurs or the system has large air volume, the value of polytropic process is close to 1.0. If no heat exchange is expected or the system has small air volume with fast response times, the value is 1.4 and the process can be assumed to be fast transient process. Often an average value of 1.2 is used in design calculations [Wylie et al., 1993; Lee, 1998 and 2000]. This research uses a polytropic exponent of 1.4 for numerical and experimental verifications because gas cavity size is very small and time response is fast in the accumulator on rapid transient events.

Eq. 7.12 can be rewritten by introducing the integrated continuity equation, $dV_a / dt = -Q$. The minus sign indicates that the air volume reduces with positive inflow of fluid into the cavity.

$$\left(H^{/} - z + H_b\right) \cdot \left[V_a^k - \Delta t\left(Q_3^k + Q_3^{k-1}\right)\right]^n = C_A \qquad (7.13)$$

where *k* represents the computational time level. The above equations are incorporated into the conservative solution scheme to estimate the entrapped single or multiple air pockets in transient pipe flows. Unlike the traditional transient analysis model based on the method of characteristics, the conservative scheme is still stable even if the wavespeed changes due to the presence of entrapped air pockets. The wavespeed equation for gas-liquid mixture (Eq. 7.9) is not needed to initially decide the whole computational domain following the restricted relationship between time and space step. The conservative scheme directly calculates the variation of fluid density to describe the variable wavespeeds and pressure traces of gas-liquid mixture flows during transient events.

7.3 NUMERICAL INVESTIGATION FOR ISOLATED GAS CAVITIES

Numerical experiments have been carried out to investigate the dynamic behaviour of transient pipe flows with various air pocket sizes and locations under different initial pressure conditions. The pipeline system shown in Fig. 7.2 has been used for numerical experiments. This system is identical with the laboratory pipeline system presented in Chapter 4. The total inside pipe volume is 1.4396 * 10^{-2} m^3. The pressure of tank 2 is

assumed to be atmospheric pressure during the numerical tests. Therefore, the system is tank-pipeline-valve system.

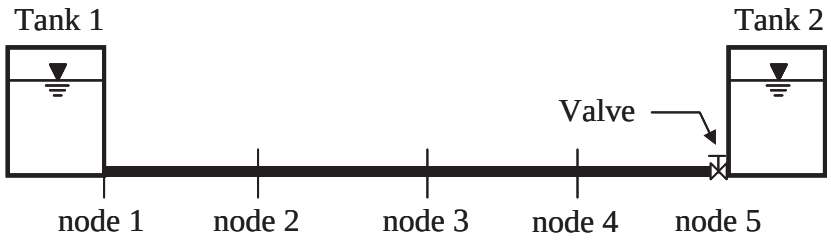

Figure 7.2 Pipeline System for Numerical Experiments

For all numerical investigations for isolated gas cavities, transient events are generated by instantaneous valve closure. Pressure data are observed at the middle of pipe (node 3) and/or the downstream valve (node 5). Table 7.1 shows the air pocket volumes and their void fractions and Table 7.2 shows the initial flows and pressures (at tank 1) used for all numerical tests in this section (pressure variations according to different pressure conditions, single or multiple air pockets, and the change of air pocket size and location).

Table 7.1 Air Pocket Volumes and Void Fractions Used for Numerical Tests

Air Pocket	Air Pocket Volume (m^3)	Void Fraction
No Air Pocket	-	-
Air Pocket #1	$5*10^{-9}$	$3.47*10^{-7}$
Air Pocket #2	$5*10^{-8}$	$3.47*10^{-6}$
Air Pocket #3	$5*10^{-7}$	$3.47*10^{-5}$
Air Pocket #4	$5*10^{-6}$	$3.47*10^{-4}$
Air Pocket #5	$5*10^{-5}$	$3.47*10^{-3}$

Table 7.2 Initial Flows and Pressure (at tank 1) Used for Numerical Tests

System Condition	Velocity (m/s)	Tank Pressure (kPa)
Condition 1 (low pressure)	0.084	186
Condition 2 (high pressure)	0.136	480

Figs. 7.3 and 7.4 show pressure transients at the downstream end (node 5) and at the middle of pipe (node 3) induced by the rapid valve closure at node 5 when the pipeline has various sizes of a single air pocket at the middle of pipeline (node 3) in Fig. 7.2. The condition 2 in Table 7.2 is used for the initial system condition. The relative proportions of

air and water in a pipeline system give rise to different patterns of pressure wave and these patterns are very dependent on the size of air pocket. When the void fraction is less than $3.47*10^{-7}$, the result at node 5 is almost the same as the result of pure liquid transients. From the air pocket #2, pressure waves at node 5 show the shock waves (high frequency spikes with steepening wave front) caused by interaction between water and air. The results at node 5 of air pocket #4 and #5 have excessive pressure spikes and wavespeeds are significantly reduced by air pockets.

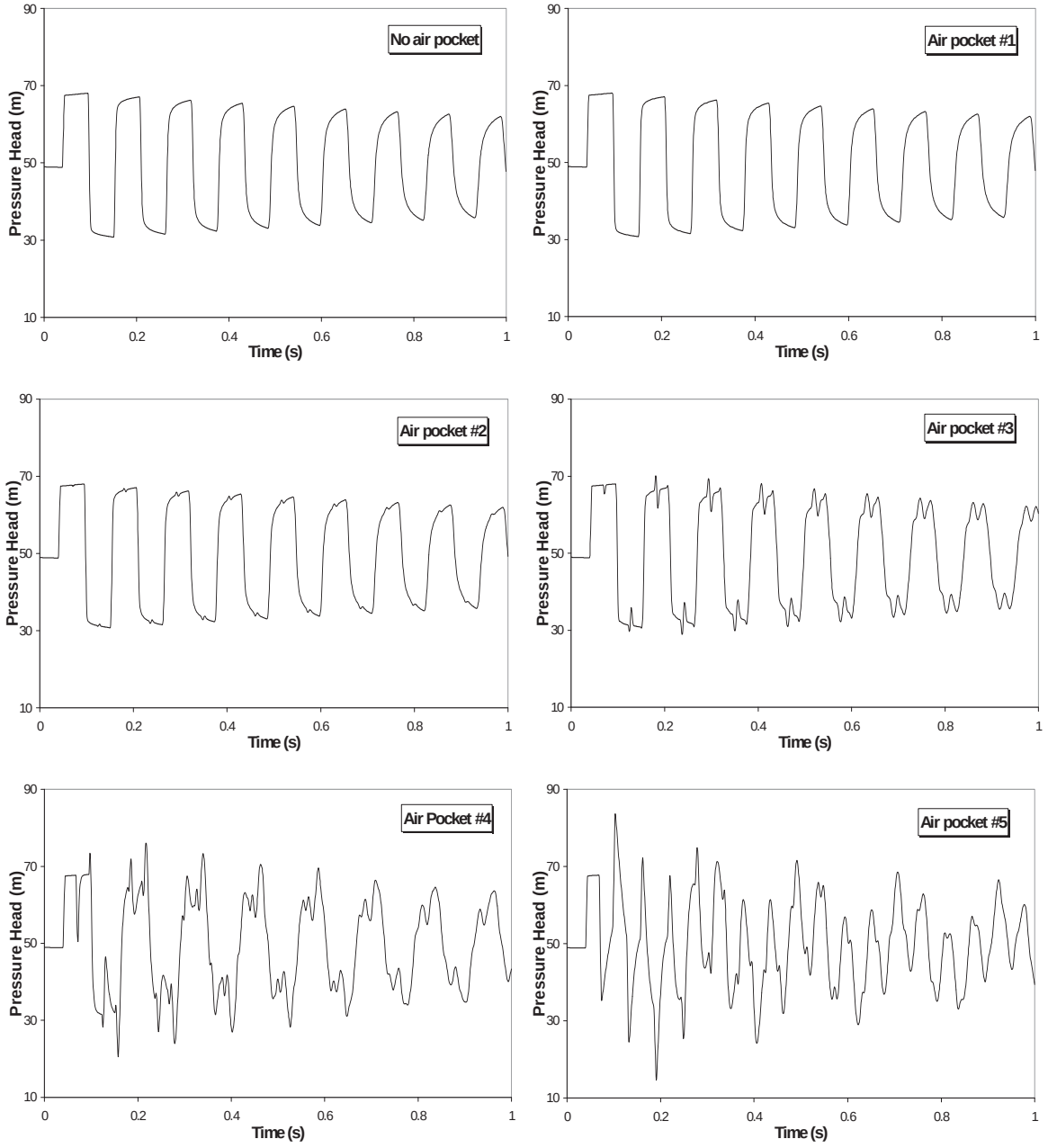

Figure 7.3 Pressure Waves at Node 5
according to the Change of Air Pocket Size Located at Node 3

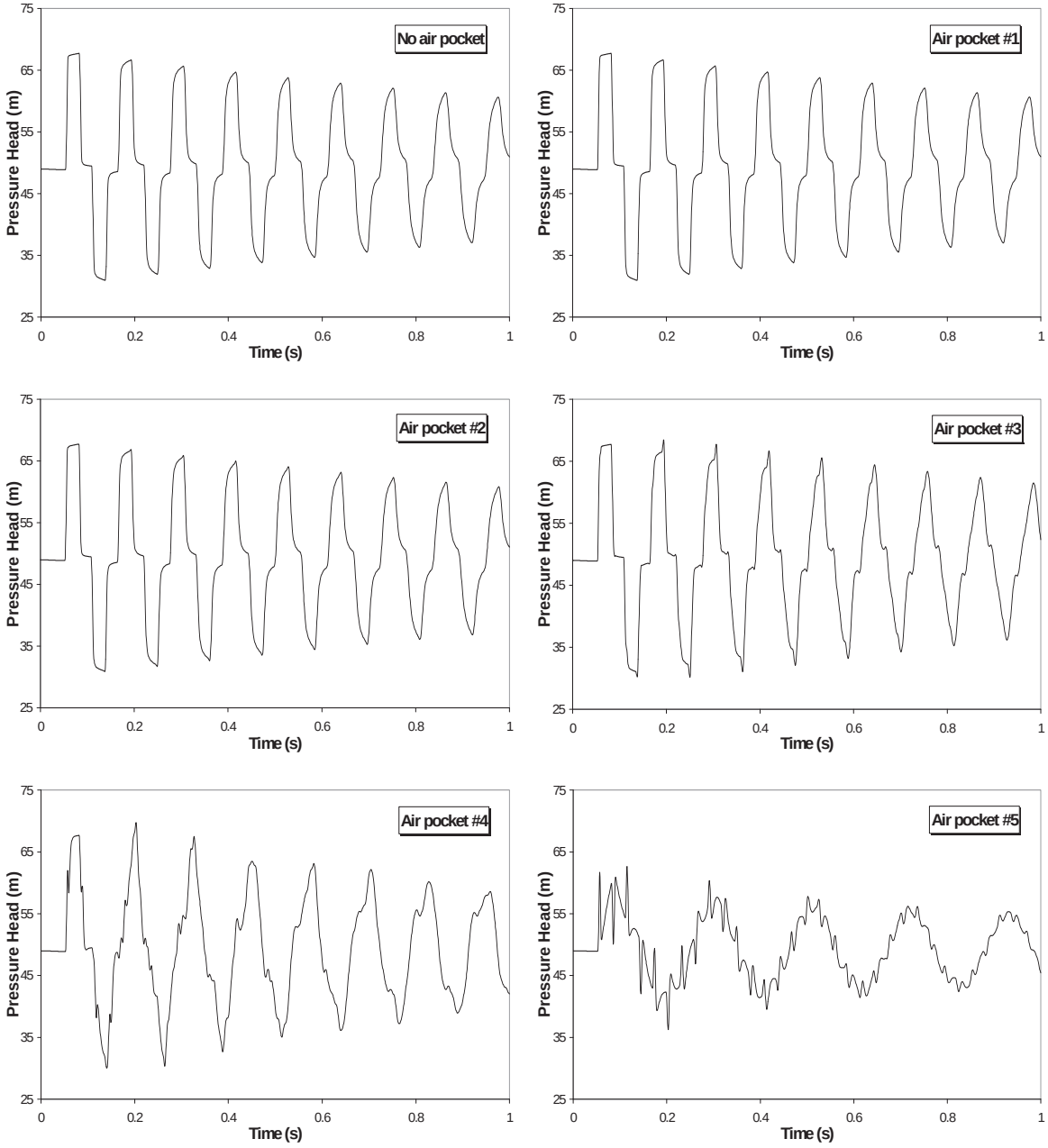

Figure 7.4 Pressure Waves at Node 3
according to the Change of Air Pocket Size Located at Node 3

The results of air pocket #1, #2, and #3 in Fig. 7.4 are similar to the results when the pipeline has no air pocket. However, the results at node 3 with air pocket #4 and #5 show the significant reduction of wave propagation speeds. In particular, the pressure wave at node 3 with air pocket #5 shows large pressure damping by air pocket #5. The effects of entrapped or entrained air on surge pressures in the pipeline systems can be either

beneficial or detrimental. The outcome is entirely dependent on the characteristics of the pipeline, the amount and location of the air, and the nature and cause of the transients.

In hydraulic transients, generally, the presence of large air pockets results in pressure waves that are strongly damped and deformed. However, the numerical results indicate that small accumulations of air have an effect on pressure transients that actually enhance the maximum and minimum peak pressures by high frequency pressure spikes. The propagation velocity decreases when the pipeline has air pockets. Fig. 7.5 shows the wavespeeds of the above numerical experiments. These wavespeeds are compared with the values at around 1 second because the wavespeed is continually changing as simulation time goes on. When the void fraction is larger than $3.47*10^{-4}$ (air pocket #4), air pocket significantly reduces the propagation velocity of a pressure wave in the pipeline system.

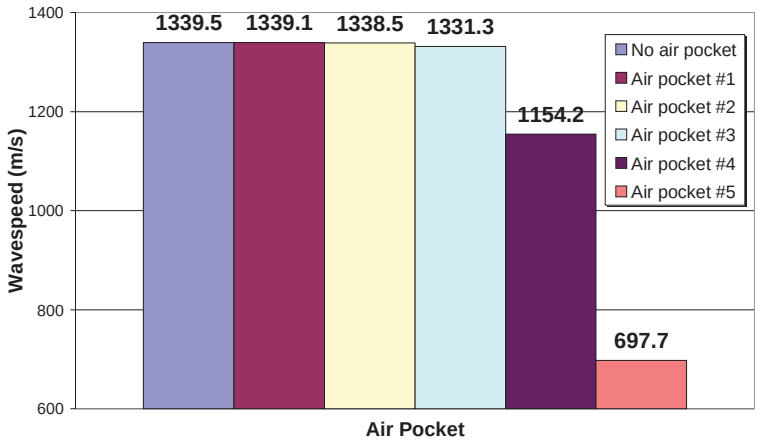

Figure 7.5 Wavespeeds according to the Change of Air Pocket Size

Fig. 7.6 shows pressure waves at the downstream end (node 5) according to the change of the location of air pocket #4. The condition 2 in Table 7.2 is used for the initial system condition. The high frequency narrow spike of the first pressure rise, which is caused by sudden pressure drop when the pressure wave meets air pocket, may be used to indicate the location of the air pocket. When the air pocket is located at the end of pipeline (node 5, near the valve for transient generation), the first pressure rise has a continuous pressure oscillation because of the interaction between air pocket and dead-end after closure of the valve. Fig. 7.6 shows that the location of air pocket has a great effect on the pressure waves, despite the size of air pocket being the same. The shapes of the pressure waves observed at the downstream end (node 5) are remarkably different when the air pocket is

located in the valve used for transient generation. The interaction of pressure wave between air pocket and closed valve produces high frequency oscillations as shown in Fig. 7.6.

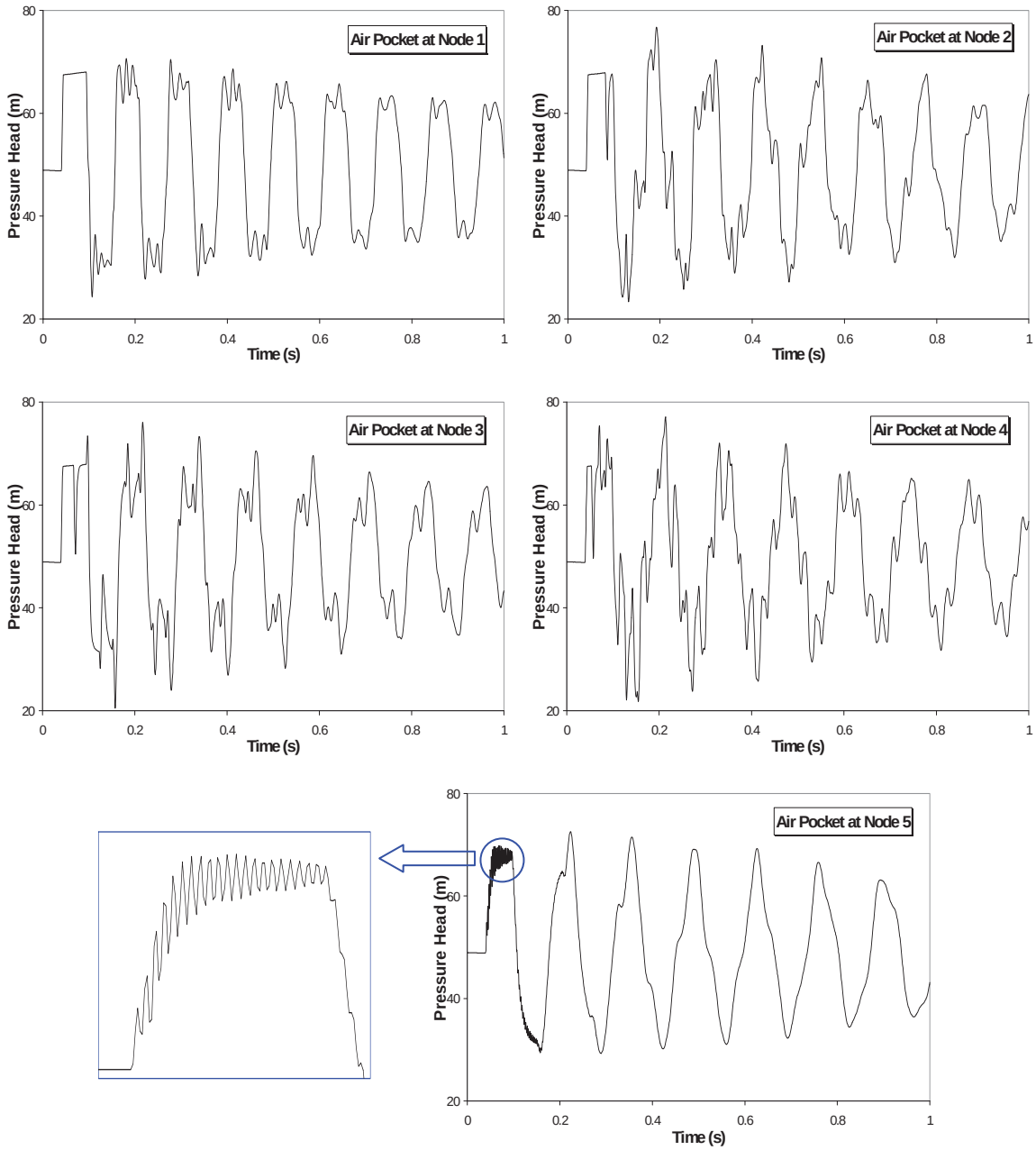

Figure 7.6 Pressure Waves at Node 5 according to the Change of Air Pocket Location

Fig. 7.7 shows the results of numerical experiments according to different initial pressure conditions (high and low initial pressure conditions) as shown in Table 7.2 when the pipeline system has air pocket of $2.5*10^{-6}$ m^3 at the middle of pipeline (node 3). Pressure waves are measured at the end of pipeline (node 5). The effect of an air pocket on

transients is less when the initial pressure condition is high. Naturally, the initial size of air pocket is more contracted by a higher initial pressure condition, therefore the actual size of air pocket in the high pressure condition is smaller than that in the low pressure condition. As a result, the pressure wave under the low pressure condition is more deformed by relatively large air volume.

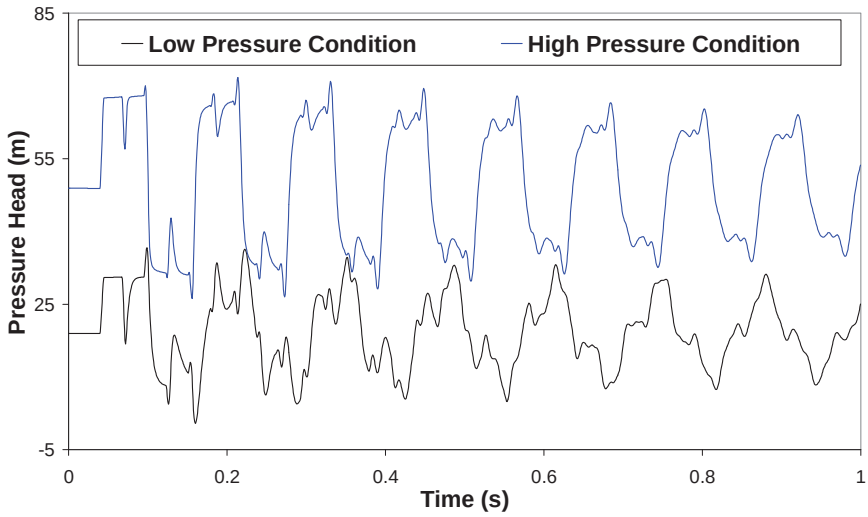

Figure 7.7 Pressure Waves at Node 5 according to Different Pressure Conditions

Fig. 7.8 shows the comparison results when the pipeline has air pocket of $2.5*10^{-6}$ m^3 at only node 3 and at both node 2 and 4. Pressure waves are measured at the end of pipeline (node 5). The high frequency narrow spikes of first pressure rise may be used to indicate the location of the air pockets. Although the result of multiple air pockets has bigger pressure spikes until approximately 0.4 seconds, it shows a larger damping effect of the magnitude of the pressure wave as the simulation time goes on. Also, the comparison of two results clearly shows the difference of shapes of pressure wave affected by air pockets. The wavespeed of a pipeline with multiple air pockets is much slower than that of single air pocket because the total air volume of multiple air pockets is double of that of the single air pocket.

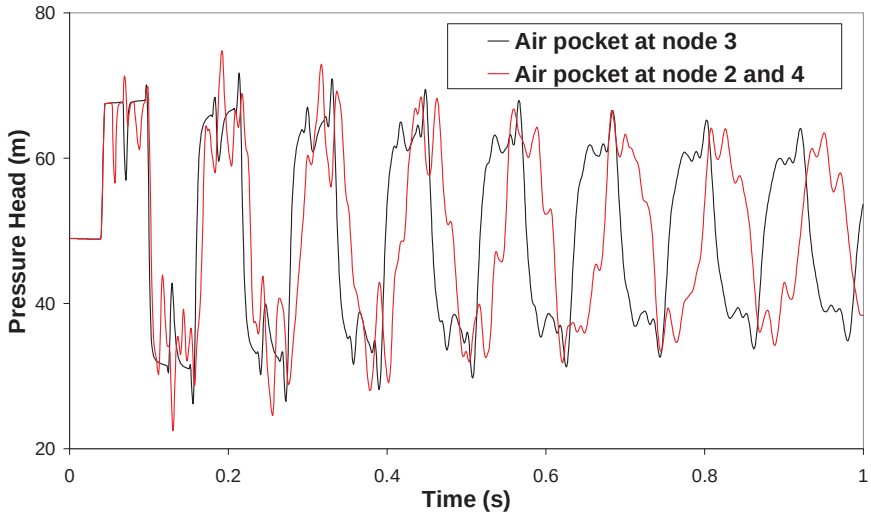

Figure 7.8 Pressure Waves (at Node 5) with Single and Multiple Air Pockets

Fig. 7.9 shows the comparison of results when the pipeline has air pocket of $5.0*10^{-6}$ m^3 at only node 3 and when the volume of the air pocket ($5.0*10^{-6}$ m^3) is equally divided at 5, 10, and 40 nodes respectively through the pipeline. Pressure waves are measured at the end of pipeline. Table 7.3 shows the test conditions.

Table 7.3 Test Conditions for Distributed Multiple Air Pockets

Test Condition	Location of Air Pockets	Individual Air Pocket Volume (m^3)
Single Pocket	At the middle of pipe	$5.0*10^{-6}$
5 Pockets	Equally distributed at 5 nodes	$1.0*10^{-6}$
10 Pockets	Equally distributed at 10 nodes	$0.5*10^{-6}$
40 Pockets	Equally distributed at 40 nodes	$1.282*10^{-7}$

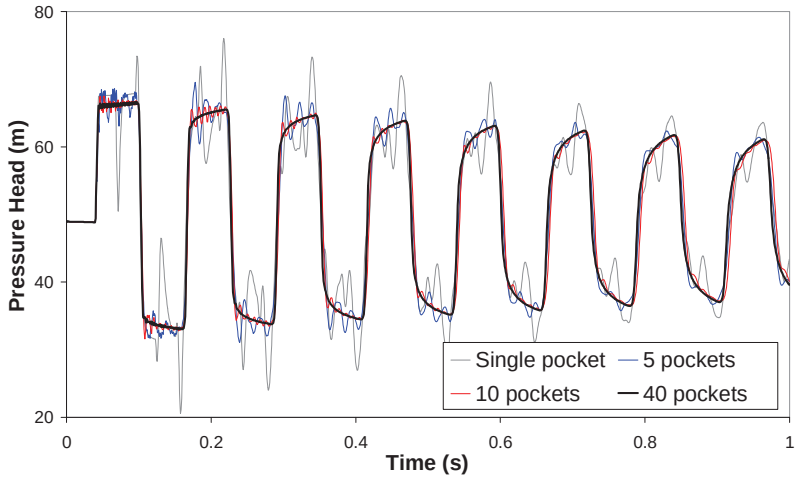

Figure 7.9 Effect of Distributed Multiple Air Pockets (results during 1 second)

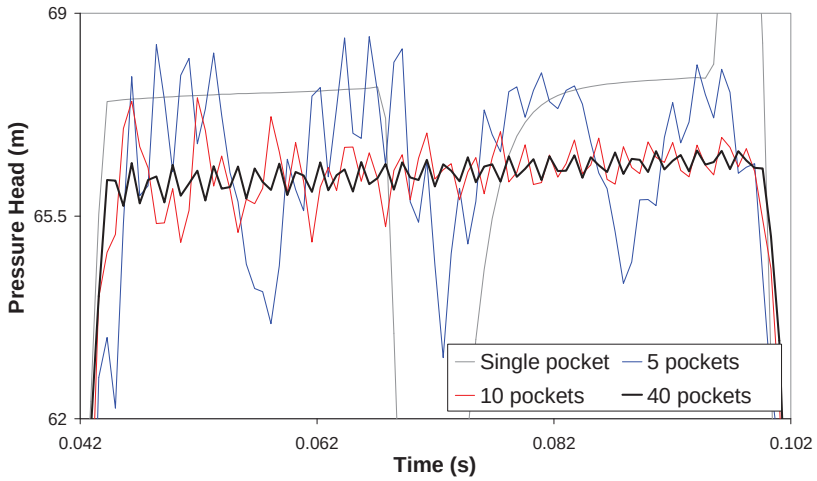

Figure 7.9 Effect of Distributed Multiple Air Pockets (continued)
(details of the first pressure rise)

The test results of 4 different conditions have the same wavespeed because all test conditions have same void fraction. The locations of air pockets are reflected in the first pressure rise of simulated results as shown in the second graph of Fig. 7.9. Although the results clearly indicate the locations of air pockets when the pipeline has single pocket or 5 air pockets, it is difficult to discriminate the locations of air pockets when the air pocket of $5.0*10^{-6}$ m^3 are equally distributed at 10 or 40 nodes because there are so many interactions by air pockets during the transient event. Another important physical phenomenon of distributed air pockets is the pattern of pressure damping. The large single pocket gives rise to strong pressure spikes during transients, but the distributed air pockets appear to soften the pressure spikes. Finally, the results of 40 air pockets in the first graph of Fig 7.9 shows that the shape of pressure wave is similar to the results without an air pocket with the exception of the speed of pressure propagation. This flow can be regarded as a homogenously mixed bubbly flow.

7.4 EXPERIMENTAL SYSTEM AND TEST PROCEDURE

Laboratory experiments have been undertaken for the verification of proposed air pocket model and investigation of real physical phenomena of entrapped air pockets during transients. The experiments provide special cases of localized air cavities at one position in a sloping pipeline. The experimental apparatus is described in Chapter 4. The layout of the pipeline system is repeated in Fig. 7.10.

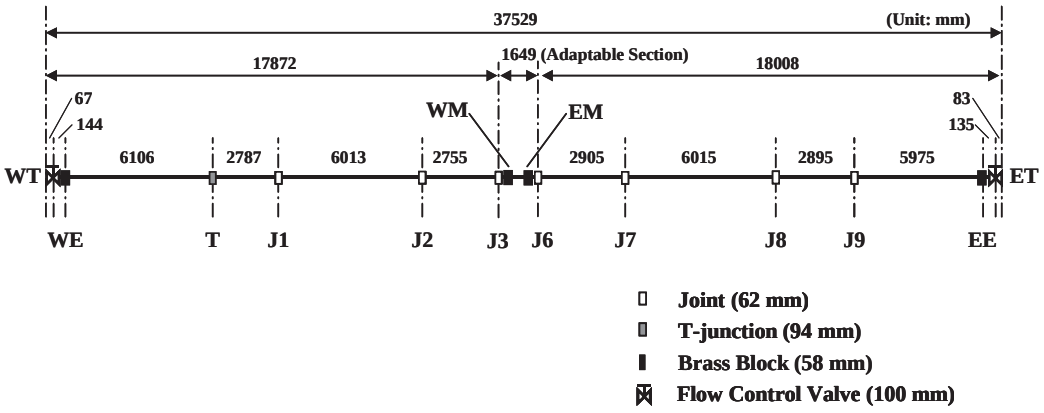

Figure 7.10 Pipeline System Layout

Transient events are generated by fast closing solenoid valve at the WE. The pipeline system is regarded as a tank-pipe-valve system. Water and surrounding temperature are 21 and 22^{o}C respectively. The sampling frequency of measured data is 4 kHz. Tests were undertaken under the specified 6 different flow conditions shown in Table 7.4 used for previous chapters. The initial velocities are adjusted by the pressure conditions of the boundary tank pressurised by an air compressor. These flow conditions range from laminar flow to low Reynolds number turbulent flow.

Table 7.4 Test Conditions

Test Condition	Tank Pressure at ET (kPa)	Initial Velocity (m/s)	Reynolds Number
Condition 1	117.6	0.0599	1338
Condition 2	200.0	0.0824	1827
Condition 3	297.2	0.1031	2307
Condition 4	397.4	0.1208	2672
Condition 5	502.2	0.1368	3000
Condition 6	612.1	0.1495	3326

Fig. 7.11 (a) shows three screw bolt type devices for air pockets with relatively small air volumes. The screw bolts have a hole drilled in the middle. These devices can be inserted into brass blocks of laboratory pipeline system as shown in Fig. 7.11 (c) and (d). Therefore, these screw bolt type devices for air pockets can be regarded point-boundary condition without computational length. The right side of Fig. 7.11 (b) shows an air pocket device for a relatively large air volume. Table 7.5 shows the specification of air pocket devices. An air pocket device with the smallest cavity volume is denoted by air pocket #1.

The cavity volumes of air pocket devices can be measured by using the diameter and depth of holes or by using 1.25 mL micro centrifuge tube with a conical bottom.

Table 7.5 Specification of Air Pocket Devices

Air Pocket	The Volume of Air Pocket (mL)	Void Fraction
Air pocket #1	0.043	$2.99*10^{-6}$
Air pocket #2	0.120	$8.34*10^{-6}$
Air pocket #3	0.393	$2.73*10^{-5}$
Air pocket #4	4.800	$3.33*10^{-4}$

(a) Air Pocket Devices with Small Air Volumes

(b) Air Pocket Devices with Large Air Volumes

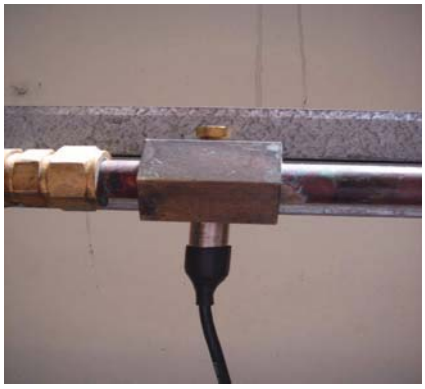

(c) Brass Block with an Air Pocket Device

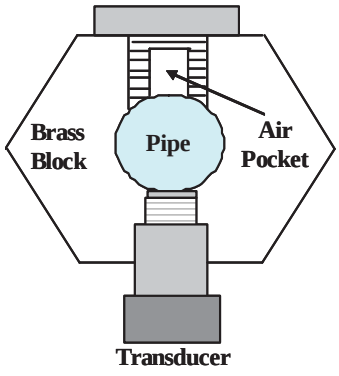

(d) Layout of Brass Block with an Air Pocket Device

Figure 7.11 Air Pocket Devices

The procedure for the experimental tests for investigating the effect of air pockets in transient pipe flows is important because we have to remove any residual air of pipeline before the transient tests. Even a very small volume of air can change the phase and shape of surge pressure wave. All tests were executed by closing the flow control valve near the west tank, therefore the pipeline system for air pocket tests can be regarded as tank (east

tank) – pipe – valve (solenoid valve installed near the west tank) system. The procedure below is the method of controlling any residual air problems and venting of the entrapped air in the laboratory pipeline system as shown in Fig. 7.10.

1. Fill the pipeline slowly from a slightly pressurised east tank to the end of the pipe (near the west tank) after closing the flow control valve near the west tank (the most important procedure).
2. Open the solenoid valve (functions as an air valve) during pipeline filling. After opening the solenoid valve, the valve makes some 'hissing sound' noises because of the release of trapped air through the solenoid valve at the end of pipeline.
3. Check the sound of the solenoid. If the pipeline is fully filled by water, the noise dies away and the solenoid valve discharges water.
4. Close the solenoid valve when the solenoid valve discharges water.
5. Flush the pipeline system after opening the flow control valve near the west tank at moderate velocities and low pressure to remove the additional air that is attached at the valve, joints, pipe, or connection.
6. Open the screw type plug at the brass block to install air pocket device after closing the flow control valve near the west tank and at the very low pressure condition of east tank. There is a very low water discharge through the plug hole of the brass block.
7. Install the air pocket device carefully. The volume of hole of air pocket device is air pocket volume for tests at the atmospheric pressure.
8. Pressurise east tank to obtain proper test condition.
9. Open the solenoid valve. The pipeline has steady state flow (initial flow condition).
10. Fast closure of the solenoid valve. The pipeline has a pressure surge due to rapid flow change.

7.5 MEASURED TRANSIENT DATA WITH AIR POCKETS

This section shows various experimental data with dynamic behaviour of an entrapped air pocket during transients. Figs. 7.13 to 24 show the measured transient data at the end of pipeline (WE) and middle of pipeline (WM) under the various test conditions (shown in Table 7.4) when the pipeline has various air pockets (shown in Table 7.5) at the middle of

the pipeline (EM). The pressure data with various air pockets are plotted on the same scale graphs to compare the pressure variation, wavespeed, and pressure wave shape during the test conditions (except for the air pocket #4 in test condition 1 and 2). Table 7.6 shows the wavespeeds of measured pressure waves. These wavespeeds were obtained from the measured data of the end of pipeline at around 1 second because the wavespeed continually changes as time goes on. The propagation velocities definitely decrease when the pipeline has air pockets. When the pipeline has air pocket #4, the air pocket significantly reduces the propagation velocity of a pressure wave in pipeline systems. The wavespeed under test condition 1 and with air pocket #4 is almost half when compared to the wavespeed for the pipeline system without an air pocket.

Table 7.6 Measured Wavespeeds in Experimental Pipeline

	Test condition 1	**Test condition 2**	**Test condition 3**	**Test condition 4**	**Test condition 5**	**Test condition 6**
No air pocket	1334.4	1331.4	1334.4	1331.4	1331.4	1334.4
Air pocket #1	1316.8	1322.6	1331.4	1331.4	1328.4	1332.8
Air pocket #2	1288.6	1308.6	1328.4	1331.4	1328.4	1331.4
Air pocket #3	1245.8	1302.2	1313.9	1327.6	1327.6	1328.4
Air pocket #4	703.1	977.9	1062.7	1170.5	1215.5	1240.6

Fig. 7.12 shows the comparison of wavespeeds according to the sizes of air pockets and flow conditions. The wavespeed of the system is slower at low pressurised systems because the initial size of air pocket in the low pressure condition is larger than that in the high pressure condition.

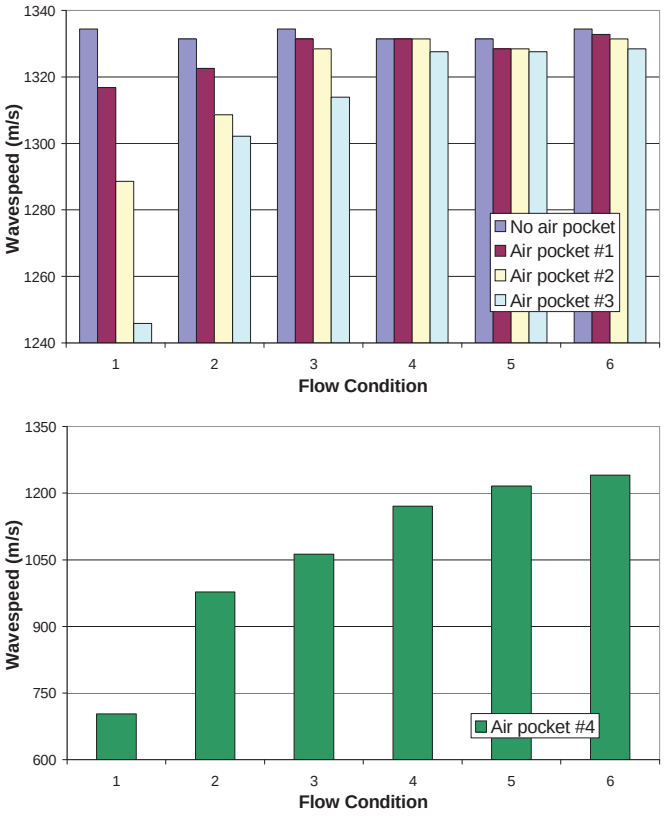

Figure 7.12 Comparison of Measured Wavespeeds According to Air Pocket Size and Flow Condition

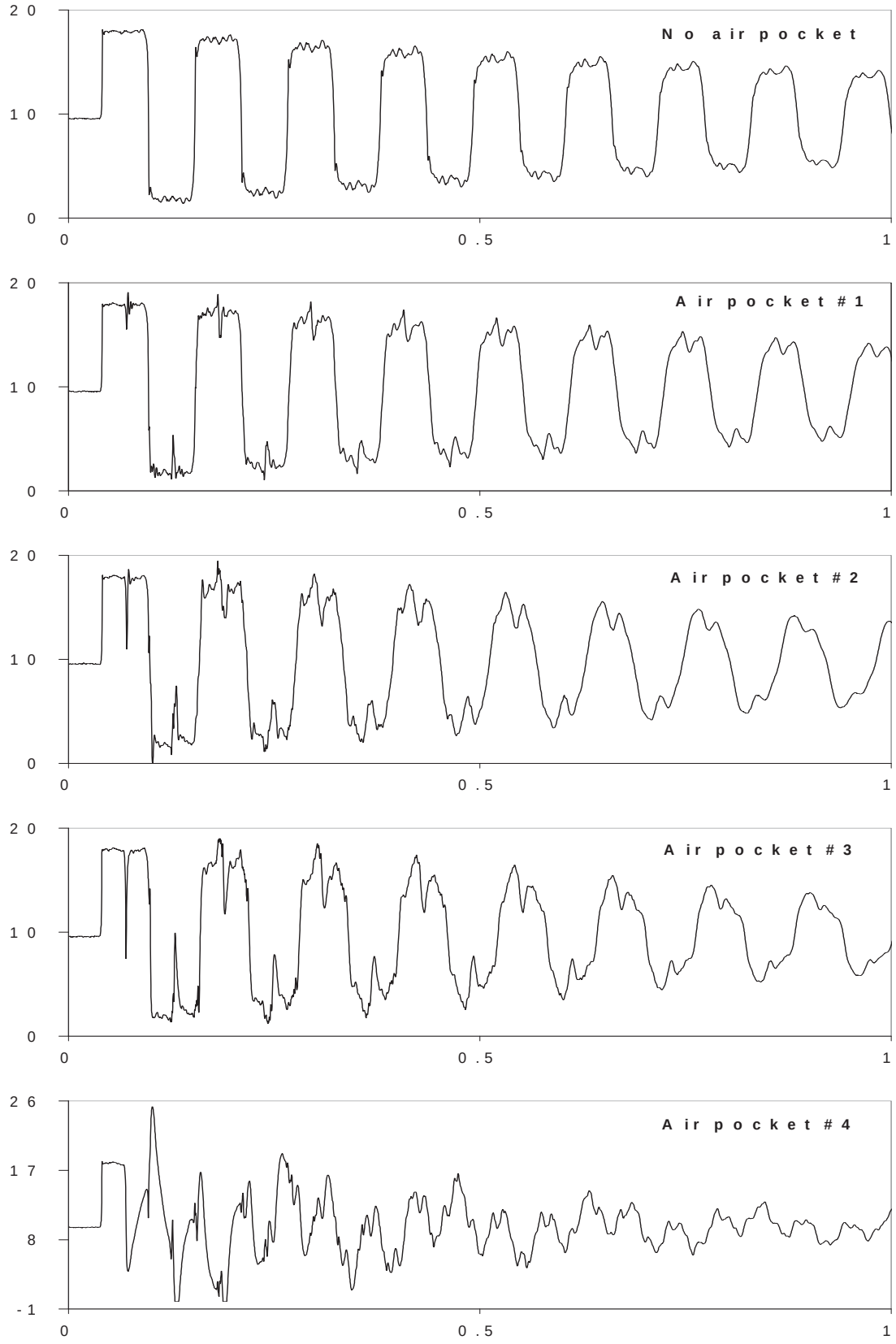

Figure 7.13 Measured Data at the End of Pipeline (WE) during Flow Condition 1 (Air pocket is located the middle of pipeline (EM) and initial velocity is 0.0599 m/s)

(x-axis: measured time (s) and y-axis: pressure head (m))

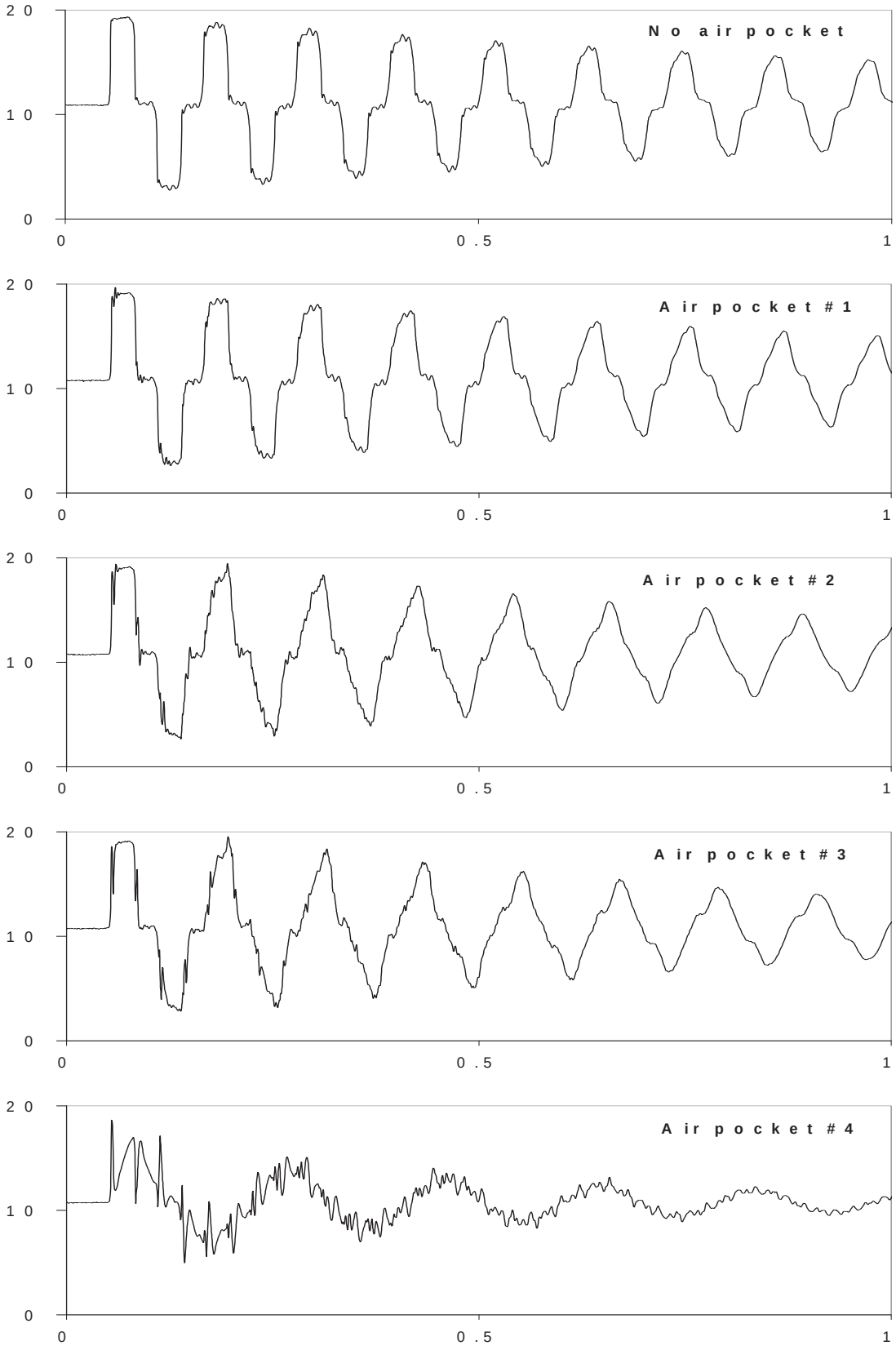

Figure 7.14 Measured Data at the Middle of Pipeline (WM) during Flow Condition 1 (Air pocket is located the middle of pipeline (EM) and initial velocity is 0.0599 m/s)

(x-axis: measured time (s) and y-axis: pressure head (m))

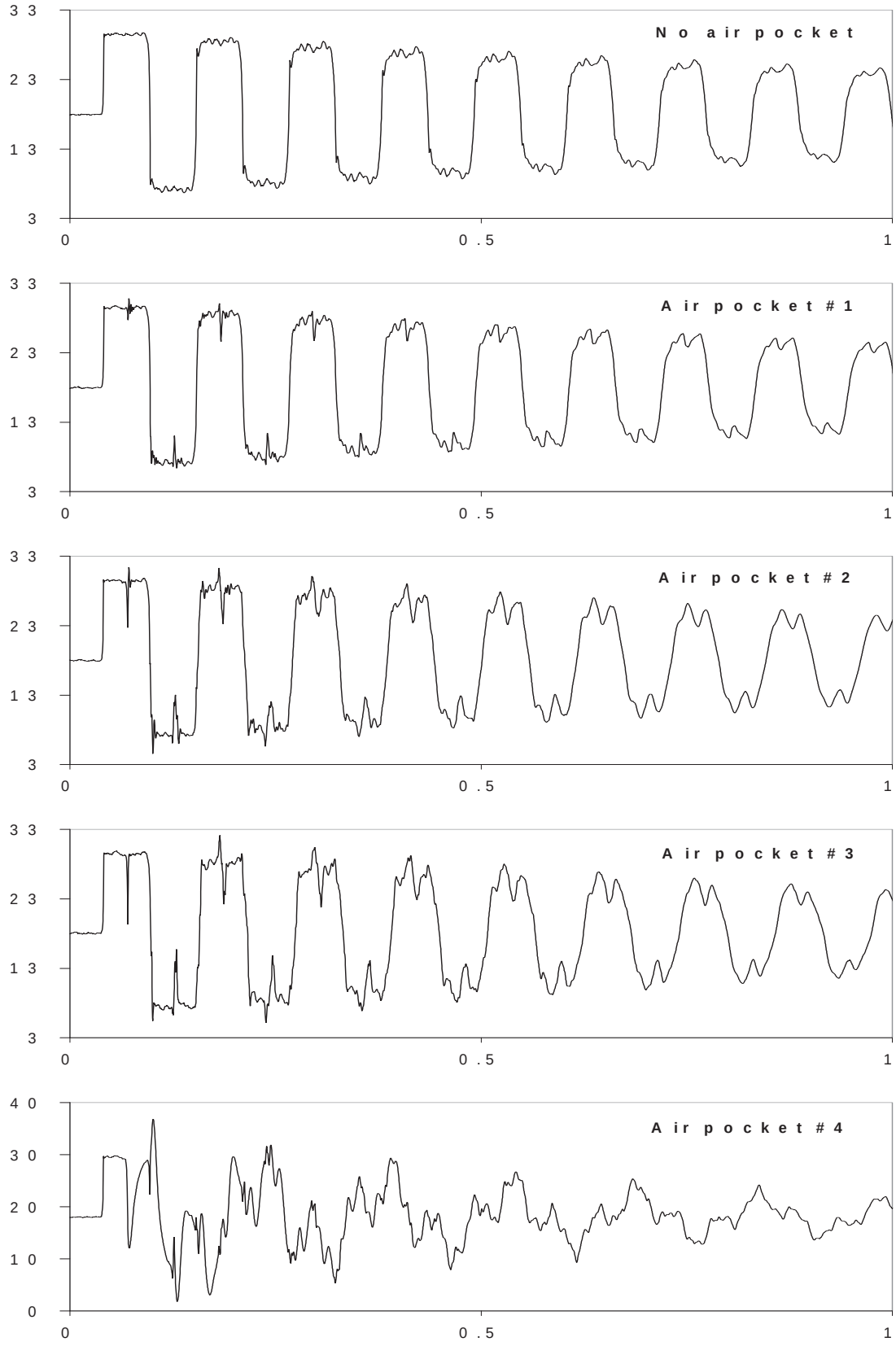

Figure 7.15 Measured Data at the End of Pipeline (WE) during Flow Condition 2 (Air pocket is located the middle of pipeline (EM) and initial velocity is 0.0824 m/s)

(x-axis: measured time (s) and y-axis: pressure head (m))

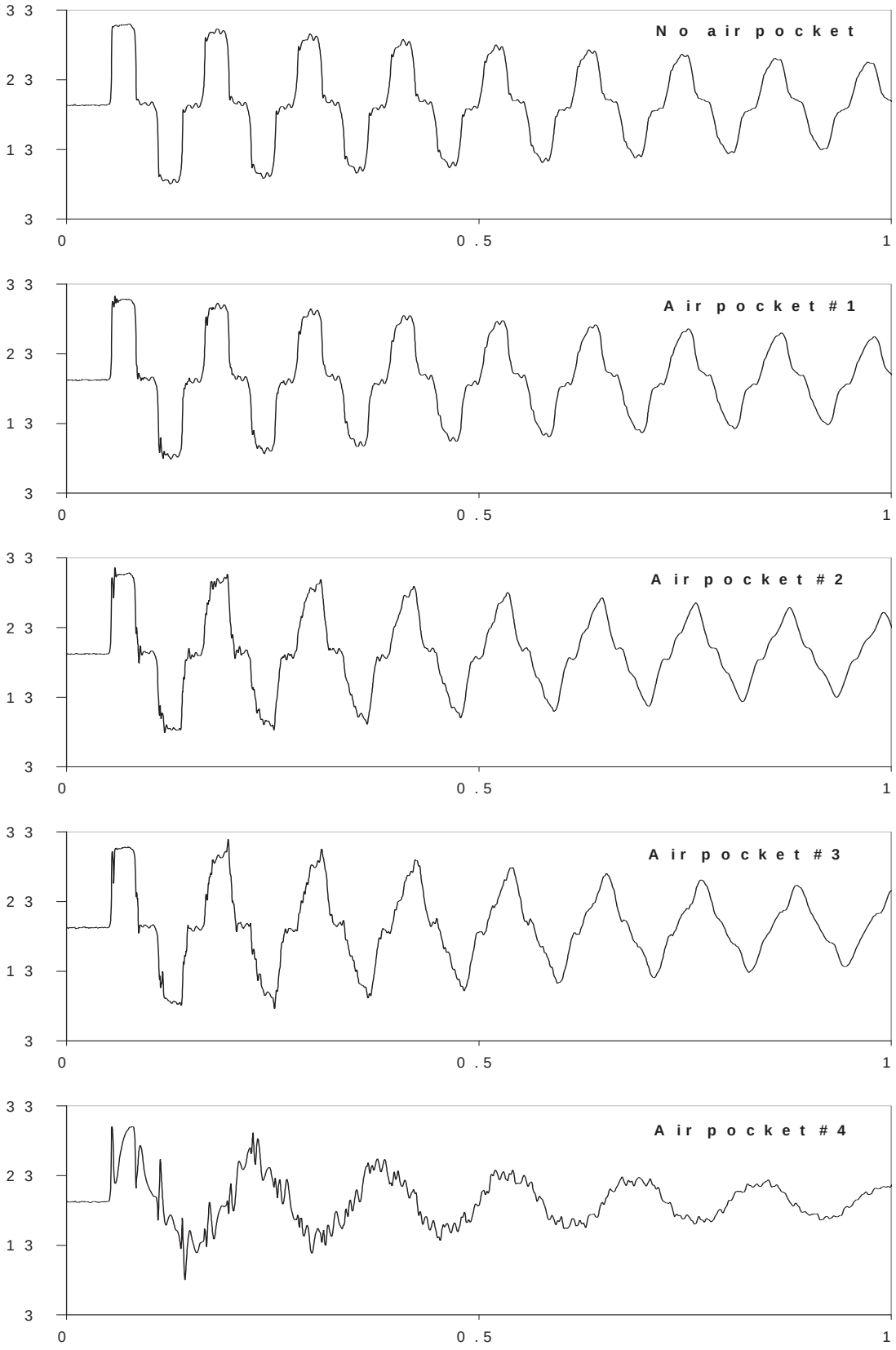

Figure 7.16 Measured Data at the Middle of Pipeline (WM) during Flow Condition 2 (Air pocket is located the middle of pipeline (EM) and initial velocity is 0.0824 m/s)

(x-axis: measured time (s) and y-axis: pressure head (m))

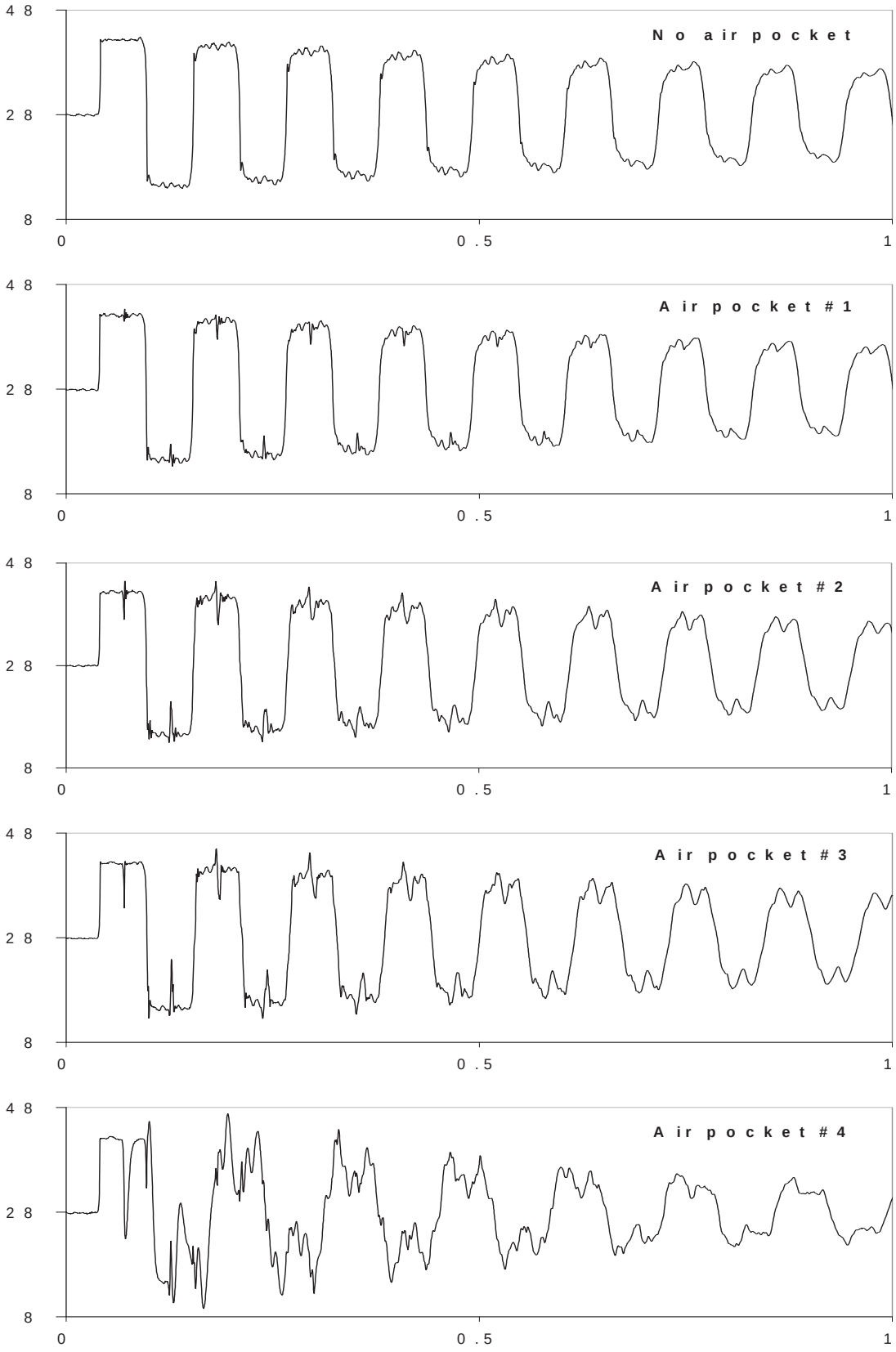

Figure 7.17 Measured Data at the End of Pipeline (WE) during Flow Condition 3 (Air pocket is located the middle of pipeline (EM) and initial velocity is 0.1031 m/s)

(x-axis: measured time (s) and y-axis: pressure head (m))

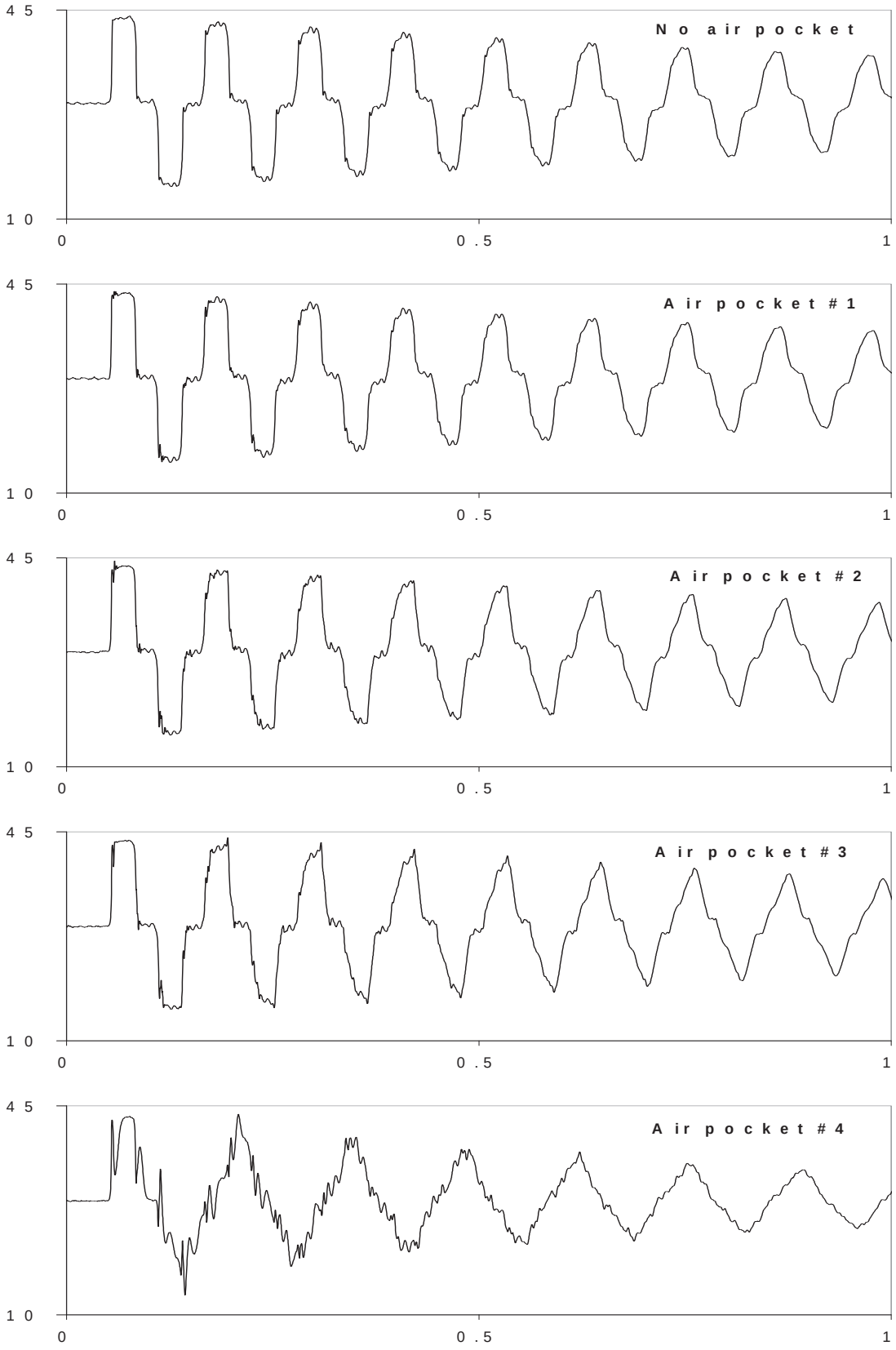

Figure 7.18 Measured Data at the Middle of Pipeline (WM) during Flow Condition 3 (Air pocket is located the middle of pipeline (EM) and initial velocity is 0.1031 m/s)

(x-axis: measured time (s) and y-axis: pressure head (m))

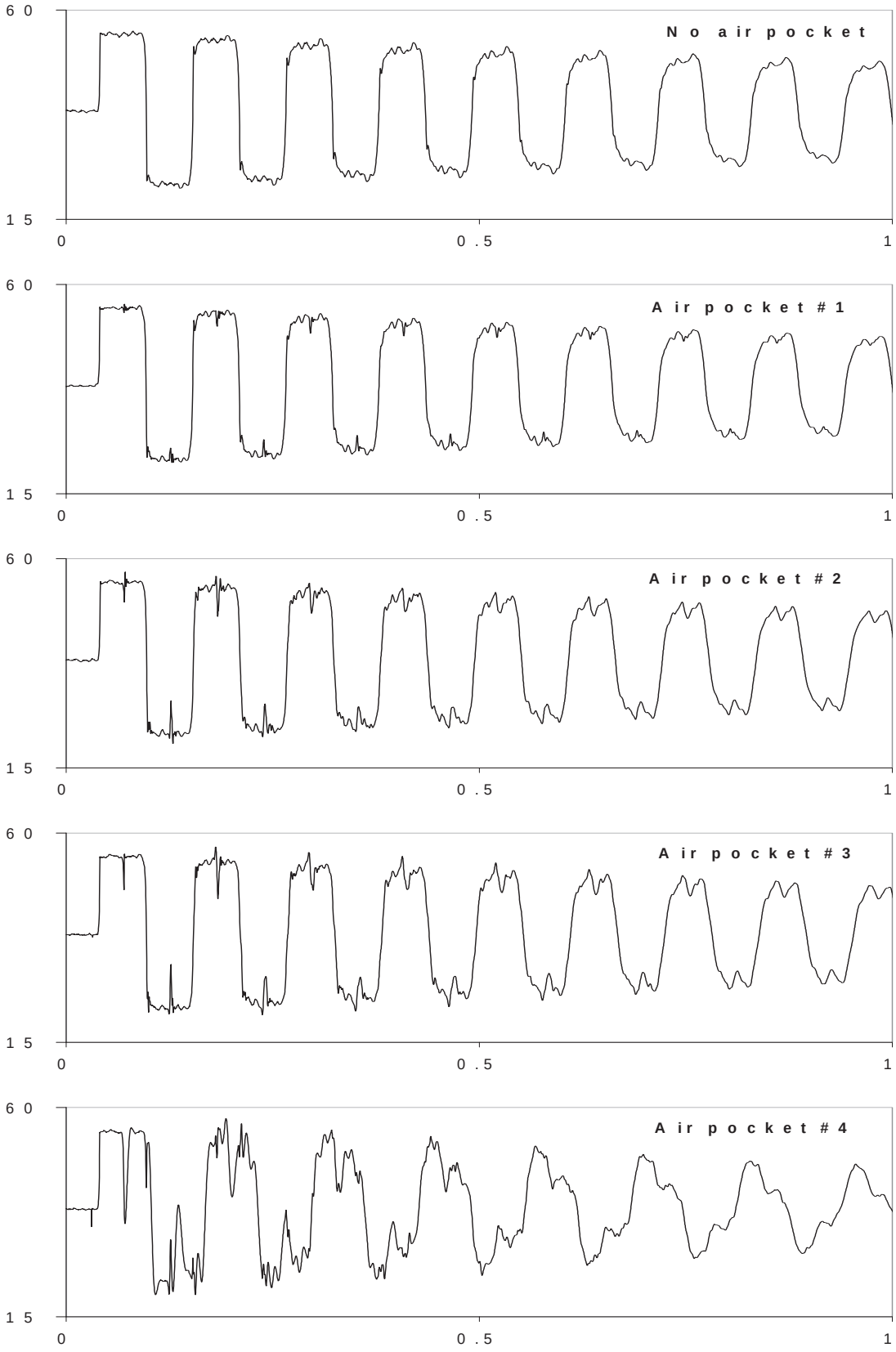

Figure 7.19 Measured Data at the End of Pipeline (WE) during Flow Condition 4 (Air pocket is located the middle of pipeline (EM) and initial velocity is 0.1208 m/s)

(x-axis: measured time (s) and y-axis: pressure head (m))

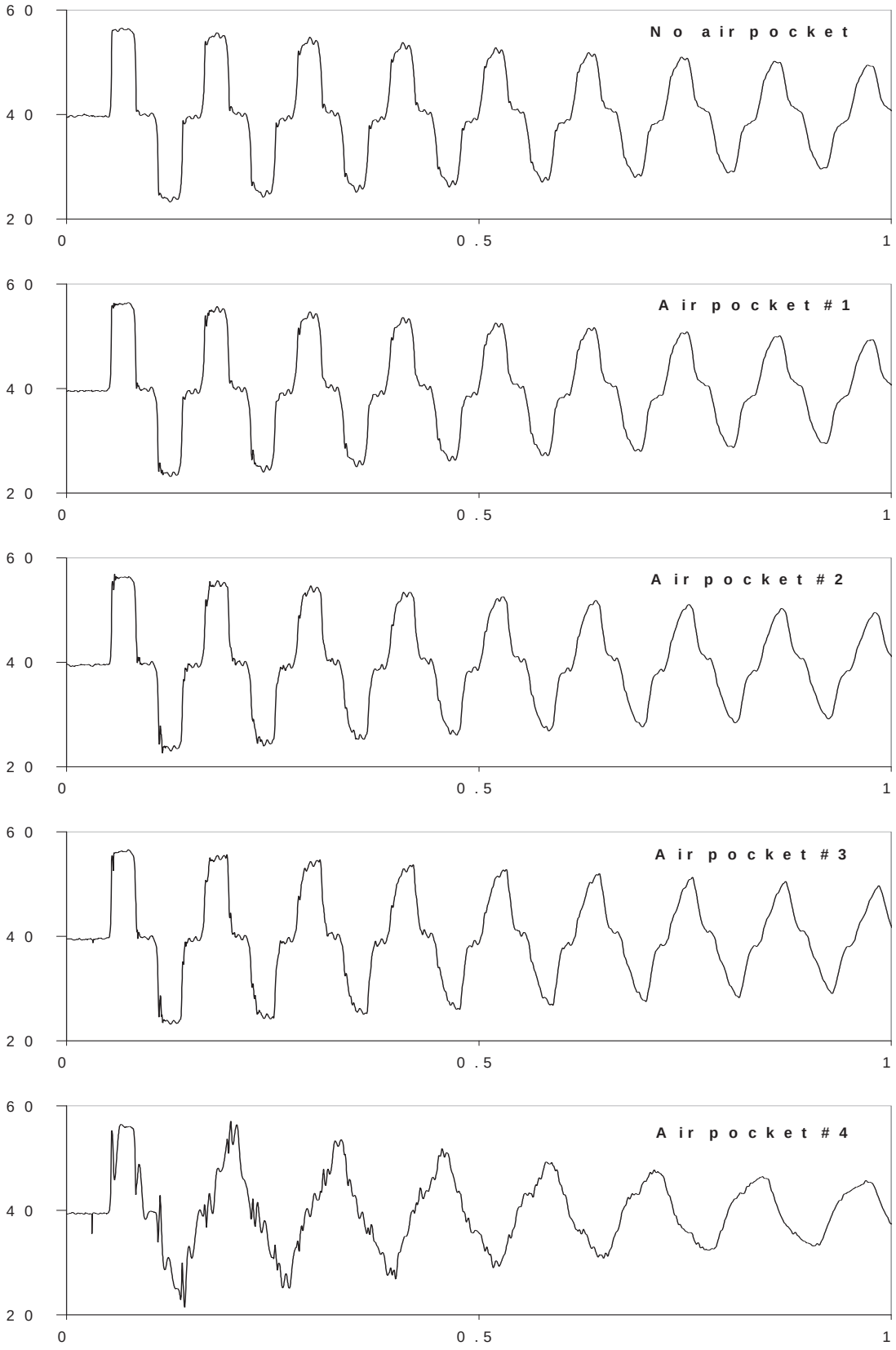

Figure 7.20 Measured Data at the Middle of Pipeline (WM) during Flow Condition 4 (Air pocket is located the middle of pipeline (EM) and initial velocity is 0.1208 m/s)

(x-axis: measured time (s) and y-axis: pressure head (m))

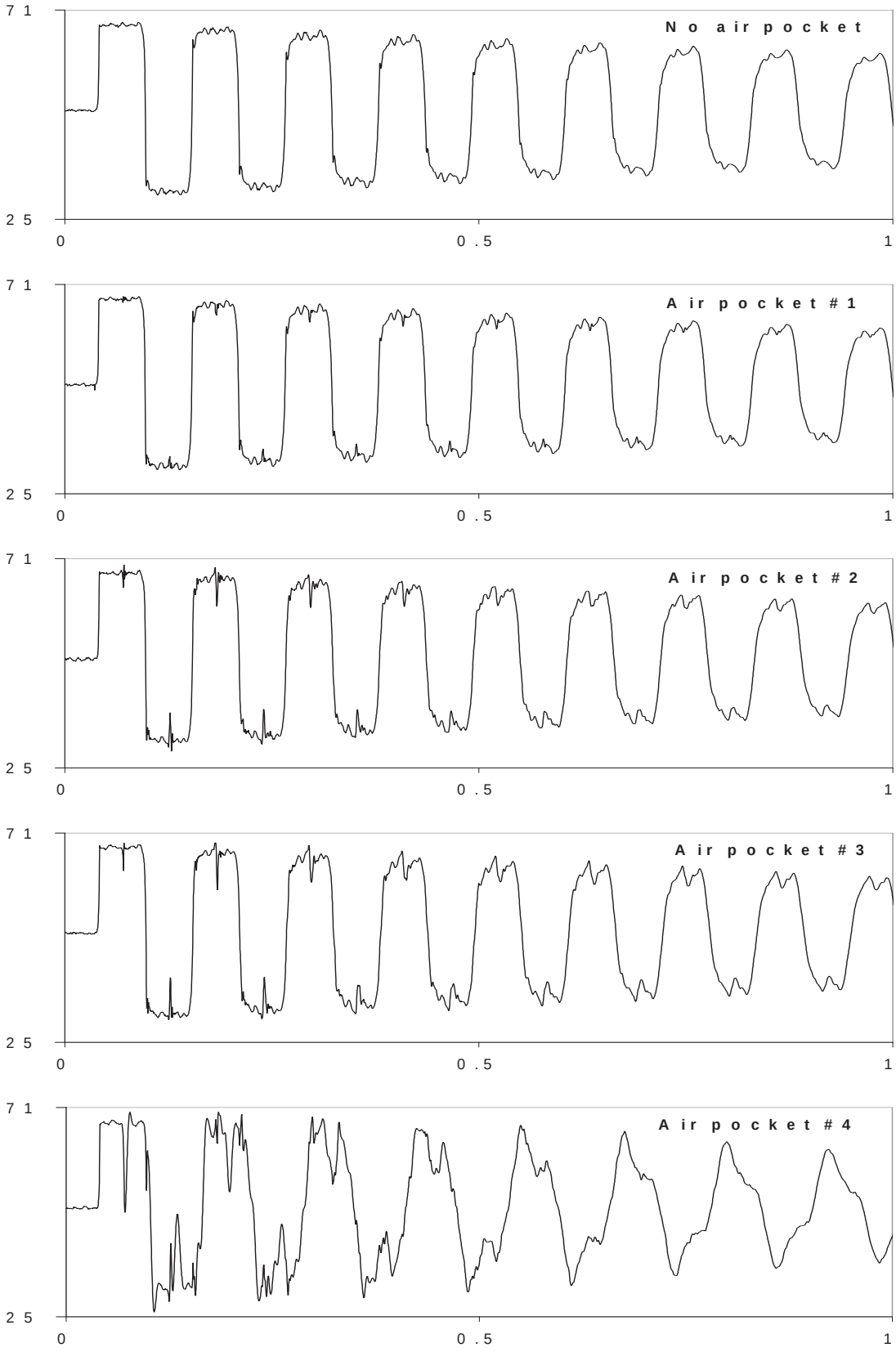

Figure 7.21 Measured Data at the End of Pipeline (WE) during Flow Condition 5 (Air pocket is located the middle of pipeline (EM) and initial velocity is 0.1368 m/s)

(x-axis: measured time (s) and y-axis: pressure head (m))

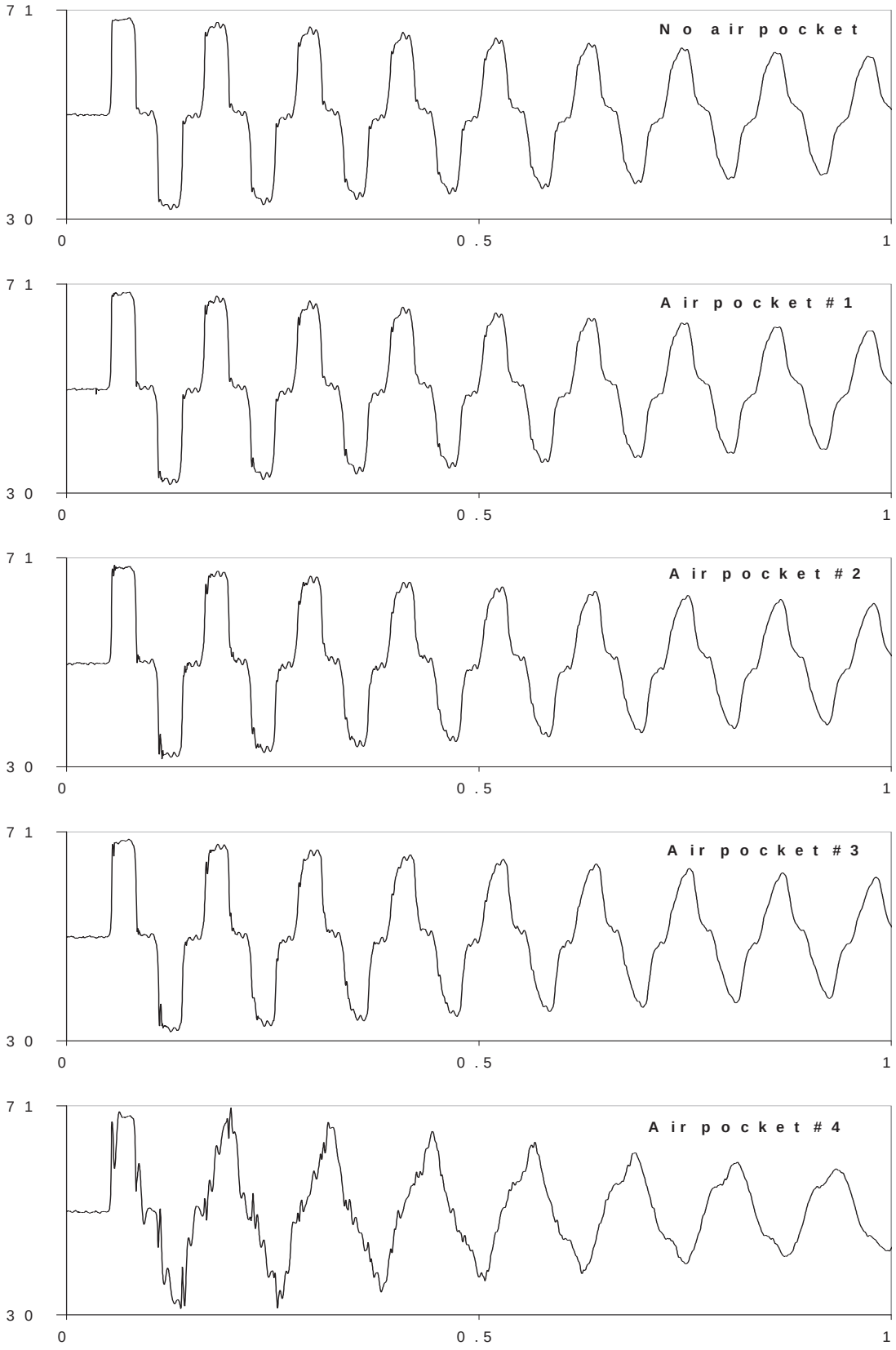

Figure 7.22 Measured Data at the Middle of Pipeline (WM) during Flow Condition 5 (Air pocket is located the middle of pipeline (EM) and initial velocity is 0.1368 m/s)

(x-axis: measured time (s) and y-axis: pressure head (m))

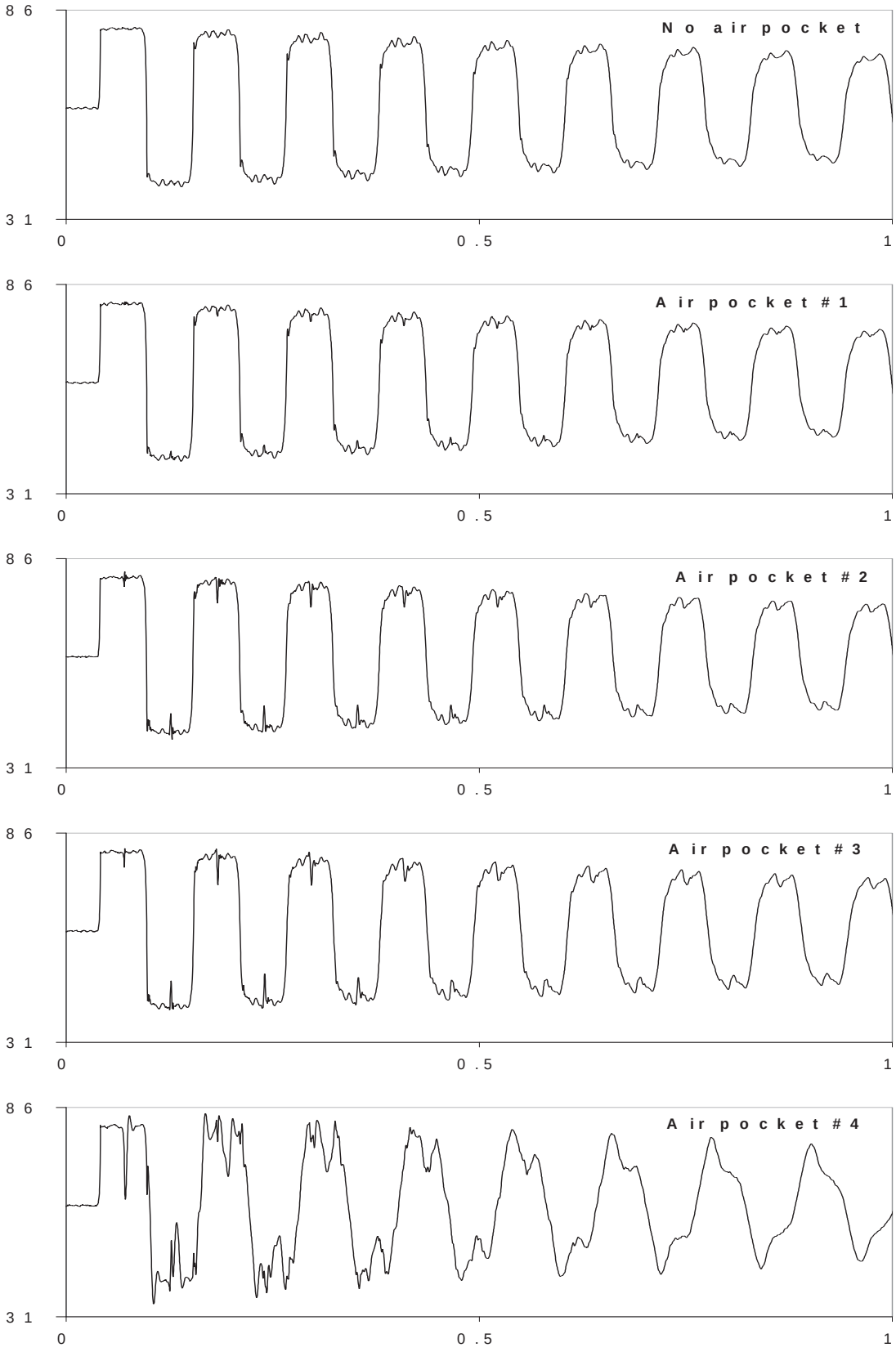

Figure 7.23 Measured Data at the End of Pipeline (WE) during Flow Condition 6 (Air pocket is located the middle of pipeline (EM) and initial velocity is 0.1495 m/s)

(x-axis: measured time (s) and y-axis: pressure head (m))

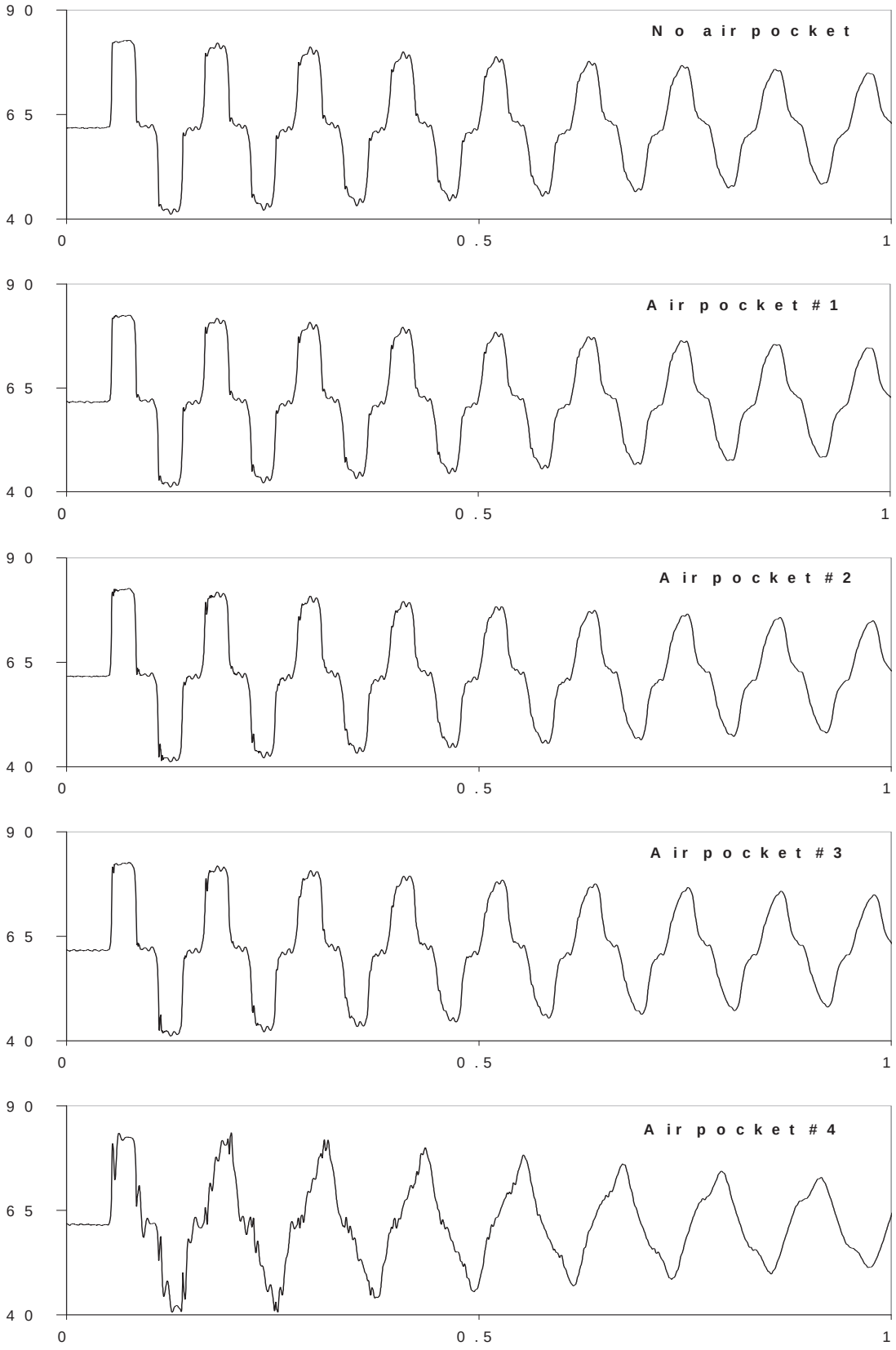

Figure 7.24 Measured Data at the Middle of Pipeline (WM) during Flow Condition 6 (Air pocket is located the middle of pipeline (EM) and initial velocity is 0.1495 m/s)

(x-axis: measured time (s) and y-axis: pressure head (m))

The measured data illustrate that air pockets not only reduce the wavespeed, but also cause a major change in the shape and the magnitude of the pressure waves. Similar to the numerical experiment results, the relative proportions of air and water in a pipeline system lead to different patterns of pressure wave and speeds of pressure propagation and these are very dependent on the size of air pocket and pressure condition of the experiment. Air pockets create high frequency deep valleys when the pressure waves meet the air pockets of the pipeline because of the sudden drop of fluid density (compression of an isolated air cushion). The magnitudes of these valleys are reduced as the initial test pressure increases or the size of air pocket decreases.

The presence of air is generally beneficial in reducing waterhammer pressures in the longer term transients (extended time period). Also, the entrapped air can increase peak pressures by shock waves (high frequency spikes). In case of air pocket #4 under the low pressure conditions, the measured data demonstrates significant peak pressures. The formation of shock waves is associated with the dynamic interaction between water and air phases. The shock wave occurs due to the reflection of a pressure wave by air pocket. The instantaneous compression of the air pocket by the passing pressure wave leads to the characteristic recovery. This generates the reflection of the compression wave and this reflection can increase the peak pressure. The peak pressure becomes bigger as the size of air pocket increases due to the rise of the reflection of the compression wave. In the propagation process of the high pressure conditions, the peak pressure by the pressure reflection is relatively small because the size of air pocket diminish owing to the higher pressure. Estimation of the maximum pressure by shock wave is highly important in safety analysis.

Figs. 7.25 and 7.26 show the comparative graphs of measured pressure waves (as shown in Figs. 7.13 to 24) at the end of pipeline (WE) according to the different test conditions when the pipeline has air pockets #3 and #4 in the middle of pipeline (EM). The comparative graphs clearly show the changes of wavespeeds and pressure shapes. In particular, the change is drastic in the pipeline with the larger air pocket shown in Fig. 7.26.

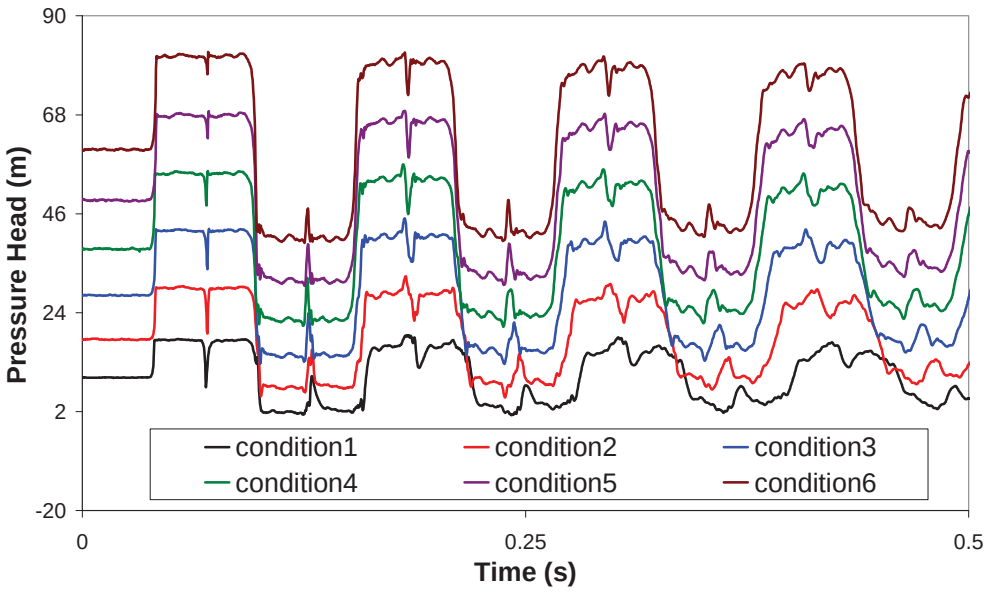

Figure 7.25 Comparison of Pressure Waves according to Different Flow Conditions (when the pipeline has air pocket #3) - see Table 7.4 for test condition details

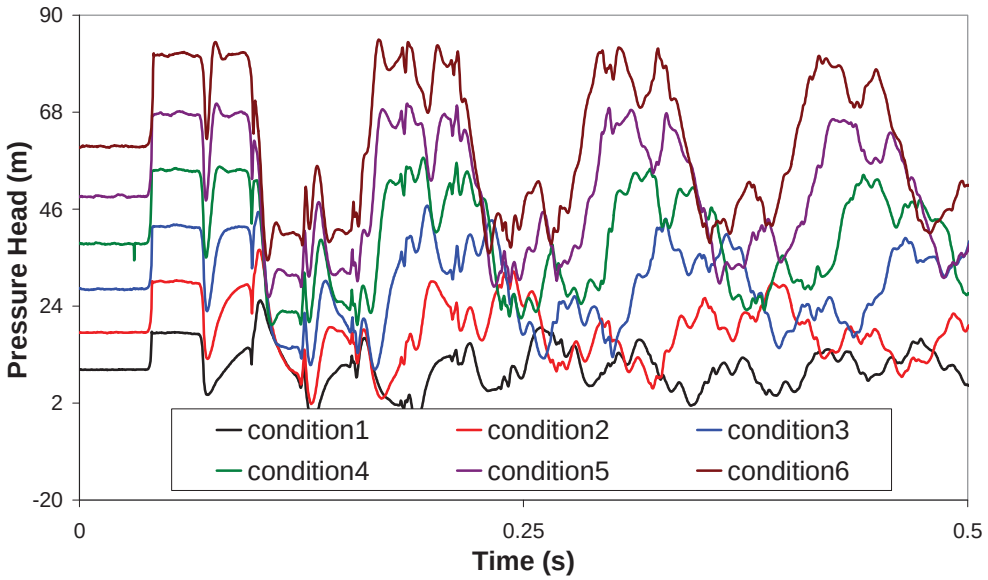

Figure 7.26 Comparison of Pressure Waves according to Different Flow Conditions (when the pipeline has air pocket #4) - see Table 7.4 for test condition details

Figs. 7.27 and 7.28 show the comparative graphs of measured pressure waves (as shown in Figs. 7.13 to 24) at the end of pipeline (WE) according to the different sizes of air pocket under the same test condition to demonstrate the pressure damping effect by different sized air pockets. The test conditions used are condition 2 for low pressure scenario and condition 5 for high pressure scenario. The graphs show the measured data over an

extended period of time. The damping rate of the pressure wave affected by the air pocket is more severe when the pipeline is at a lower pressure. In the high pressure test scenario, the pressure damping effects by air pockets are less, although the change of wavespeed still looks like a significant factor for transient analysis.

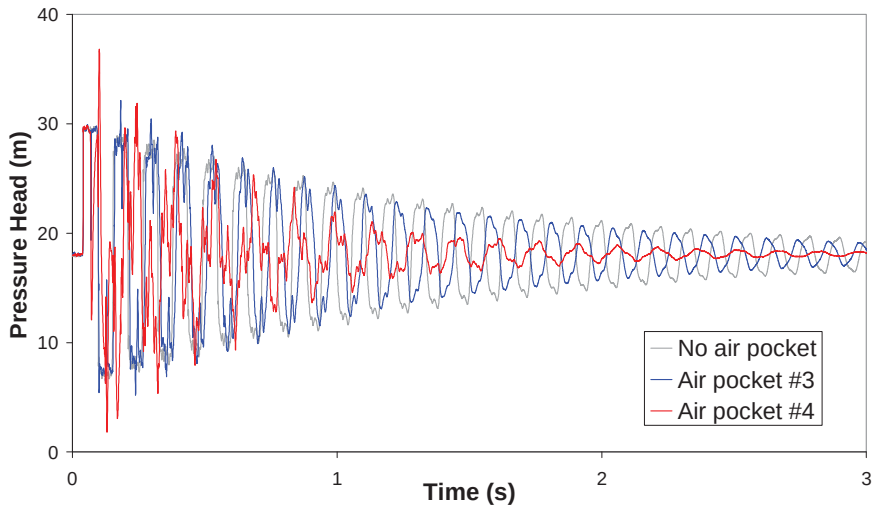

Figure 7.27 Comparison of Pressure Waves according to Different Sizes of Air Pocket under the Test Condition 2 (Low Pressure Condition) - see Table 7.5 for air pocket volume

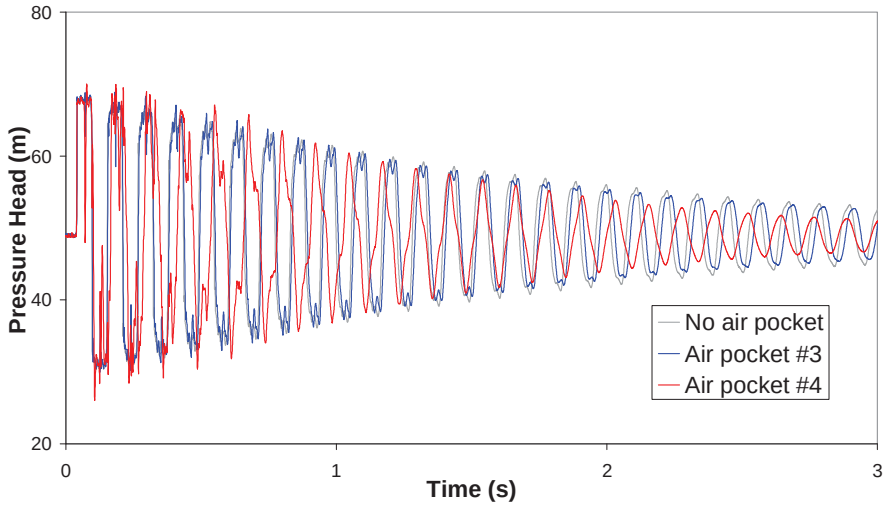

Figure 7.28 Comparison of Pressure Waves according to Different Sizes of Air Pocket under the Test Condition 5 (High Pressure Condition) - see Table 7.5 for air pocket volume

7.6 SIMULATION RESULTS FOR AIR POCKET TESTS

Figs. 7.29 to 7.32 show the comparison between measured pressure data (introduced in the previous section) and their simulation results by proposed model under the test condition 2 (low pressure condition) and 5 (high pressure condition). The pressure data used are the measurements at the middle (WM) and end (WE) of pipeline. The black line represents the measured pressure data and the gray broken line represents the simulation results by traditional method of characteristics without unsteady friction and entrapped air pocket effects during transients. The red or blue line is the simulation results by the conservative solution scheme including the proposed air pocket model.

The simulation results by traditional MOC without an air pocket show significant discrepancies of pressure patterns and wavespeeds when compared with the measured pressure waves. The simulation results given by the conservative scheme model show that the timing of the positive and negative pressure waves matches the experimental pressure waves quite closely. Also, the model predicts well the detailed shapes of pressure waves affected by entrapped air pockets during transients. However, the model overestimates the magnitude of pressure waves for the measured data of test condition 2. This situation is similar to the simulation results of Figs. 5.17 and 5.18 in Chapter 5. The detailed reasons for these discrepancies is explained in the Section 5.5.1.

Figs. 7.31 and 7.32 show good agreement between the experimental data and the simulation results. Although the pressure peaks of the simulation model slightly exceed the measured data, the magnitudes, shapes, and timing of the two transients are quite similar. These results indicate that the pressure transients affected by entrapped air can be estimated fairly precisely by the conservative solution scheme including the proposed discrete air pocket model.

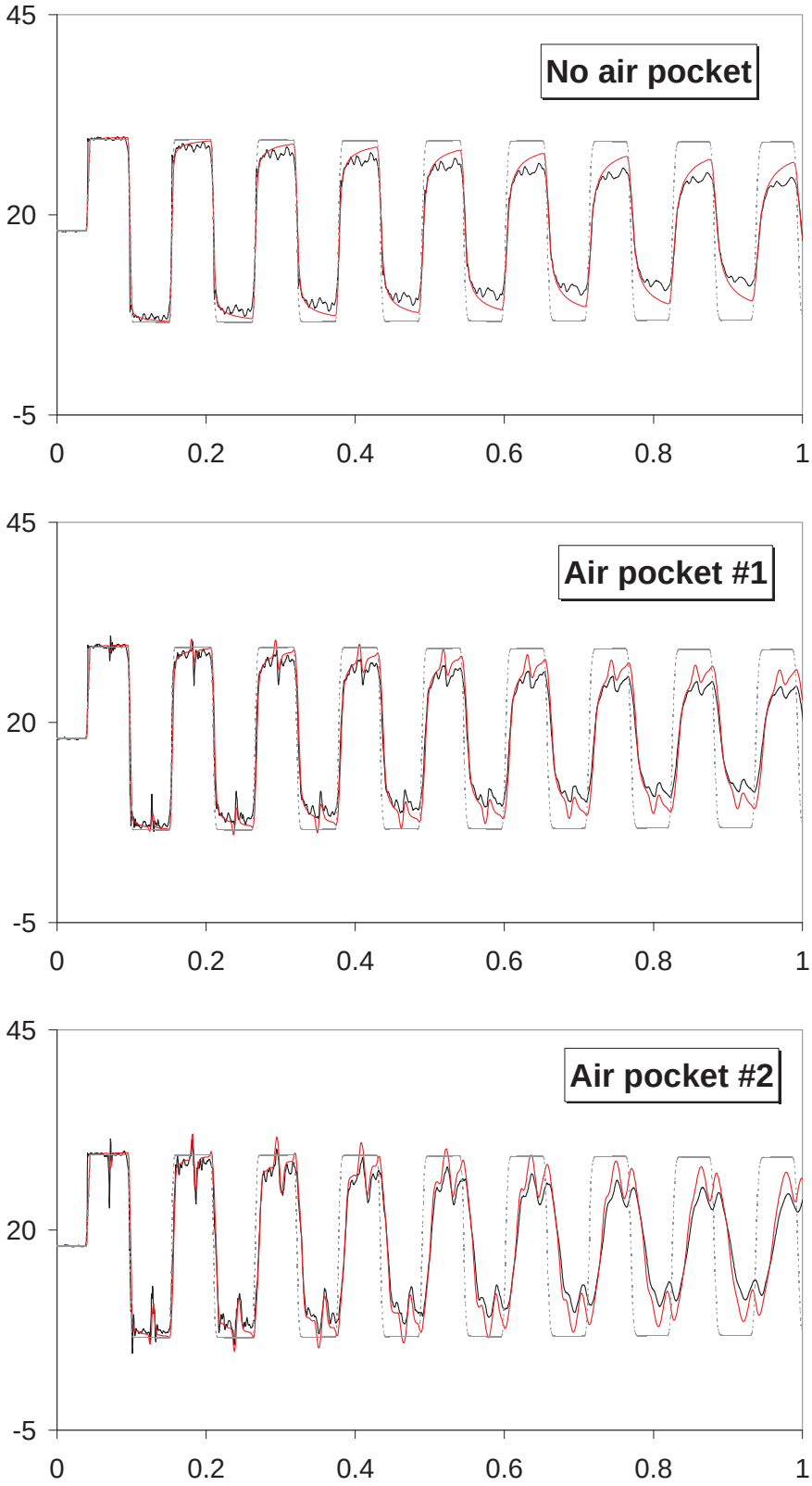

Figure 7.29 Comparison between Measured Pressure Data and Simulation Results at the End of Pipeline (WE) under the Test Condition 2

(black line: measured data, red line: simulation result, gray broken line: simulation result by traditional MOC without unsteady friction and air pocket models)

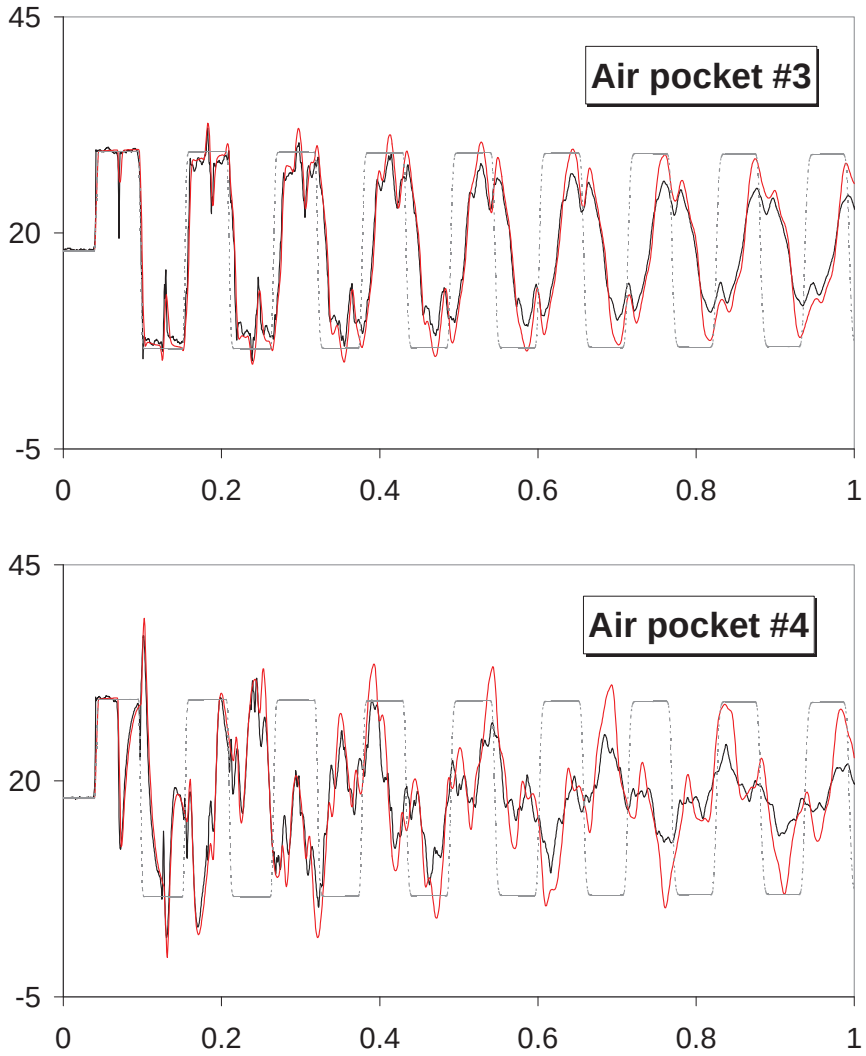

Figure 7.29 Comparison between Measured Pressure Data and Simulation Results at the End of Pipeline (WE) under the Test Condition 2 (continued)

(black line: measured data, red line: simulation result, gray broken line: simulation result by traditional MOC without unsteady friction and air pocket models)

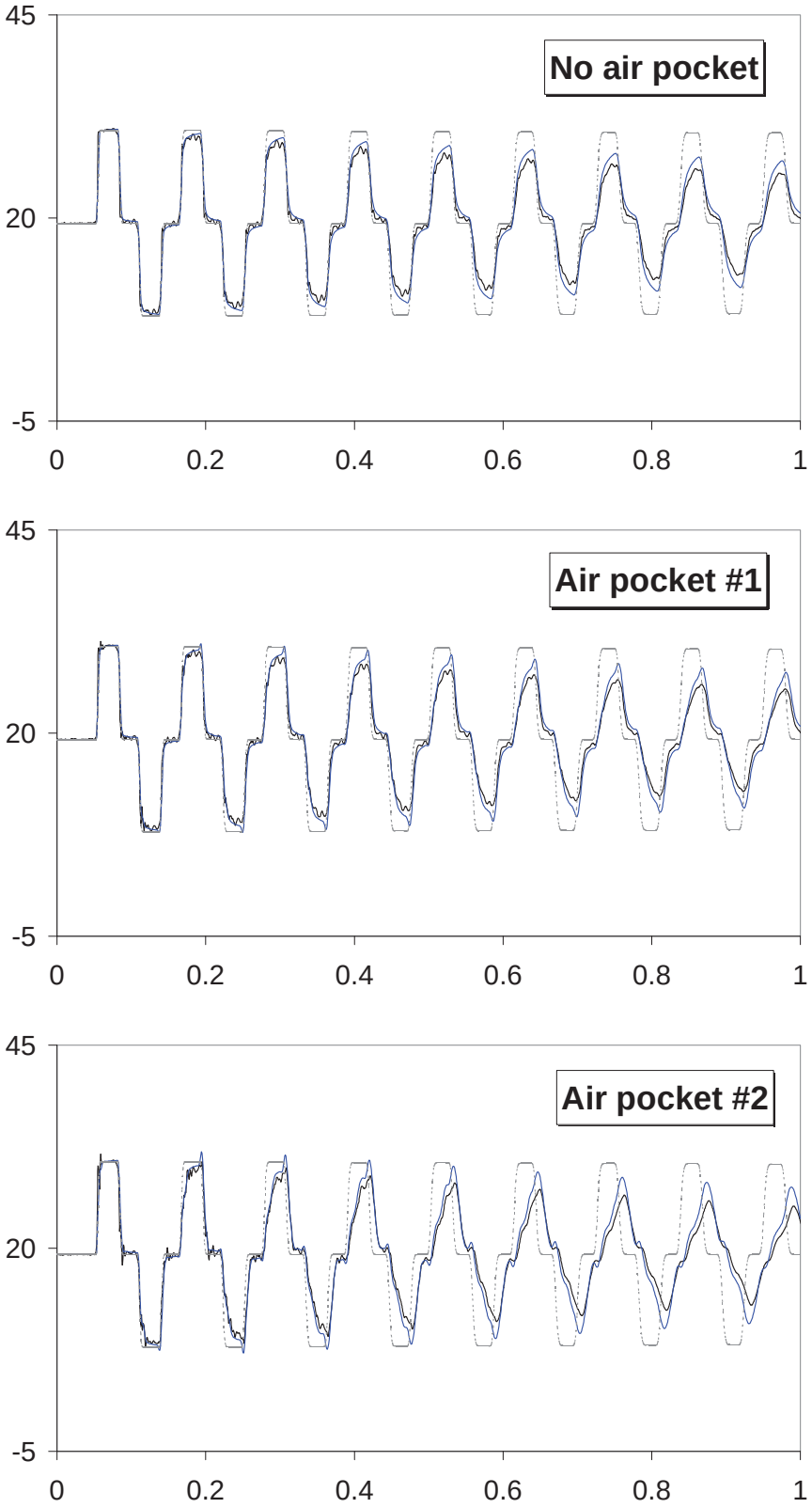

Figure 7.30 Comparison between Measured Pressure Data and Simulation Results at the Middle of Pipeline (WM) under the Test Condition 2

(black line: measured data, blue line: simulation result, gray broken line: simulation result by traditional MOC without unsteady friction and air pocket models)

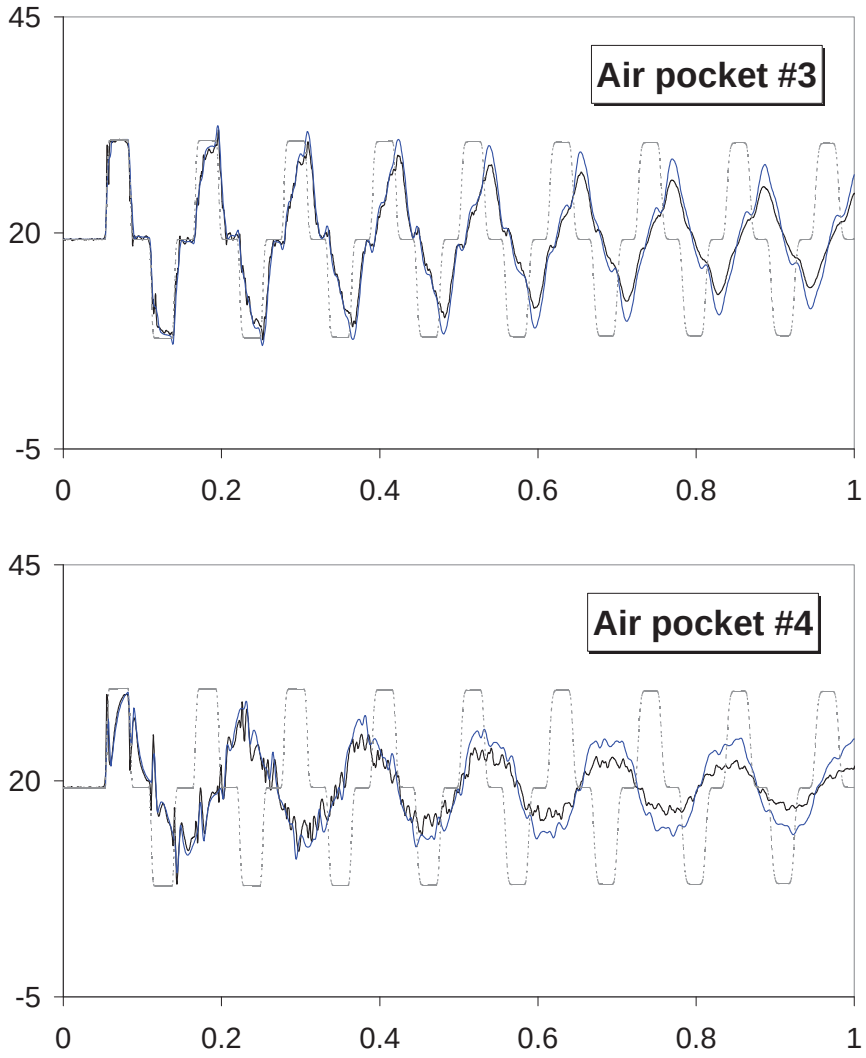

Figure 7.30 Comparison between Measured Pressure Data and Simulation Results at the Middle of Pipeline (WM) under the Test Condition 2 (continued)

(black line: measured data, blue line: simulation result, gray broken line: simulation result by traditional MOC without unsteady friction and air pocket models)

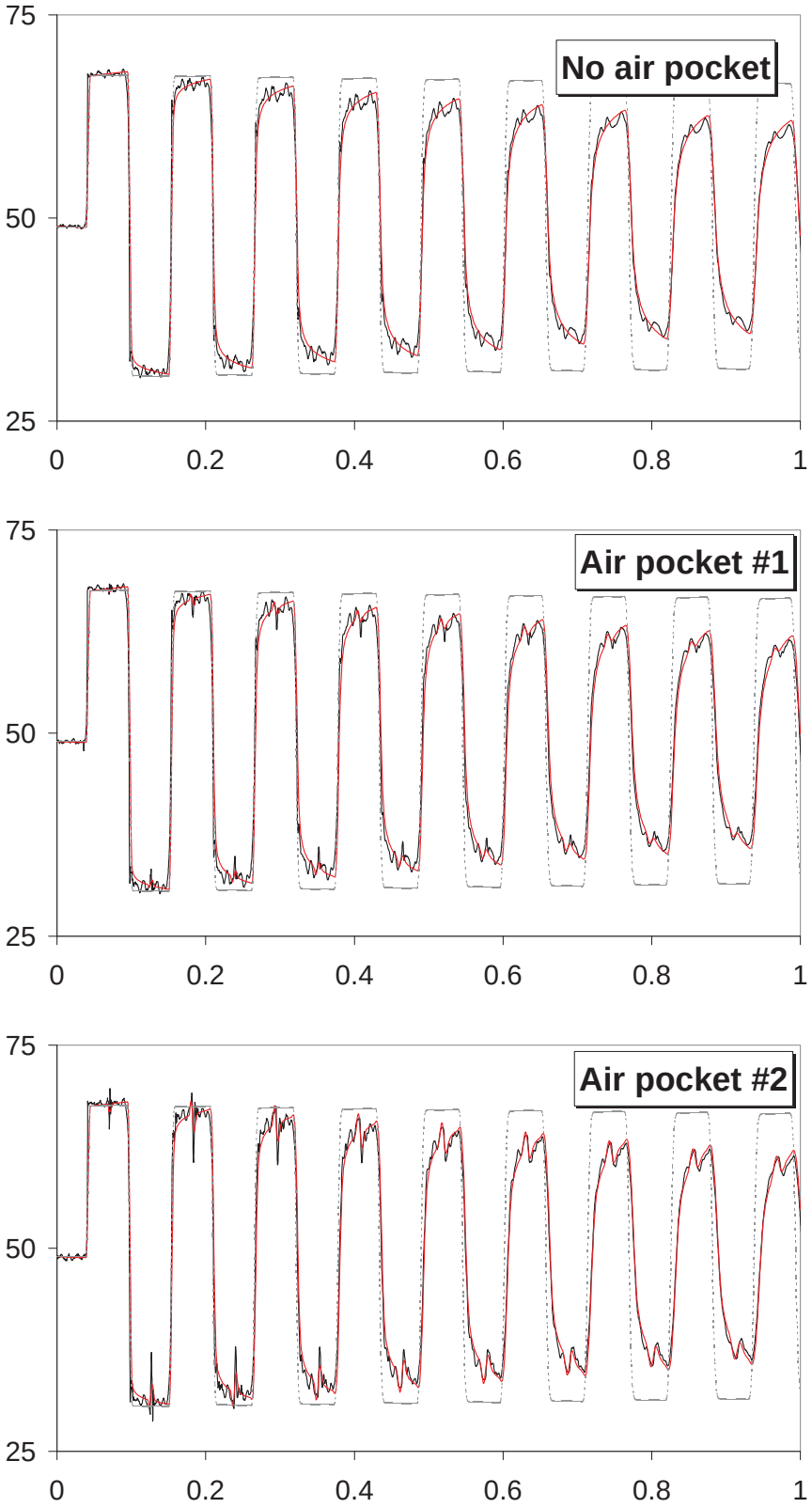

Figure 7.31 Comparison between Measured Pressure Data and Simulation Results at the End of Pipeline (WE) under the Test Condition 5

(black line: measured data, red line: simulation result, gray broken line: simulation result by traditional MOC without unsteady friction and air pocket models)

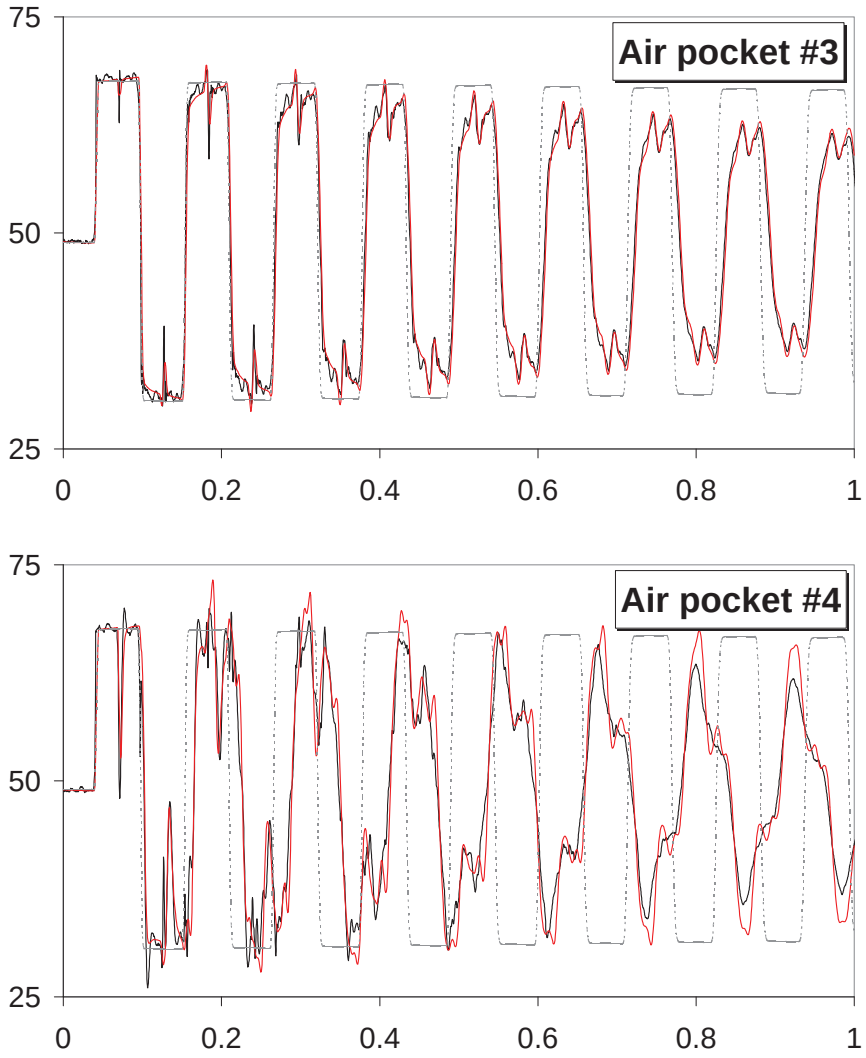

Figure 7.31 Comparison between Measured Pressure Data and Simulation Results at the End of Pipeline (WE) under the Test Condition 5 (continued)

(black line: measured data, red line: simulation result, gray broken line: simulation result by traditional MOC without unsteady friction and air pocket models)

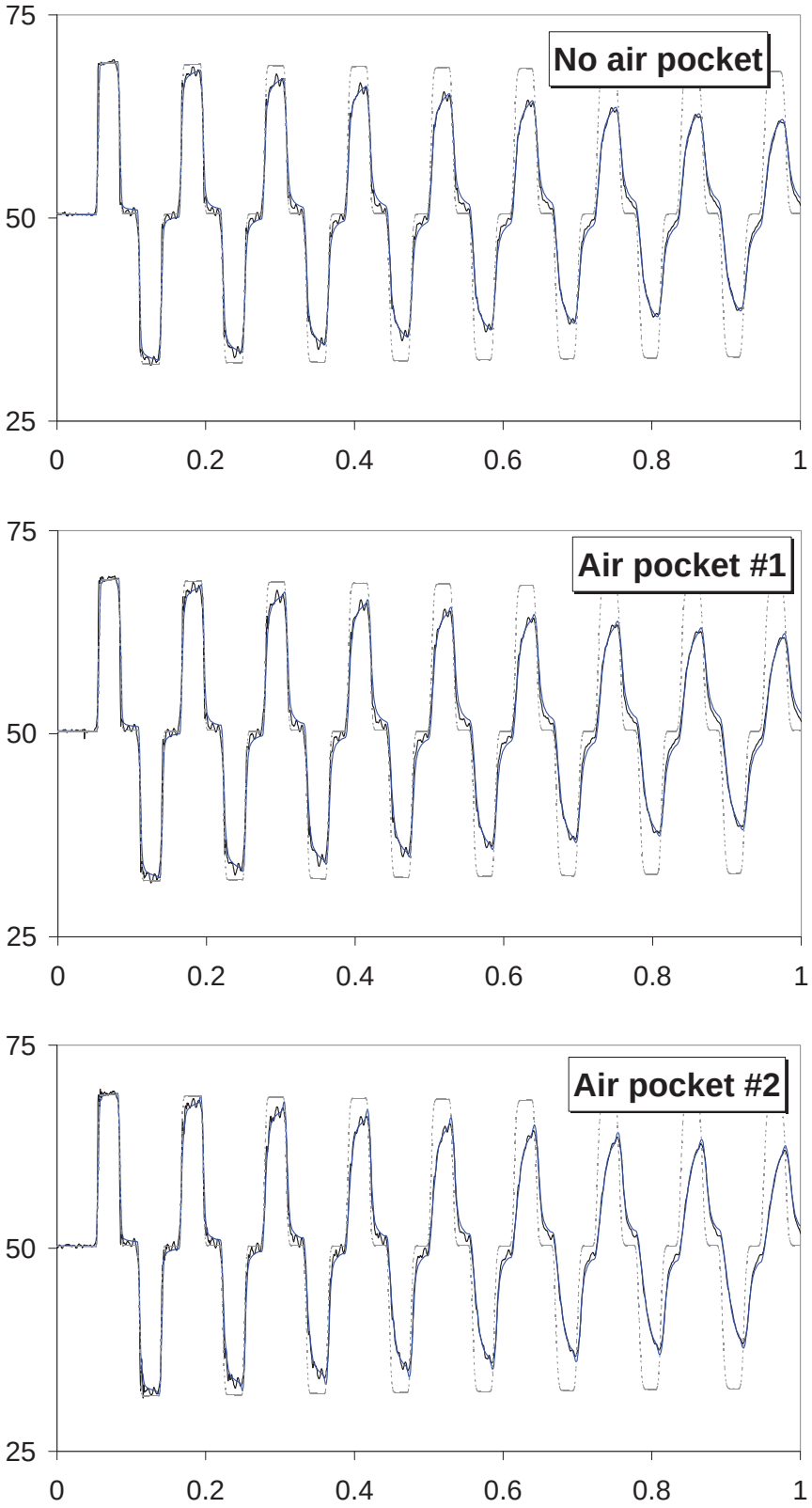

Figure 7.32 Comparison between Measured Pressure Data and Simulation Results at the Middle of Pipeline (WM) under the Test Condition 5

(black line: measured data, blue line: simulation result, gray broken line: simulation result by traditional MOC without unsteady friction and air pocket models)

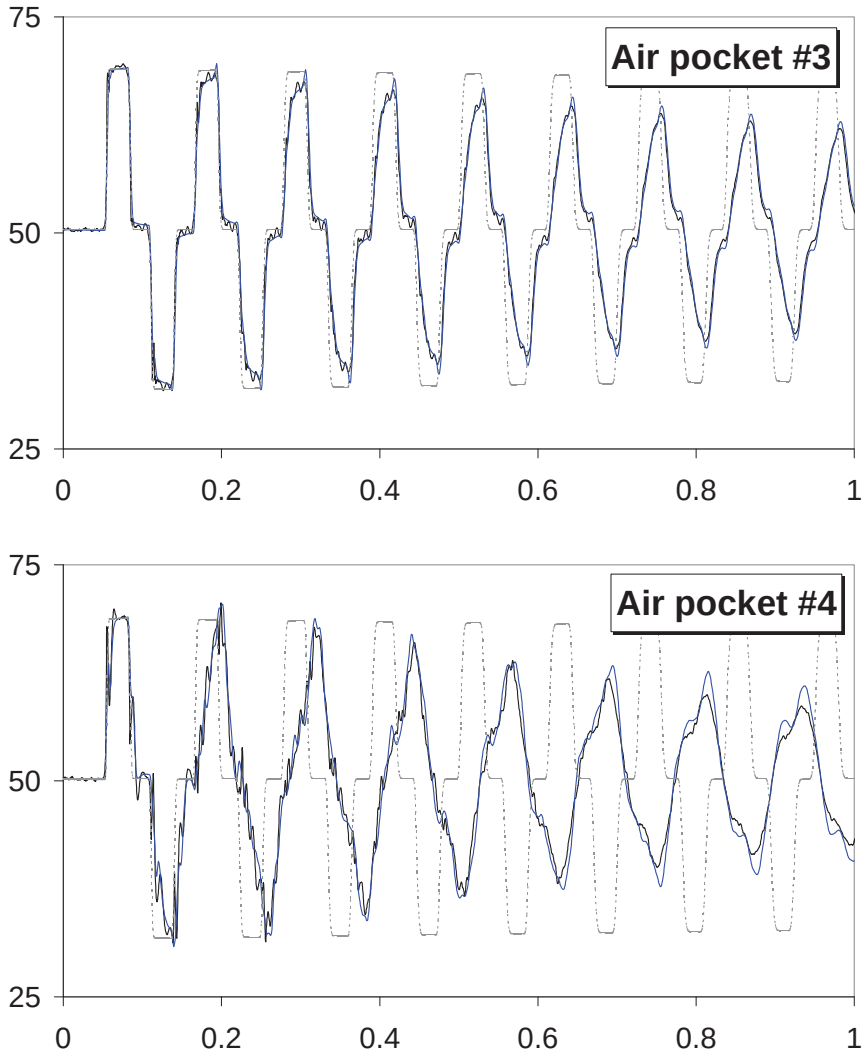

Figure 7.32 Comparison between Measured Pressure Data and Simulation Results at the Middle of Pipeline (WM) under the Test Condition 5 (continued)

(black line: measured data, blue line: simulation result, gray broken line: simulation result by traditional MOC without unsteady friction and air pocket models)

7.7 SUMMARY AND CONCLUSIONS

The measured data has shown that gas cavities in a liquid pipeline system, even in very small volumetric proportions, not only significantly reduces the wave propagation speed, but also causes a major change in the shape and magnitude of the transient pressure waves. The sudden and rapid change in fluid velocity when the pipeline has an air pocket creates excessively high frequency pressure spikes that are greater than those that occur without any cavity due to the reflection from the boundary surface between the two-phase and

single-phase flows. On the other hand, a large air cavity acts as an effective accumulator and suppresses the maximum and minimum pressures because of the increase in elasticity of the mixture. The patterns of pressure wave and speed of pressure propagation have been shown to be very dependent on the size of air pocket and initial pressure condition of pipeline system.

Mathematical model for simulating the effect of entrapped air pocket on transient pipe flows have been presented by using an accumulator (air chamber) model that yields practical results. Incorporating the model into the conservative solution scheme leads to the discrete gas cavity analysis model for single or multiple isolated cavities. The gas cavity model is effective in treating relatively small gas volumes, for which the gas volume is significantly less than the liquid volume. The model has been applied to a number of numerical and experimental examples with the pressure dependent wavespeeds and shock waves during transient events. This model has been shown to accurately calculate the overall pressure trace with variable wavespeeds, high frequency pressure spikes, and the change of pressure magnitude. The range of applicability of the model varies for different proportions of air to liquid systems, discrete vapour cavities, or homogenous gas-liquid mixtures.